INVESTIGATING THE GENERATION EFFICIENCY, GROWTH AND STRUCTURE OF FLOCS PRODUCED BY ELECTROCOAGULATION

by

Sin Yin Lee

Submitted in partial fulfilment of the requirements
for the degree of Doctor of Philosophy

at

Dalhousie University
Halifax, Nova Scotia
October 2015

TABLE OF CONTENTS

LIST OF TABLES

LIST OF FIGURES

ABSTRACT

Electrocoagulation (EC) is a water treatment technology that releases metal cations into solution from sacrificial anodes. Compared to chemical coagulation (CC), EC's advantages (e.g., solid metal electrodes, reduced alkalinity consumption) make it potentially better suited for use in emergency situations or remote areas. However, EC is not commonly used, suffering from a lack of standardized design and operational procedures, and a dearth of research regarding its functional mechanisms. This thesis addresses this research gap, focusing on the generation efficiency, growth and structure of EC flocs. It was found that using a stainless steel cathode rather than an aluminum cathode resulted in faster and more efficient iron generation; this was attributed to the difference in the rate of hydrogen evolution at the cathode surface. The EC system also produced more iron per unit power when operated at lower voltages, suggesting that it is more efficient to operate using more electrodes at low power, rather than vice versa. Regarding the growth of iron precipitate EC flocs, changes in particle size were reflected by changes in scattering exponent. Flocs initially spanned a broad size range and formed loose, open structures; these initial aggregates then broke and formed into more compact structures. While operating at higher current densities resulted in larger and faster stabilizing flocs, comparing plots of scattering exponent against time revealed that the described structural progression was otherwise unaffected. Flocs were also more compact when formed from CC rather than EC, in low rather than high salt solution, and at pH 8.3 rather than pH 6.0. Flocs formed in low salt and at pH 8.3 were more stable in solution than their counterparts, likely requiring more collisions to form and producing denser structures. Transmission electron microscopy revealed that CC and EC flocs were structurally distinct, possibly affecting the scattering exponent. Flocs were also larger when produced via CC and in low salt solution; because these conditions resulted in denser flocs, they were likely less prone to breakage. Because all research was conducted at the bench-scale using synthetic solutions, further testing is required before inferences can be made regarding full-scale EC performance.

LIST OF ABBREVIATIONS USED

CC	Chemical coagulation
COD	Chemical oxygen demand
DLA	Diffusion limited aggregation
EC	Electrocoagulation
HER	Hydrogen evolution reaction
NOM	Natural organic matter
RLA	Reaction limited aggregation
RO	Reverse osmosis
SEEC	Specific electrical energy consumption
SEM	Scanning electron microscopy
SS	Stainless steel
TEM	Transmission electron microscopy

ACKNOWLEDGEMENTS

There are many people without whom this thesis would have been a great deal more difficult, if not impossible. Each and every one of them has my sincere gratitude.

Foremost, I would like to acknowledge my supervisor, Dr. Graham Gagnon, for providing me with this tremendous opportunity for research and learning. His support and guidance have been invaluable. I would also like to thank my supervisory committee members, Dr. Margaret Walsh and Dr. George Jarjoura, for their advice and support.

I am sincerely grateful to Heather Daurie, Shelley Oderkirk, and Elliott Wright, who advised me in the lab and processed many of my samples. I would also like to acknowledge Dan Chevalier, Gerald Fraser, and Dr. Ping Li for their assistance with certain analytical instruments. Furthermore, I would like to thank Jesse Keane, Brian Kennedy, and Blair Nickerson, who helped me build my experimental system.

I would also like to thank all the students and staff associated with the Centre for Water Resources Studies for their help and discussion and company. In particular, I would like to acknowledge Tarra Chartrand, without whom all would be impossibly disorganized, and Jessica Younker, for her camaraderie and reassurance.

I am also thankful to the office staff in the Department of Civil and Resource Engineering for handling my paperwork, and in particular, June Ferguson, who was instrumental to scheduling my defence.

Finally, I gratefully acknowledge the financial contributions provided by the Natural Sciences and Engineering Research Council of Canada (NSERC), Petroleum Research Atlantic Canada (PRAC), Encana, and Dalhousie University.

CHAPTER 1: INTRODUCTION

1.1 Research Rationale and Objective

Electrocoagulation (EC) functions by releasing metal cations into solution to destabilize particles and thus aid their aggregation. These cations can also react to form metal hydroxide compounds, which provide a surface for particle adsorption. EC has a number of advantages over CC that potentially make it better suited for use in remote areas or emergency situations: (a) EC uses solid sacrificial electrodes instead of corrosive chemical salts, which are easier to handle and store; and (b) EC consumes less alkalinity than CC, reducing the need for pH adjustment (Bagga et al. 2008; Zhu et al. 2005). However, despite these advantages and having been available for nearly a century, EC has never become a widely used water treatment technology (Holt et al. 2005).

There are no established design or operational procedures for EC, and there is limited research available regarding the mechanisms of EC. The available literature mostly presents results from bench-scale EC case studies, which are difficult to compare as they are generally based on custom-designed systems which have unique operating conditions. This thesis attempts to address selected aspects of this extensive research gap by focusing on scale invariant parameters and outcomes, namely cathode material, electrolyte composition, and floc characteristics.

The objective of this research was to study the formation of EC flocs, specifically investigating production efficiency, process of growth and structure. Two sub-objectives were developed from this statement. The first was to explore the factors that affect the

efficiency of cation generation at the anode in order to advance the design and operation of EC systems. The second was to conduct a detailed investigation into the characteristics and structural progression of EC flocs, and to compare these results against those for CC. All research was conducted at the bench-scale using synthetic solutions. Experiments were executed in three phases, corresponding to Chapters 4, 5, and 6.

1.2 Organization of Thesis

Chapters 2, 4, 5 and 6 were originally prepared as manuscripts for potential publication in peer reviewed journals. They retain much of their original formatting, including individual abstract and conclusions sections. Each subsequent chapter is described briefly below:

- Chapter 2 provides a literature review regarding the design and operation of EC systems. This Chapter has been published in the journal *Environmental Reviews.*
- Chapter 3 summarizes the materials and methods that are common to Chapters 4, 5, and 6.
- Chapter 4 presents experimental work investigating the rate and efficiency of iron generation in an EC system. This work has been published in the journal *Environmental Technology.*
- Chapter 5 presents experimental work regarding the growth and structure of EC flocs.

- Chapter 6 is an extension of the work conducted in Chapter 5, and provides a comparison of the growth and structure of CC and EC flocs under various conditions.
- Chapter 7 gives overall conclusions for the entire thesis.

CHAPTER 2: REVIEW OF THE FACTORS RELEVANT TO THE DESIGN AND OPERATION OF AN ELECTROCOAGULATION SYSTEM FOR WASTEWATER TREATMENT[1]

2.1 Abstract

Electrocoagulation (EC) is a water treatment technology that has been proven effective at the bench scale for the removal of a wide variety of contaminants from water and wastewater. It is an electrochemical process that involves using a sacrificial anode to generate cations for coagulation. It also evolves hydrogen gas at the cathode, which some researchers have suggested can be used for natural flotation. EC has a number of advantages over conventional chemical coagulation (CC). For instance, solid metal electrodes tend to be easier to move and store than corrosive chemical salts. Furthermore, EC tends to increase solution pH, rather than consume alkalinity like chemical coagulants. However, unlike with CC, there are no standardized procedures for jar testing with EC, or for designing EC systems. Much of the current EC literature focuses on the treatment of a specific water or wastewater using custom EC systems. In an attempt to

[1] This work is published in the journal *Environmental Reviews.* It is available online at: http://www.nrcresearchpress.com/doi/abs/10.1139/er-2014-0009

Full reference: Lee, S. Y., & Gagnon, G. A. (2014). Review of the factors relevant to the design and operation of an electrocoagulation system for wastewater treatment. *Environmental Reviews, 22*(4), 421-429.

provide guidance for EC cell design, this Chapter reviews some of the current literature in four parts: electrodes, electrolyte, power source, and operational parameters.

2.2 Introduction

Electrocoagulation (EC) is a water treatment technology that involves electrolytically producing metal cations from a sacrificial anode for coagulation (Holt et al. 2005). EC has proved effective at the bench scale for the removal of a wide variety of contaminants from water and wastewater. The process has been studied for a broad range of applications, including (but not limited to) the pretreatment of seawater for desalination, the removal of fluoride from drinking water, and the treatment of heavily contaminated and highly colored textile industry wastewater (Timmes et al. 2010; Vasudevan et al. 2009; Wei et al. 2012).

EC has a number of advantages over conventional chemical coagulation (CC). For example, electrodes are usually entirely composed of metal, unlike chemical coagulants, which contain only a fraction of metal. Ferric chloride hexahydrate, for instance, is only about 21% iron, as determined from its chemical formula. Solid metal electrodes are also easier to store and move than corrosive, liquid, chemical coagulant salts. This gives EC a potential advantage when working in remote areas or emergency situations (Zhu et al. 2005). EC also typically produces less sludge than CC, since a pure source of cations is generated from anode oxidation (Vasudevan et al. 2009; Zhu et al. 2005). Furthermore, the EC process should not theoretically consume bulk alkalinity, since the protons produced at the anode are consumed at the cathode (see Section 2.2.1) (Zhu et al. 2005).

This may eliminate or reduce the need for pH adjustment, which is often required with CC.

However, EC also faces a number of challenges in regards to implementation for water treatment. Unlike with CC, there are no standardized procedures for designing an EC system and thus scale up from bench scale testing (e.g., jar testing) is not commonly reported in the literature. Not surprisingly, there is a gap in the literature regarding pilot or full scale setups. It is also difficult to compare results across research studies, as most papers are focused on the treatment of a specific wastewater using their own custom EC cell setup. Holt et al. (2005) notes that while EC has been available since the late 19th century, it has never become a widely used water treatment technology; they attribute this to the absence of an established method for reactor design, as well as a lack of published operational data.

To provide guidance for EC cell design, this Chapter reviews and summarizes some of the current EC literature, focusing on some of the key operational and design factors. By providing a review of the current state of the literature, this Chapter could be used as a planning tool to assist in future experimental design.

2.2.1 System Overview and Electrochemical Reactions

At its most basic, an EC system is simply an electrolytic cell. As seen in Figure 2.1, it must include a current source that is connected to at least one anode-cathode pair submerged together in an electrolyte. The electrolyte, which is the water or wastewater that is to be treated, completes the electrical circuit by allowing charges to migrate

between the electrodes. In this Chapter, EC is described in four sections: electrodes, electrolyte, power source, and operational parameters.

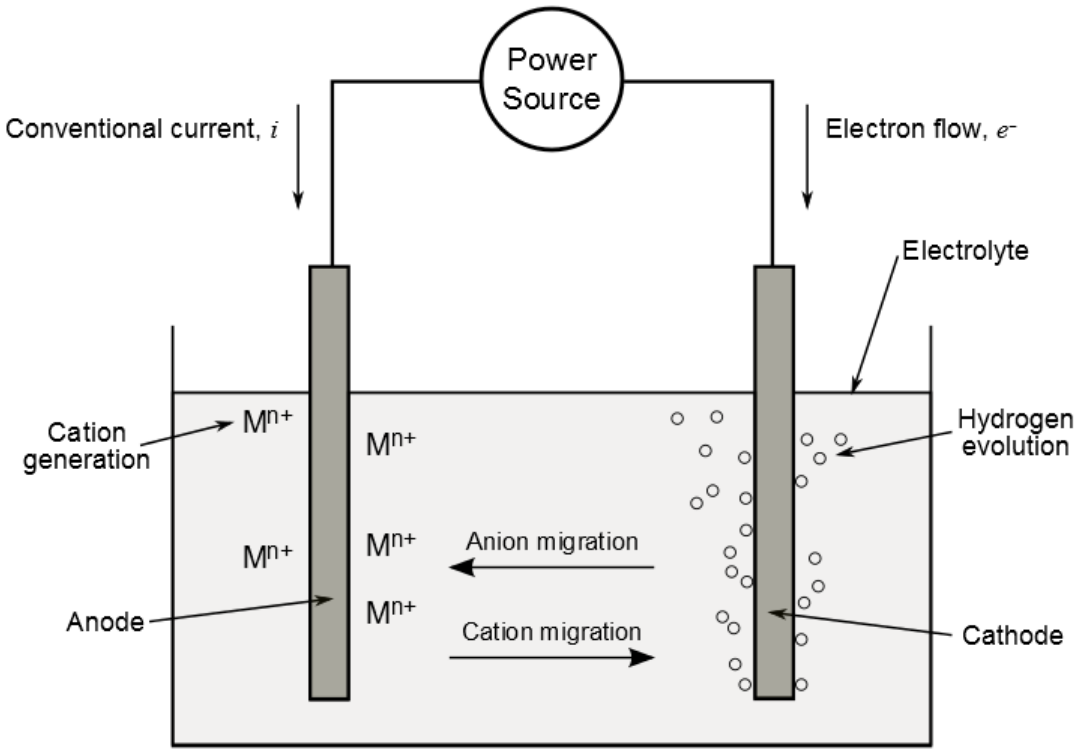

Figure 2.1: Diagram of an EC cell

Current is applied to promote the generation of metal cations at the anode, and the evolution of hydrogen gas at the cathode. Table 2.1 provides an overview of the electrochemical reactions for an iron anode (Bagga et al. 2008; Inan et al. 2004; Zhu et al. 2005). For an aluminum anode, the reactions are very similar—simply substitute Fe with Al, and disregard path 1 entirely, as aluminum does not have a divalent cation form.

Table 2.1: Electrochemical reactions

Chemical Equations	Notes
Cathode Reactions	
$2H_3O^+ + 2e^- = H_2 + 2H_2O$	Acidic
$2H^+ + 2e^- = H_2$	Acidic
$2H_2O + 2e^- = H_2 + 2OH^-$	Basic
$H_{ads} + H_3O^+ + e^- = H_2 + H_2O$	H_{ads} = H atom adsorbed onto cathode (Bockris et al. 2000)
Divalent Iron Reactions (Path 1)	
$4Fe\ (s) = 4Fe^{2+} + 8e^-$	Anode
$4Fe^{2+} + O_2 + 4H^+ = 4Fe^{3+} + 2H_2O$	Oxidation
$4Fe^{3+} + 12H_2O = 4Fe(OH)_3\ (s) + 12H^+$	Hydrolysis, formation of $Fe(OH)_3$ (s)
$4Fe\ (s) + O_2 + 10H_2O = 4Fe(OH)_3\ (s) + 8H^+ + 8e^-$	Overall cation reaction
$4Fe\ (s) + O_2 + 10H_2O = 4Fe(OH)_3\ (s) + 4H_2$	Overall reaction, divalent iron
Trivalent Iron Reactions (Path 2)	
$Fe\ (s) = Fe^{3+} + 3e^-$	Anode
$Fe^{3+} + 3H_2O = Fe(OH)_3\ (s) + 3H^+$	Hydrolysis, formation of $Fe(OH)_3$ (s)
$Fe\ (s) + 3H_2O = Fe(OH)_3\ (s) + 3H^+ + 3e^-$	Overall cation reaction
$2Fe\ (s) + 6H_2O = 2Fe(OH)_3\ (s) + 3H_2$	Overall reaction, trivalent iron

At the cathode, hydrogen gas is evolved. Stated in Table 2.1 are both the acidic and basic forms of this reaction, as well as the reaction at the cathode surface, as given by Bockris et al. (2000). Gas evolution at the cathode can be described in three phases: nucleation, growth, and detachment (Khosla et al. 1991). In the case of hydrogen evolution, nucleation begins when electrons at the cathode combine with protons from solution to form hydrogen atoms that are chemisorbed onto the cathode (Nørskov et al. 2005). From here, there are two possible "pathways" depending on the material of the cathode. For non-catalytic metals (such as aluminum and iron), the amount of adsorbed hydrogen on the cathode surface increases, filling up the available reaction sites. When the percentage of covered surface area is sufficiently high, collisions between hydronium ions (H_3O^+) and the surface adsorbed hydrogen become significant. Hydrogen can then desorb off of the cathode and combine with the hydronium to form hydrogen gas. This collision-desorption is likely the rate limiting step for hydrogen evolution (Bockris et al. 2000). The hydrogen bubbles grow by merging with other bubbles at the electrode, or by dissolved gas diffusion at the bubble surface. Buoyancy and/or liquid shearing forces can detach the bubbles away from the electrode (Khosla et al. 1991).

Iron cations are released at the anode in either divalent (path 1) or trivalent (path 2) form. A divalent iron cation can oxidize to its trivalent form, before reacting with water to form solid ferric hydroxide, the key compound for sweep flocculation. A trivalent cation can skip this oxidation step and directly react with water. Because reactions with water are quite complicated and highly pH dependent, note that these equations are simplifications, and that a variety of metallic hydroxides can actually be formed.

Overall, because hydrogen ions are produced at the anode and consumed at the cathode, the alkalinity of the bulk solution theoretically should not be consumed (Zhu et al. 2005). This is a distinct advantage of EC, one that suggests that EC systems may not require the same degree of pH adjustment as CC systems.

Secondary reactions can also occur at the anode if its potential is sufficiently high. Organic matter, water molecules, and chloride ions can all be directly oxidized at or near the anode (Adhoum and Monser, 2004). In particular, in acidic conditions, chloride ions can be oxidized to chlorine gas in the EC cell (Bukhari, 2008; Zaied and Bellakhal, 2009).

2.2.2 Faraday's Law and Methods of Describing Efficiency

The theoretical mass of metal cation generated through EC can be calculated using Faraday's law (Equation 2.1):

$$m = \frac{ItM}{ZF} \tag{2.1}$$

where

m = mass of metal cation generated, in grams

I = current, in amperes

t = elapsed time, in seconds

M = molecular weight of the metal, in g/mol

Z = number of electrons transferred per metal atom

F = Faraday's constant, 96 485 C/mol

For aluminum anodes, Z is equal to 3. For iron anodes, Z can be equal to 2 or 3, depending on the iron species generated. Tanneru and Chellam (2012) reported that the iron concentrations generated in their EC system best matched the quantities predicted by Faraday's law when Z was 2. In contrast, Zhu et al. (2005) found that their experimental iron concentrations fit the theoretical values well when Z was 3.

A theoretical value obtained using Faraday's law can be compared against an actual quantity of metal generated in order to determine current efficiency (η), reported as a percentage (Equation 2.2) (Zodi et al. 2013):

$$\eta = \frac{Mass\ of\ metal\ generated}{Mass\ of\ metal\ expected\ theoretically} \times 100 \tag{2.2}$$

Another parameter used for comparing energy usage is the specific electrical energy consumption (SEEC), defined in Equation 2.3, and reported in units of kWh/kg (Zodi et al. 2013):

$$SEEC = \frac{Power}{Mass\ of\ Metal\ Generated} \tag{2.3}$$

2.3 Electrodes

Table 2.2 summarizes the specifications for the electrodes used in a variety of papers.

Table 2.2: Electrode specifications used in various EC studies

Reference	Number	Materials	Geometry	Surface area	Configuration	Spacing
Bagga et al. 2008	2	1018 Steel (a), 316SS (c)	Cylindrical rod (a), porous cylindrical sheathe (c)	38 cm^2 anode area	Monopolar	n. r.
Bukhari, 2008	2	SS	n. r.	44 cm^2/electrode	Monopolar	3 cm
Carmona et al. 2006	2	2017-Al	Rectangular	50 cm^2/electrode	Monopolar	2 cm
Chavalparit and Ongwandee, 2009	2	Al (a), Graphite (c)	Flat rectangular	52.5 cm^2/electrode *	Monopolar	1.5 cm
Chen et al. 2000	1 (a), 3 (b), 1 (c)	Al or Fe	Rectangular	56 cm^2/electrode	Bipolar	6 mm
Den and Wang, 2008	3 (a), 2 (c)	Al (a), SS (c)	Flat rectangular	288 cm^2/electrode *	Monopolar	4 cm
Den and Wang, 2008	1 (a), 3 (b), 1 (c)	Al (a, b), SS (c)	Flat rectangular	288 cm^2/electrode *	Bipolar	4 cm

Reference	Number	Materials	Geometry	Surface area	Configuration	Spacing
Dubrawski and Mohseni, 2013	Up to 6 (a), 6 (c)	1018 Steel (a), 304SS (c)	n. r.	18.65 cm^2/electrode	Monopolar	2 mm
El-Naas et al. 2009	2	Al, SS, or Fe	Flat rectangular	48 cm^2/electrode	Monopolar	1 – 4 cm
Gomes et al. 2009	n. r.	Al or Fe	Rectangular	220 cm^2/electrode *	Bipolar	n. r.
Inan et al. 2004	8 (a), 8 (c)	Al or Fe	Rectangular	35 cm^2/electrode	Monopolar	3 mm
Malakootian et al. 2010	3 (a), 3 (c)	Fe	Cylindrical rods	n. r.	Monopolar	2 cm
Un et al.2009	3 (a), 3 (c)	Al	Rectangular	36.8 cm^2/electrode *	Monopolar	8 mm
Wan et al. 2011	2	Fe	Cylindrical rods	57 cm^2/electrode	Monopolar	2 cm
Wang et al. 2009	3 (a), 3 (c)	Al	Rectangular	24 cm^2/electrode *	Monopolar	10 mm
Wei et al. 2012	2	Fe (a), Steel (c)	Rectangular (a), steel wool sheathe (c)	28 cm^2 anode area, 591 cm^2 cathode area	Monopolar	1 mm
Zaied and Bellakhal, 2009	3 (a), 3 (c)	Al or Fe	Flat	50 cm^2/?	Monopolar	5 mm

Reference	Number	Materials	Geometry	Surface area	Configuration	Spacing
Zhu et al. 2005	3 (a), 3 (c)	Fe (a), SS (c)	Cylindrical rods (a), porous cylindrical sheathes (c)	100 cm^2 combined anode area	Monopolar	1.85 mm *
Zodi et al. 2013	1 (a), 4 (b), 1 (c)	Al	Rectangular	240 cm^2/electrode *	Bipolar	10 mm

*Denotes values calculated based on details given in paper.

Note: n. r., not reported; (a), anode; (b), bipolar; (c), cathode.

2.3.1 Anode Material

Many metals can be used for anodes, but certain metals are better suited to certain applications. For example, Vasudevan et al. (2009) found that an anode made of a magnesium-aluminum-zinc alloy was better at removing fluoride from drinking water than one made of mild steel or pure magnesium. However, the metals most commonly used are aluminum and iron (or steel), likely because there is a well established body of research regarding aluminum and iron-based chemical coagulants.

Literature that compare iron and aluminum electrodes have varied results, depending on the specific properties of the water being treated. Zaied and Bellakhal (2009) found that both metals were similarly effective at removing COD and polyphenol from paper industry black liquor. However, treatment with iron electrodes resulted in an effluent that appeared greenish at first, then became yellow and turbid. As color is commonly associated with iron corrosion products (Moreno et al. 2009), this is likely due to an overdose of iron cation. Chen et al. (2000) reported similar results for the treatment of restaurant wastewater. In contrast, El-Naas et al. (2009) found that aluminum electrodes were more than 2.5 times more effective at removing sulphate from petroleum refinery wastewater than either iron or stainless steel (SS) electrodes. They attributed this difference to the reaction of sulphate ions with aluminum hydroxide to form a precipitate. As aluminum sulphate forms faster and has a lower solubility than ferrous sulphate, aluminum electrodes have a clear advantage over iron electrodes for the removal of sulphates.

When using iron anodes, both ferrous and ferric iron can be generated. Using surface water, Bagga et al. (2008) found that their experimental iron concentrations were accurately modeled by Faraday's law when a two-electron transfer ($Z = 2$) was assumed. In other words, ferrous iron was generated at the anode rather than ferric. This is disadvantageous as ferrous iron is highly soluble and thus incapable of colloid destabilization by sweep flocculation. However, under proper solution conditions, ferrous iron will oxidize to ferric iron (Bagga et al. 2008).

Ferrous iron oxidation is dependent on factors such as the pH, the distribution of oxygen, and the anions that are present in solution. Under acidic conditions, hydroxide, phosphate, sulphate, and chloride will all slow the oxidation of ferrous iron (Stumm and Lee, 1961). Ferrous iron will also form complexes with natural organic matter (NOM), preventing oxidation (Bagga et al. 2008). Furthermore, below about pH 4, ferrous iron is the dominate iron species as the oxidation rate is very slow. Between pH 4 and 8, the oxidation rate is strongly pH dependent, and above pH 8, ferric iron tends to dominate (Morgan and Lahav, 2007). Likewise, Bagga et al. (2009) found that substantial amounts of ferrous iron were only present at low pH conditions and low dosages; the presence of soluble ferrous iron resulted in smaller flocs. At higher coagulant doses, it was suggested that pH increases during the operation of the EC cell created conditions that favored ferric iron formation.

2.3.2 Cathode Design

From corrosion engineering, the rule of thumb is to avoid a large cathode to anode surface area ratio in order to reduce the risk of severe galvanic corrosion (Ahmad, 2006). As such, with EC, where the intent is to promote anode corrosion using a minimum amount of energy, the reverse of this rule is applicable. Wei et al. (2012) used in their experiments a steel wool cathode, which had a tremendous amount of surface area. They found that dye removals were much quicker with the steel wool cathode than with either iron or SS plate cathodes which were of the same size as the anodes. They also found that using the steel wool cathode caused the solution pH to increase more rapidly, which may in turn have resulted in greater ferric iron concentrations (see Section 2.3.1). Note, however, that because the total amount of current applied was the same, in all cases the total iron generated was the same. Nevertheless the power draw was lower, due to lower resistance resulting from a bigger cathode surface area and smaller electrode spacing.

With regards to electrode geometry, electrodes should be designed such that the current paths from all points on the cathode to the anode are equivalent in distance. Current densities will not be perfectly uniform across an anode, but will be highest where the anode is closest to the cathode. In general, non-uniform current densities in electrochemical systems can result in ineffective use of the electrode area (Bard and Faulkner, 2001).

Cathode material will also affect the rate of metal cation generation. While cations are shed at the anode, hydrogen gas is formed at the cathode. It is this latter half-reaction that is likely the rate limiting factor of the overall reaction. Different metals have

different exchange current densities; this parameter is a measure of the inherent rate of an electrochemical reaction at an electrode at equilibrium, where a higher exchange current density means a faster rate of reaction, and vice versa (Ahmad, 2006). For example, the exchange current density for the hydrogen evolution reaction on a cathode surface is roughly four orders of magnitude greater on iron than on aluminum (Roberge, 2008). Therefore, using an iron-based cathode is expected to result in a higher rate of anode corrosion than if using an aluminum cathode.

For aluminum cathodes several studies (Carmona et al. 2006; Chen et al. 2000) noted that the amount of aluminum released into solution was higher than the amount predicted by Faraday's law. Picard et al. (2000) argued that this disparity is most likely caused by chemical dissolution of the cathode. According to the half reactions that describe an electrochemical cell, a cathode should not be dissolving. However, during the reduction of water to form hydrogen gas, hydroxyl ions are generated and attack the cathode. Picard et al. (2000) supported this premise by measuring the amount of hydrogen gas created at the cathode and comparing it to the theoretical amount predicted by Faraday's law. They determined that, as the yield of hydrogen gas was greater than 100%, there must be a chemical reaction underway as well as an electrochemical one.

2.3.3 Electrode Configurations

Electrodes can be arranged in monopolar or bipolar configurations. A monopolar configuration consists of anode-cathode pairs that are strung in parallel with each other; for example, if there are four electrodes in total, two would be anodes, two would be

cathodes, and each electrode would be directly connected one of the terminals of the power source. However, in the case of a bipolar configuration, one electrode would be an anode, two would be bipolar (becoming both negatively and positively charged), and one would be a cathode. Only the cathode would be connected to the positive terminal of a power source, and only the anode would be connected to the negative terminal, creating one series circuit (Den and Wang, 2008; Gomes et al. 2009). Bipolar configurations tend to be more energy intensive than monopolar ones, as there is greater resistance in a series circuit (Den and Wang, 2008). It logically follows that bipolar configurations would function more efficiently in high conductivity wastewaters, and that monopolar configurations would be better suited to low conductivity water systems.

There is very little in the literature regarding the effects of electrode configuration. However, Den and Wang (2008) concluded that when using aluminum electrodes, a bipolar system was more effective than a monopolar system for removing dissolved silica from brackish water. In addition, Timmes et al. (2010) treated seawater using a pilot scale EC reactor in bipolar mode for 222 hours, much longer than any of the bench scale experiments discussed; they found that the electrodes that were directly powered had the thickest corrosion scale.

2.4 Electrolyte

2.4.1 Solution Composition

The composition of the electrolyte can have a direct affect on the state of the electrodes. Table 2.3 gives examples of solutions that have been treated via EC.

The study of corrosion inhibitors is extensive and beyond the scope of this literature review. There are many substances (most of which are organic compounds) that can be added to solution in order to hinder corrosion. The ability of an organic molecule to be a corrosion inhibitor is dependent upon the strength with which it binds to a surface, its concentration in solution, and its solubility (the less soluble, the greater the tendency to adsorb). Some commonly applied corrosion inhibitors for iron alloys are benzene derivatives, pyrroles, and sulphur containing compounds (Bockris and Reddy, 2000).

There are also those substances that can encourage corrosion by breaking down protective passive layers. Passivation is a process wherein a metal oxide layer forms on an electrode surface, creating a barrier between the metal and the solution (Ahmad, 2006). Passive layers are amorphous in structure, preventing the easy diffusion of metal cations through said layer and into solution. The breakdown of a passive layer begins with the adsorption of an anion such as chloride. The anion diffuses through the layer, meeting and displacing the hydroxide species that are present. When dealing with an iron-based system, chloride-iron complexes will form and exit the layer. Other ions that can cause depassivation include iodide and bromide (Bockris and Reddy, 2000).

Table 2.3: Electrolytes used in various EC studies

Reference	Treated water	Conductivity	Initial pH
Bagga et al. 2008	Surface water for potable use	n. r.	7.3 – 7.5
Bukhari, 2008	Municipal wastewater	4 mS/cm	6.9 – 7.1
Carmona et al. 2006	Emulsions of soluble oils and kerosene in water	3.8 – 4.9 mS/cm	8.6, 9
Chavalparit and Ongwandee, 2009	Biodiesel wastewater	0.350 mS/cm	4 – 9
Chen et al. 2000	Restaurant wastewater	0.443 – 2.850 mS/cm	3 – 10
Den and Wang, 2008	Synthetic brackish water with silica	5.0 mS/cm	7.0
Dubrawski and Mohseni, 2013	Synthetic solution of NOM in potable water	0.300 mS/cm	7.0 ± 0.05
El-Naas et al. 2009	Petroleum refinery wastewater	9.76 mS/cm, 16.36 mS/cm	6 – 9

Reference	Treated water	Conductivity	Initial pH
Gomes et al. 2009	Produced water	80 – 298 mS/cm	6.0 – 9.1
Inan et al. 2004	Olive oil mill wastewater	11.5 mS/cm	4 – 9
Malakootian et al. 2010	Hardness in drinking water	1.612 mS/cm	3 – 10
Un et al.2009	Vegetable oil refinery wastewater	1.62 mS/cm	1.4 – 9
Wan et al. 2011	Synthetic solution of arsenic in potable water	n. r.	5 – 9
Wang et al. 2009	Synthetic laundry wastewater	0.334 mS/cm	2.5 – 9.5
Wei et al. 2012	Synthetic textile dye wastewater	n. r.	3.8 – 10
Zaied and Bellakhal, 2009	Paper industry black liquor	42.72 mS/cm	2 – 12
Zhu et al. 2005	Synthetic fresh water with viruses (MS2 bacteriophage)	10^{-7}, $6x10^{-3}$, $1.8x10^{-2}$ M (ionic strength)	6.3 – 8.3
Zodi et al. 2013	Synthetic textile dye wastewater	2.575 mS/cm	7.5

Note: n. r., not reported.

Wang et al. (2009) found that addition of 0.25 g/L NaCl to synthetic laundry wastewater enhanced removal efficiency. However, efficiencies decreased when more NaCl was added to solution, perhaps due to the formation of aluminum-chloride complexes that are less useful as coagulants.

2.4.2 Optimal pH Ranges

Cañizares et al. (2009) compared CC and EC and found that removals were dependent on dosage and pH, but not the technology used. Dosing aluminum coagulant into salt water (without a pollutant), Cañizares et al. (2009) compared the zeta potentials of CC and EC flocs. For both technologies, the particles became negatively charged above pH 8, and positively charged below. This suggests that the species of hydrolyzed aluminum formed are not dependent on the type of technology used. Furthermore, Cañizares et al. (2009) conducted experiments comparing EC and CC where the final pH conditions after treatment were approximately equal. Testing two different wastewaters, they found that the final concentrations and removal trends for chemical oxygen demand (COD) were very similar. This implies that the established jar testing procedures for CC, used to pick parameters such as dose and pH, may be applied to EC as well.

There is a well established body of literature regarding the effective use of chemical coagulants. Based on solubility diagrams at 25 °C, the effective pH range for sweep flocculation using aluminum-based coagulants is around 5.5 to 7.7; for iron-based coagulants, the effective pH range is around 5 to 8.5. Promoted within these pH ranges is the precipitation of solid, amorphous aluminum or ferric hydroxide, respectively. Note

that iron tends to be more insoluble than aluminum; it is also able to work effectively over a broader pH range (MWH et al. 2005). Furthermore, aluminum tends to be more soluble (and thus less effective) than iron in seawater due to its ionic strength. Based on the solubility curves for amorphous aluminum hydroxide in seawater, the minimum solubility at 10 °C occurs at pH 6.8, and results in about 27 μg/L of residual soluble aluminum. At 35 °C, the minimum solubility occurs at pH 6, and results in about 270 μg/L of residual soluble aluminum. In comparison, iron is quite insoluble over a broad pH range. Within the pH range of 6 to 8, for both 10 °C and 35 °C, there is less than 1 μg/L of residual soluble iron in solution (Edzwald and Haarhoff, 2011).

Unsurprisingly, most studies reported optimal removals between pH 5 and pH 7 (Bagga et al. 2008; Chavalparit and Ongwandee, 2009; Inan et al. 2004; Wan et al. 2011; Zaied and Bellakhal, 2009). These papers encompassed both drinking water and wastewater treatment, as well as iron, steel, and aluminum electrodes. Others also reported optimal removals at slightly alkaline pH levels. For example, when using iron anodes, Inan et al. (2004) found that their best COD removals were around pH 9, which is somewhat more basic than expected.

There may also be localized pH effects near the electrodes; as protons are produced at the anode and hydroxide ions at the cathode, these areas are respectively more acidic and basic than the bulk solution. Zhu et al. (2005) found that EC outperformed CC in regards to virus removal from drinking water. As negatively charged viruses migrated towards a positive anode, they interacted with locally higher concentrations of iron hydroxide complexes. Zhu et al. (2005) suggests that virus

adsorption occured primarily in this low pH region near the anode, where iron hydroxide complexes would be more positively charged than in the bulk solution.

2.4.3 pH Changes during Operation

Unlike CC, a process that consistently consumes solution alkalinity and often requires pH adjustment, EC can cause solution pH to increase (which is most common), decrease, or have no significant change at all. As of yet, there are no definite rules or conditions to define when each of these three cases should occur. Reviewing the literature, it is difficult to reach any consensus, as each study used different coagulants, doses, retention times, and treated different waters.

It has been observed that solution pH increased during the operation of the EC cell (Adhoum and Monser, 2004; Malakootian et al. 2012; Un et al. 2009; Wei et al. 2012). Adhoum and Monser (2004) observed that solutions with initial pH levels below 9 underwent pH increases, while those that started at pH 9 or above remained relatively consistent. Un et al. (2009) noted that pH increased gradually during operation, until the solution reached about pH 9. Malakootian et al. (2010) found that solution pH increased until it reached over pH 10; in one case, this was a drastic increase from pH 3 to 10.37. Harif et al. (2012) also noticed pH increases during operation. Consider the basic form of the hydrogen evolution reaction given in Table 2.1. Harif et al. (2012) suggests that, while aluminum hydroxide precipitation will consume some hydroxide ion, it cannot consume all of the hydroxide ion produced. The aluminum cation can hydrolyze into a variety of metal hydroxide species, some of which are likely to be soluble. When the

hydroxide ion production rate exceeds the aluminum hydroxide precipitation rate, this causes an excess amount of hydroxide ion to build up in solution, driving up the pH (Harif et al. 2012). Another explanation for the pH increases is that carbon dioxide is released from the wastewater as a result of disturbances caused by hydrogen bubble generation. A third explanation is that certain anions (such as chloride, sulphate, etc.) can exchange with hydroxide ions in solid metal hydroxides, thus releasing hydroxide ion into solution (Chen et al. 2000).

Decreases in pH were also noted by a number of researchers (Chen et al. 2000; Wang et al. 2009; Zaied and Bellakhal, 2009). In these cases, it was observed that EC had a somewhat neutralizing effect. For example, Chen et al. (2000) observed that solutions that started with a pH below 9 became more basic, while those that started above 9 became more acidic. For Wang et al. (2009) and Zaied and Bellakhal (2009), this pivot point was around pH 8 and pH 7, respectively. It is noteworthy that each study treated solutions with very different compositions—namely, restaurant wastewater, synthetic laundry wastewater, and black liquor from the paper industry, respectively.

Others, with starting pH conditions between 7 and 9, have observed that the solution pH did not undergo any significant change (Carmona et al. 2006; Den and Wang, 2008).

2.4.4 Conductivity

A number of studies have noted that increased solution conductivity reduced energy consumption by reducing the resistance between the electrodes (Chen et al. 2000;

Un et al. 2009). However, Zhu et al. (2005) found that ionic strength did not significantly influence virus removal from drinking water. They investigated the ionic strengths from 10^{-7} M to $1.8x10^{-2}$ M, using pure deionized water at the low end, and 3.0 mM $NaHCO_3$ and 10 mM $CaCl_2$ at the high end. Similarly, Chen et al. (2000), who worked with restaurant wastewaters, found that conductivity had little effect on treatment effectiveness between approximately 0.5 and 3 mS/cm. In contrast, Gao et al. (2010) found that the addition of chloride ions (at 1.0, 3.0, 5.0, and 8.3 mM) promoted algae removal in their EC-flotation system. They attributed this to the production of chlorine (which acted as an oxidant), and enhanced aluminum corrosion at the anode.

Gomes et al. (2009) and Den and Wang (2008) both reported that the solution conductivity was not significantly altered during EC. The latter, who worked with synthetic brackish water, suggested that this was because the solution matrix did not react with the aluminum flocs they generated. However, Gomes et al. (2009), who worked with produced water, reported that analysis using scanning electron microscopy-energy dispersive x-ray spectroscopy indicated that a significant amount of sodium and chloride was captured in flocs. It is possible therefore that solution conductivity remained constant simply because the conductivity of produced water is extremely high.

2.5 Power Source

All the EC systems discussed in this Chapter used DC power. However, in order to counter electrode passivation, Bukhari (2008) used an electrical switch to periodically change the polarity of the electrodes, switching the anodes and the cathodes. Similarly,

Timmes et al. (2010), who used a pilot scale system for seawater treatment, would alter electrode polarization in variable intervals between 30 and 250 seconds in order to reduce scale formation and maintain consistent iron dosing. They found that lengthening these time intervals resulted in more consistent iron dosing, possibly due to scouring from the hydrogen bubbles generated.

A DC power source can be operated in constant voltage or constant current modes. The more common approach is the former, wherein the voltage is set to a given value and the current is allowed to fluctuate depending on the resistance of the EC cell (Malakootian et al. 2010; Wan et al. 2011; Wang et al. 2009). In constant current (galvanostatic) mode, the current is set and the voltage is allowed to fluctuate (Harif et al. 2012; Zaied and Bellakhal, 2009). Constant current operation naturally has a distinct advantage over constant voltage operation, as the cation dosing can be directly controlled according to the relationship defined by Faraday's law.

2.6 Operational Parameters

Table 2.4 summarizes some of the operational parameters that have been used in EC studies.

Table 2.4: Operational parameters used in various EC studies

Reference	Process type	Volume	Retention time or flow rate	Mixing	Clarification	Current density
Bagga et al. 2008	Batch	940 mL	n. r.	Stir bar	Microfiltration	21 mA/cm^2 *
Bukhari, 2008	Batch	1.2 L	5 – 50 min	Stir bar and paddle mixers	Sedimentation	1.1 – 18.2 mA/cm^2 *
Carmona et al. 2006	Batch	1.5 L	Up to 125 min	Hydraulic and stir bar	Sedimentation	10 – 30 mA/cm^2
Chavalparit and Ongwandee, 2009	Batch	1 L	10 – 40 min	Stir bar	n. r.	6.7 – 20.8 mA/cm^2
Chen et al. 2000	Continuous	1.5 L	6.5 – 60 min	Hydraulic	Natural flotation and Sedimentation	1.250 – 10.89 mA/cm^2

Reference	Process type	Volume	Retention time or flow rate	Mixing	Clarification	Current density
Den and Wang, 2008	Continuous	6.3 L *	20 – 60 min (75 – 225 mL/min)	Hydraulic	Sedimentation and Nanofiltration	0.29 – 1.16 mA/cm^2 (monopolar), 0.87 – 3.47 mA/cm^2 (bipolar)
Dubrawski and Mohseni, 2013	Batch	60 mL	0.5 – 2 min	n. r.	Filtration or Sedimentation	2.43 – 26.8 mA/cm^2
El-Naas et al. 2009	Batch	200 mL	Up to 120 min	Stir bar	Filtration	2 – 13 mA/cm^2
Gomes et al. 2009	Continuous	450 mL	525 mL/min (51 s *)	Hydraulic	n. r.	5 – 26 mA/cm^2
Inan et al. 2004	Batch	500 mL	2 – 30 min	Stir bar	Filtration	10 – 40 mA/cm^2
Malakootian et al. 2010	Batch	1.3 L	10 – 60 min	Stir bar	Filtration	n. r.
Un et al.2009	Batch	300 mL	15 – 120 min	Stir bar	Centrifugation	25 – 35 mA/cm^2

Reference	Process type	Volume	Retention time or flow rate	Mixing	Clarification	Current density
Wan et al. 2011	Batch	1 L	Up to 120 min	Stir bar	Filtration	0.39 mA/cm^2 *
Wang et al. 2009	Batch	1 L	Up to 40 min	Paddle mixer	n. r.	n. r.
Wei et al. 2012	Batch	500 mL	Up to 12 min	Stir bar	Centrifugation	5.4 – 21 mA/cm^2 *
Zaied and Bellakhal, 2009	Batch	300 mL	Up to 100 min	Stir bar	Filtration	1.7 – 16.7 mA/cm^2
Zhu et al. 2005	Batch or continuous	200 mL	40 s or 300 mL/min	Hydraulic	Microfiltration	0.25 mA/cm^2
Zodi et al. 2013	Continuous	18 L	167 – 467mL/min	Hydraulic	Sedimentation and Natural flotation	10 – 20 mA/cm^2

*Denotes values calculated based on details given in paper.

Note: n. r., not reported.

2.6.1 Current Density and Charge Loading

Current density is the applied current divided by the submersed surface area of the anode, commonly expressed in units of mA/cm^2. It is a key operational parameter, and used by most papers to express their electrical usage. However, a number of researchers have proposed that charge loading is a more appropriate parameter (Chen et al. 2000; Baudequin et al. 2011; Dubrawski and Mohseni, 2013; Zaied and Bellakhal, 2009). Charge loading is the amount of electrical charge (in either Faraday or coulombs) applied per unit volume of treated water (Chen et al. 2000; Den and Wang, 2008); common units include F/m^3 or C/L. Whereas current density is a measure of the *rate* of cation generation per unit anode surface area, charge loading is essentially a measure of the amount of cation per volume. As such, reporting a charge loading is directly comparable to reporting a chemical coagulant dose in mg/L. In continuous systems, charge loading would be advantageous as, unlike current density, it would be able to reflect changes in feed rate. Charge loading would also be an effective way to compare cation dosages between EC systems, particularly between monopolar and bipolar systems, as there is no clear procedure for accounting for the surface area of a bipolar electrode. Current density, however, normalizes current over anode surface area, making it easier to compare EC systems of different sizes.

As current is directly related to cation (coagulant) generation via Faraday's law, higher current densities or charge loadings generally correspond to greater pollutant removals (Wei et al. 2012; Zaied and Bellakhal, 2009). However, a number of studies observed diminishing returns once some optimum current value (of either parameter) was

exceeded, indicating coagulant overdosing (Adhoum and Monser, 2004; Carmona et al. 2006; Chavalparit and Ongwandee, 2009; El-Naas et al. 2009). Sludge volume is also naturally dependent on current, as more coagulant often results in more sludge (Zodi et al. 2013).

2.6.2 Retention Time

Longer retention times tend to equate with higher removals since more coagulant is generated. However, in most cases, authors noted that after some optimum retention time, removal rates tended to diminish and plateau. For most of the papers discussed, this occurred within 60 minutes (Bukhari, 2008; Chavalparit and Ongwandee, 2009; Den and Wang, 2008; El-Naas et al. 2009; Inan et al. 2004).

2.6.3 Floc Characterization

Using a suspension of kaolin and sodium bicarbonate in distilled water, Harif et al. (2012) compared the flocs produced from CC and EC. They found that EC flocs were more fragile, but had a faster growth rate and could be formed over a wider pH range. They suggested that the relevant flocculation mechanism for sweep flocs generated from EC was Diffusion Limited Cluster Aggregation, where the repulsive barrier between particles is low (as determined from zeta potential measurements), resulting in relatively easy ‘sticking’ upon contact. This creates flocs with loose structures that are prone to fragmenting and restructuring. This also means that growth rates and final floc sizes

increase with increases in cation dosing, as a high concentration of coagulation precursors means higher collision frequency. In contrast, the flocculation mechanism for CC is likely Reaction Limited Cluster Aggregation. In this case, there are strong repulsive barriers between particles, so collisions are required to form stable flocs. The resulting flocs tend to be stronger and have more compact structures.

Using scanning electron microscopy, Gomes et al. (2009) found that the iron based flocs formed from EC during the treatment of produced water were amorphous and nanocrystalline in nature. The flocs also contained significant amounts of sodium and chloride, as well as traces of other metals.

2.6.4 Natural Flotation

It has been suggested that the gas bubbles produced can be used for natural flotation. Chen et al. (2000), who treated restaurant wastewater, estimated that two-thirds of the sludge produced in their EC system floated; the remainder was removed via sedimentation. Gamage and Chellam (2014), who pretreated lake water before microfiltration, found that natural flotation prevented a significant fraction of foulants from reaching the membrane surface. In contrast, Bagga et al. (2008), who treated surface water, did not observe floc flotation in their system.

In regards to operation, Khosla et al. (1991) concluded that during the electrolysis of water, an increase in current density resulted in smaller bubbles (they tested between 0.05 and 0.2 mA/cm^2). Furthermore, bubble detachment can be encouraged by current interruptions (Khosla et al. 1991), which may be relevant for EC systems that regularly

switch electrode polarity during operation (such as with Timmes et al. 2010). The amount of gas that can be produced is, as with cation production, dependent on the applied current. A cation dose is tied to a given amount of hydrogen gas, and the two cannot be uncoupled. While hydrogen production can be increased with cathodic dissolution (see Section 2.3.2), this also increases the amount of metal cation released into solution (Picard et al. 2000).

2.6.5 Variations in Design and Operation

Listed in this section are some variations on the basic EC system. Un et al. (2009) added poly aluminum chloride to their solution as a coagulant aid. Wan et al. (2011) air sparged their solution at 60 mL/min to provide oxygen for the formation of ferric iron precipitates. Zhu et al. (2005) designed a system that could be operated in both batch and continuous modes; when the system was operated continuously, iron dosing was controlled by adjusting the flow rate and the electrical current. Carmona et al. (2006) designed a system where cation dosing (in other words, the electrodes) and solution mixing occurred in separate chambers; water was circulated between the two chambers in a continuous loop. Wang et al. (2009), who treated a synthetic laundry wastewater, operated their EC cell inside an ultrasonic cleaning bath, with the hope that it could help regenerate electrode surfaces, enhance electrode dissolution, and prevent gas coverage of the cathode. Removals with the ultrasound were higher than without, although it was noted that it could cause pollutants to desorb from the coagulants.

2.7 Conclusions

This Chapter reviewed the current EC literature to evaluate current operating and design criteria. Much of the current literature discusses bench scale systems treating a specific water or wastewater using a custom EC system. The main design issues reviewed were the electrodes, electrolyte make-up and power source. Concerning electrode design, it was found that there is very little in the literature regarding the effects of electrode configuration, which would be a significant issue for scale-up from laboratory to full-scale operation. Operational characteristics were also reviewed in this Chapter and it was observed that the operational procedures were largely dependent upon the characteristics of the wastewater under treatment. Thus a standard operational procedure, independent of wastewater characteristics, would assist in technology comparison and treatability studies.

CHAPTER 3: MATERIALS AND METHODS

This Chapter provides describes the bench-scale electrocoagulation (EC) system and analytical methods used in this thesis. Experiment specific details are provided with each relevant chapter.

3.1 Bench-Scale EC System

Figure 3.1 gives a diagram of the bench-scale EC system used in this thesis. The system was operated in batch mode using either a 220 mL or an 1170 mL working volume. A magnetic stir bar was used to keep the solution well mixed during operation.

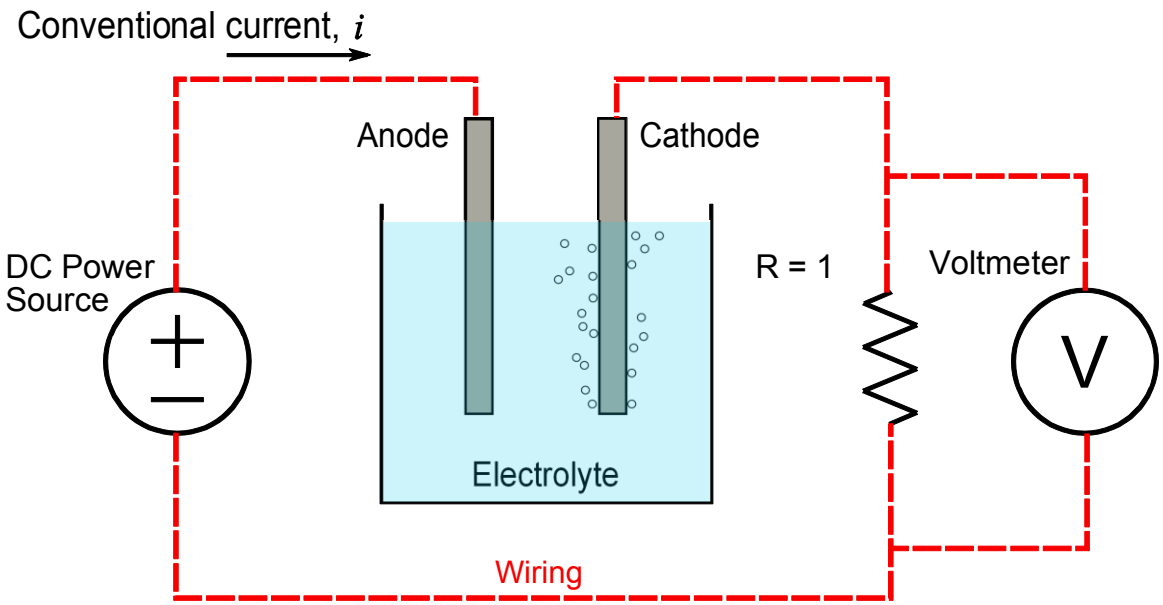

Figure 3.1: Schematic diagram of bench-scale electrocoagulation system

Current was supplied from a GPS 3030DD DC power source (GW Instek, New Taipei City, Taiwan). Its maximum voltage and current were 30 V and 3 A, respectively. As indicated in Figure 3.1, a high accuracy 1 Ω resistor (1% tolerance) was connected in series with the EC cell. A Volt101A data-logging voltmeter (MadgeTech, Warner, NH, USA) was placed in parallel with the resistor. The voltmeter was used to measure the current of the system—since there was only one path for the current to travel, the current passing through the resistor was equivalent to the system's total current. By Ohm's law, the current passing through the resistor could be determined by dividing the readings of the voltmeter by the value of the resistor (1 Ω). Thus, the total system current was equal to the voltage across the resistor.

Similarly, the voltage across the EC cell (V_{Cell}) is determined by Kirchhoff's voltage law to be equal to the voltage supplied by the power source (V_{Sys}) minus the voltage across the resistor (minus I_{Sys}, in other words). Therefore, the resistance of the EC cell (R_{Cell}) can be given by Equation 3.1 below:

$$R_{Cell} = \frac{V_{Sys} - I_{Sys}}{I_{Sys}} \tag{3.1}$$

where R_{Cell} is the resistance of the EC cell, V_{Sys} is the applied voltage or the voltage of the system, V_{Cell} is the voltage across the EC cell (calculated by $V_{Sys} - I_{Sys}$), and I_{Sys} is the steady-state current of the system, represented by the median value of the logged current.

As seen in Figure 3.2, a single anode-cathode pair was used for the electrodes. The anode was a pure iron cylindrical wire with a diameter of 2 mm and a submerged height of 5.1 cm, resulting in a submerged surface area of 3.20 cm^2. Depending on the

experiment, the cathodes were either stainless steel (SS) or aluminum. The cathodes were identically shaped half-cylinders with a wall thickness of 0.25 cm, an outer diameter of 2.1 cm, and a submerged height of 5.1 cm, resulting in a submerged surface area of 32.2 cm^2. The surface area ratio of the cathode to the anode was thus 10.0. The gap between the anode and the inner surface of the cathode was 0.7 cm. The electrodes were physically clamped into place using non-conductive plastic plates, allowing for easy assembly and disassembly. Between experimental runs, the electrodes were scrubbed with steel wool and rinsed with reverse osmosis (RO) water.

Figure 3.2: Anode and cathode

3.2 Analytical Methods

3.2.1 General Water Quality Parameters

Conductivity and pH were measured using an Accumet Excel XL50 meter with the respective probes (Fisher Scientific, Waltham, MA, USA). Zeta potential was measured using a Malvern Zetasizer Nano-ZS (Malvern Instruments, Worcestershire, UK); for each sample, zeta potential was measured in triplicate. Iron samples were prepared following Standard Methods 3010 and 3125 and analyzed using a Thermo Scientific XSeries2 ICP-MS (Thermo Fisher Scientific, Waltham, MA, USA).

3.2.2 Transmission Electron Microscopy

Images of flocs were taken using a Tecnai12 transmission electron microscope (FEI, Hillsboro, Oregon, USA) with an ORIUS SC1000 CCD camera (Gatan, Warrendale, PA, USA). As samples subject to TEM must necessarily be very small, the flocs were sonicated in solution in order to uniformly reduce their size. Using pipets, 10 μL samples were then dropped onto 200 mesh copper grids with carbon support films (Electron Microscopy Sciences, Hatfield, PA, USA). The grids were dried at room temperature before image analysis.

While dehydration damages flocs, Cornelisson et al. (1997) could not find the same damage on floc images produced by transmission electron microscopy (TEM) that they could on the ones produced by light microscopy or scanning electron microscopy

(SEM). They attributed this to the necessarily small size of the particles subject to TEM analysis.

3.2.3 Particle Size

Particle size, reported as the diameter of a volume equivalent sphere, was measured using the Malvern Mastersizer 3000 (Malvern Instruments, Worcestershire, UK). The Mastersizer 3000 operates using small angle light scattering. In short, particles in the solution scatter light proportionally to their size, where smaller particles scatter light at higher angles, and larger particles scatter light at lower angles.

During tests, solution was slowly looped between the test jar and the Mastersizer's measurement chamber using a peristaltic pump. The pump was placed after the measurement chamber in order to minimize floc damage. The instrument was typically set to take measurements once per minute.

3.2.4 Scattering Exponent

Because of their complex and irregular structures, flocs are commonly described using fractal geometry. Flocs are mass fractal objects that exhibit repeating, self-similar patterns regardless of the scale of observation; in other words, images of a floc at different magnifications should all look similar. Due to this property, they can be described by the relationship:

$$M \propto R^{d_f} \tag{3.2}$$

where M is the mass, R is the size (typically the diameter), and d_f is the mass fractal dimension. For three dimensional objects, d_f can have a value between 1 and 3. A Low d_f value indicates that an aggregate is open and highly branched, whereas a high value suggests that it is tightly packed (Gregory, 1997; Jarvis et al. 2005b; Li and Ganczarczyk, 1989; Li et al. 2006).

Along with particle size, the Mastersizer 3000 reports both scattered light intensity, *I,* and scattering wave vector, *Q,* which are related by Equation 3.3:

$$I \propto Q^{-d_f} \tag{3.3}$$

When *log(I)* is plotted against *log(Q),* the fractal dimension, d_f, is the slope of the linear region. The boundaries of the linear region were visually established for each plot. If no linear region exists, then the aggregates do not have fractal tendencies. Equation 3.3 is only applicable when Q is simultaneously much larger than the primary particles and much smaller than the aggregated particles (Biggs et al. 2000; Gregory, 1997; Jarvis et al. 2005b; Li et al. 2006; Waite, 1999; Wilén et al. 2003). This limited the determination of d_f to flocs no greater than 100 nm, as calculated from Q following the process described by Jarvis et al. (2005b). Because of the variability in floc aggregate structure and the limitations of the analytical method, it could not be confirmed that the calculated d_f represented the "true" fractal dimension; as such, this thesis uses the term "scattering exponent" as an approximation.

CHAPTER 4: THE RATE AND EFFICIENCY OF IRON GENERATION IN AN ELECTROCOAGULATION SYSTEM[2]

4.1 Abstract

The rate and efficiency of iron generation in a bench-scale electrocoagulation (EC) system was investigated when variations were made to operating voltage, cathode material, and electrolyte composition. Two electrolytes were tested, one with organic compounds (naphthalene, acenaphthene, and 4-nonylphenol), and one without. While aromatic structures often make good corrosion inhibitors, in this case they had no discernible effect. This is a positive indicator that EC systems will not have adverse effects when treating wastewaters associated with oil and gas production. Using a stainless steel (SS) cathode rather than an aluminum one resulted in 35% more production of iron at the anode per volt per minute; it also resulted in greater iron production given equivalent quantities of power. This likely occurred because the rate limiting hydrogen evolution reaction (HER) at the cathode occurs more quickly on iron

[2] This is a preprint of an article whose final and definitive form has been published in *Envionmental Technology* © 16th April 2015 Copyright Taylor & Francis; *Environmental Technology* is available online at:
http://www.tandfonline.com/doi/full/10.1080/09593330.2015.1032367
Reference: Lee, S. Y., & Gagnon, G. A. (2015). The rate and efficiency of iron generation in an electrocoagulation system. *Environmental Technology, 36*(19), 2419-2427.

than on aluminum. It was also observed that the EC system (using either cathode) produced more iron per unit power when operated at lower voltages. At lower voltages, the corrosion that occurred spontaneously in the absence of an applied current may have contributed more significantly to the total amount of iron released. This research suggests that it is more efficient to design EC systems using iron-based cathodes rather than aluminum ones. It also indicates that it is more energy efficient to use more electrodes at low power, rather than fewer electrodes at high power.

4.2 Introduction

4.2.1 Electrocoagulation

Electrocoagulation (EC) is a process for water or wastewater treatment that uses sacrificial anodes in order to produce metal cations for coagulation. It is often compared to chemical coagulation (CC), which uses chemical salts to induce coagulation. EC has successfully treated a variety of water types at the bench-scale, including (but not limited to) biodiesel wastewater, surface water for potable use, and petroleum refinery wastewater (Chavalparit and Ongwandee, 2009; Bagga et al. 2008; El-Naas et al. 2009).

In its most basic form, an EC system is an electrochemical cell operated electrolytically. At the anode, metal cations are released into the electrolyte (the water under treatment), and at the cathode, hydrogen gas is generated. For this research, iron was used for the anode, which has both divalent and trivalent cation forms. Once released, the iron cations react with water to form solid iron hydroxides, the desired

species for adsorption. The chemical equations below describe this process assuming only ferric iron generation for simplicity:

Anode: Fe^{3+} generation

$$Fe\ (s) \rightarrow Fe^{3+} + 3e^{-} \tag{4.1}$$

Anode: Reaction with H_2O to form $Fe(OH)_3$ (s)

$$Fe^{3+} + 3H_2O \rightarrow Fe(OH)_3\ (s) + 3H^{+} \tag{4.2}$$

Anode: Adding Equations (4.1) and (4.2)

$$Fe\ (s) + 3H_2O \rightarrow Fe(OH)_3\ (s) + 3H^{+} + 3e^{-} \tag{4.3}$$

Cathode: H^2 gas evolution at the cathode surface

$$2H^{+} + 2e^{-} \rightarrow H_2 \tag{4.4}$$

Overall:

$$2Fe\ (s) + 6H_2O \rightarrow 2Fe(OH)_3\ (s) + 3H_2 \tag{4.5}$$

The chemical equations for ferrous iron generation are similar, and are provided by Lee and Gagnon (2014). Note however, that these equations are simplifications; iron cation reactions with water are complex and dependent on pH as well as any other chemical species present (Duan and Gregory, 2003; Jolivet et al. 2004; Morgan and Lahav, 2007). In particular, pH affects the number of hydroxyl ions bound to a ferric cation. For

example, Fe^{3+} (no hydroxyl ions) can occur under acidic pH conditions, while $Fe(OH)_4^-$ (four hydroxyl ions) becomes dominant under more alkaline conditions. The solid, uncharged metal hydroxide, $Fe(OH)_3$, is maximized by targeting some solution dependent optimal pH (typically around 6 to 9) (Duan and Gregory, 2003).

In an electrochemical system, the theoretical amount of metal cation produced at the anode is equated to the current by Faraday's law (Equation 2.1):

$$m = \frac{ItM}{ZF} \tag{2.1}$$

where m is the mass of metal cation produced (g), I is the current (A), t is the elapsed time (s), M is the molecular mass of the metal (g mol^{-1}), Z is the number of electrons transferred per atom (2 for ferrous iron, 3 for ferric iron), and F is Faraday's constant (96 485 C mol^{-1}).

Unfortunately, there are no standard practices for either EC design or operation. Much of the current literature focuses on the treatment of specific wastewaters using custom EC systems (Holt et al. 2005). As such, EC has never become a conventional water treatment technology, despite having been available for about a hundred years. To help address this information gap, this research investigates the effect of cathode material, electrolyte composition, and operating voltage on the rate and efficiency of iron generation.

4.2.2 Cathode Material

Regarding cathodes, current literature has focused on surface area availability rather than materials. For example, Zhu et al. (2005) and Bagga et al. (2008) both designed bench-scale EC systems with cathodes in the shape of cylindrical sheathes in order to facilitate a high cathode-to-anode surface area ratio. Furthermore, Wei et al. (2012) found that the removal of dye occurred up to 4.4 times more quickly when using steel wool (which had an extremely high surface area) as their cathode rather than either iron or stainless steel (SS) plate cathodes. They also noted a significantly lower power draw. However, there was no discussion of the electrochemical effects of cathode material.

The reactions at the anode and at the cathode are two halves of a whole, and cannot exceed each other in rate. Therefore, one of these half-reactions must be the rate limiting step for the overall reaction. This Chapter hypothesizes that it is the hydrogen evolution reaction (HER) at the cathode that is rate limiting. Comparing the exchange current densities for the HER on each material, it further hypothesizes that using an iron-based cathode rather than an aluminum one will result in a higher rate of anode dissolution. When a reaction at an electrode is at equilibrium and the net current is zero, the exchange current density, i_0, is equal to both the forward and reverse currents. A larger exchange current density indicates a faster inherent reaction rate (Ahmad, 2006). On iron, the exchange current density for the HER is four orders of magnitude greater than it is on aluminium (Roberge, 2008).

4.2.3 Electrolyte Composition

While the study of both corrosion inhibitors and enablers is extensive, little has been applied experimentally to EC systems. There are a number of substances that, when present in solution, may encourage or inhibit corrosion. For example, passive oxide layers can breakdown over time in the presence of chloride ions, promoting corrosion (Bockris and Reddy, 2000). As for corrosion inhibitors, Bockris and Reddy (2000) list organic compounds including aromatics, aliphatic unsaturated compounds, and alicyclics. Unlike with CC, EC researchers need to be concerned with not just the chemistry of coagulants once in solution, but also with a solution's effect on an EC system's operation.

Regarding electrolytes, current literature tends to focus on solution conductivity. For example, Wang et al. (2009) observed that the addition of 250 mg/L of NaCl to a simulated laundry wastewater significantly increased chemical oxygen demand (COD) removal. Furthermore, Timmes et al. (2010) noted the formation of corrosion scales on their electrodes when operating a pilot-scale EC system in seawater. This Chapter explores whether operation in an electrolyte with aromatic organic compounds, which are common in wastewaters associated with oil or natural gas production (Ahmadun et al. 2009), will have an adverse effect on EC performance.

4.3 Materials and Methods

4.3.1 Bench-Scale EC System

The bench-scale EC system used in this experiment is described in Section 3.1. It used a 220 mL working volume, and tested both SS and aluminum cathodes.

4.3.2 Electrolyte

This research used two electrolyte solutions, one with the addition of organic compounds, and one without. The base solution (without organics) was made by dissolving 25 g/L of sodium chloride and 15 g/L of calcium chloride dihydrate into reverse osmosis (RO) water. With the addition of organic compounds, the solution was intended to emulate produced water from oil and gas production. To this end, 4.0 mg/L of 4-nonylphenol, 2.4 mg/L of acenaphthene, and 2.7 mg/L of naphthalene (Fisher Scientific, Waltham, MA, USA) were added to the salt solution. In order to more easily dissolve these organics into an aqueous solution, they were first combined together in acetone to form an organic stock solution. Table 4.1 gives the formula for this synthetic wastewater. As an aside, the Canadian water quality guideline for naphthalene in marine environments is 1.4 μg/L. For nonylphenols, the guideline is 0.7 μg/L. No guideline for acenaphthene in the marine environment currently exists (CCME, 2007).

Table 4.1: Synthetic wastewater formula

Component	Unit	Quantity
Salts		
NaCl	g/L	25.0
$CaCl_2 \cdot 2H_2O$	g/L	15.0
Chloride	g/L	22.4
Organics		
Organic stock solution	mL/L	0.5
4-Nonylphenol	mg/L	4.0
Acenaphthene	mg/L	2.4
Naphthalene	mg/L	2.7
Acetone	mL/L	0.5
Average initial parameters		
Conductivity	mS/cm	50.70 (2.45*)
pH	-	6.07 (0.13*)

*Standard deviation

4.3.3 Experimental Design and Procedure

A simple 2^2 factorial design was used, where the factors were cathode material (SS or aluminum) and electrolyte (with or without the addition of organics). The four resulting EC cell configurations are given in Table 4.2. For each configuration, a

calibration curve was created that related the mass of iron produced to the applied voltage.

Table 4.2: Electrocoagulation cell configurations and calibration values for experiment investigating iron generation rate and efficiency.

Config. No.	Electrolyte	Cathode	Calibration Curves*		R^2
1	Salts	SS	Rep1:	F = 3.15V - 1.96	0.936
			Rep2:	F = 3.51V - 2.57	0.949
			Overall:	F = 3.38V - 2.32	0.944
2	Salts, Organics	SS	Rep1:	F = 3.10V - 2.46	0.942
			Rep2:	F = 3.01V - 2.01	0.886
			Overall:	F = 3.02V - 2.20	0.919
3	Salts	Al	Rep1:	F = 2.40V - 1.97	0.915
			Rep2:	F = 2.34V - 1.81	0.942
			Overall:	F = 2.37V - 1.89	0.928
4	Salts, Organics	Al	Rep1:	F = 2.33V - 2.11	0.798
			Rep2:	F = 2.30V - 2.04	0.787
			Overall:	F = 2.31V - 2.07	0.792
SS	All SS data			F = 3.20V - 2.26	0.921
Al	All Al data			F = 2.37V - 2.01	0.869

*Where F = iron (mg), V = voltage (V), and slope has units of mg/V

Each run of the EC system began by placing the electrodes into a beaker filled with 220 mL of electrolyte. The solution was continuously mixed using a stir bar. The power source was set to the desired voltage, and then connected to the system for 60 seconds. The EC system was operated in constant voltage mode, wherein the voltage was set and the current was allowed to fluctuate. That said, fluctuations tended to be fairly minimal, and the median current value was typically assumed to be the steady-state value. At the end of the minute, the electrodes were immediately removed and the power source switched off. No clarification techniques were applied to the iron-dosed solution. The measured parameters were initial and final conductivity, initial and final pH, steady-state current (as determined from the measured current), and total iron.

To create a calibration curve, the EC system was operated over a set range of voltages (and therefore current densities) to determine the amount of iron generated at each voltage. The following voltages were tested in random order: 0.5, 1.0, 1.5, 1.X, 2.0, 2.X, 2.5, 3.0. Voltages 1.X and 2.X were allowed to be inexact, so long as they remained between 1.5 and 2.0 V, and 2.0 and 2.5 V, respectively. The resulting current densities ranged between 0 and 182 mA/cm^2.

4.3.4 Data Analysis

Outliers were first identified by calculating z-scores. For each of the four EC cell configurations given in Table 4.2, a linear model was created using applied voltage as the independent variable and mass of iron as the dependent variable. The variance for each model was estimated by calculating the mean residual sum of squares; the estimated

standard deviation was then derived from this value. A z-score was then calculated by taking the difference between the mass of iron predicted from the model and the experimental value, and dividing it by the estimated standard deviation. Any data point with an absolute value z-score greater than 1.5 was deemed an outlier, and omitted from all ensuing analyses. Overall, 6 outliers were rejected from a data set of 64 points.

Following the removal of outliers, calibration curves giving the relationship between iron and applied voltage were made for each EC cell configuration. Each calibration curve was made in duplicate, and one overall curve was made to encompass the duplicated data sets. Table 4.2 gives these equations, along with their R^2 values.

A linear regression analysis using the entire data set was also conducted in Minitab 17 statistical software, where voltage was given as a continuous predictor (or input), and electrolyte and cathode material were noted as categorical predictors. However, the accompanying ANOVA analysis suggested that, at the 95% confidence level, the electrolyte was not a significant factor. Therefore, it was deemed more relevant to give two regression equations, one encompassing all tests using a SS cathode, and another similarly for aluminum (see Table 4.2). These equations are graphed in Figure 4.1, along with their 95% confidence intervals.

4.4 Results and Discussion

4.4.1 Effect of Organics in the Electrolyte

The presence of organics in solution was not found to have any significant effect

on iron production rate, efficiency, EC cell resistance, or solution pH at the 95% confidence level. This experiment used three organics (naphthalene, acenaphthene, and 4-nonylphenol), each containing aromatic ring structures. Aromatics like benzene derivatives tend to be good corrosion inhibitors for iron alloys (Bockris and Reddy, 2000). However, the three compounds tested in this study are also fairly soluble. The more soluble an organic compound, the less likely it is to adsorb onto an electrode surface and inhibit corrosion (Bockris and Reddy, 2000). Other possible explanations include the concentration of the organic stock solution being too low to have a substantial effect, or the duration of the experimental runs being too short to allow for the organics to bind to the electrode surfaces. In the experiments conducted in this study, the organic compounds had no effect on EC performance. Sari and Chellam (2015), using an EC system with an aluminum anode, also found that organics did not contribute significantly to electrode passivation when conducting tests on hydraulic fracturing wastewater with over 1000 mg/L of dissolved organic carbon.

4.4.2 Effect of Cathode Material on Iron Generation Rate and Efficiency

From Figure 4.1, using a SS cathode rather than an aluminum one resulted in a 35% or 0.83 mg/V increase in slope (mg of iron produced per unit voltage) over a 60 second period. These results were expected as aluminum has a substantially lower exchange current density for the HER than iron (Roberge, 2008). As the rate of iron production at the anode is directly coupled to the rate of the HER at the cathode surface, less iron cation was released when using an aluminum cathode. This also confirms that it

was the cathode half-reaction that was rate limiting the overall reaction; if the rate limiting step had been the dissolution of the anode, then changing the cathode material would not have affected the iron generation rate at all.

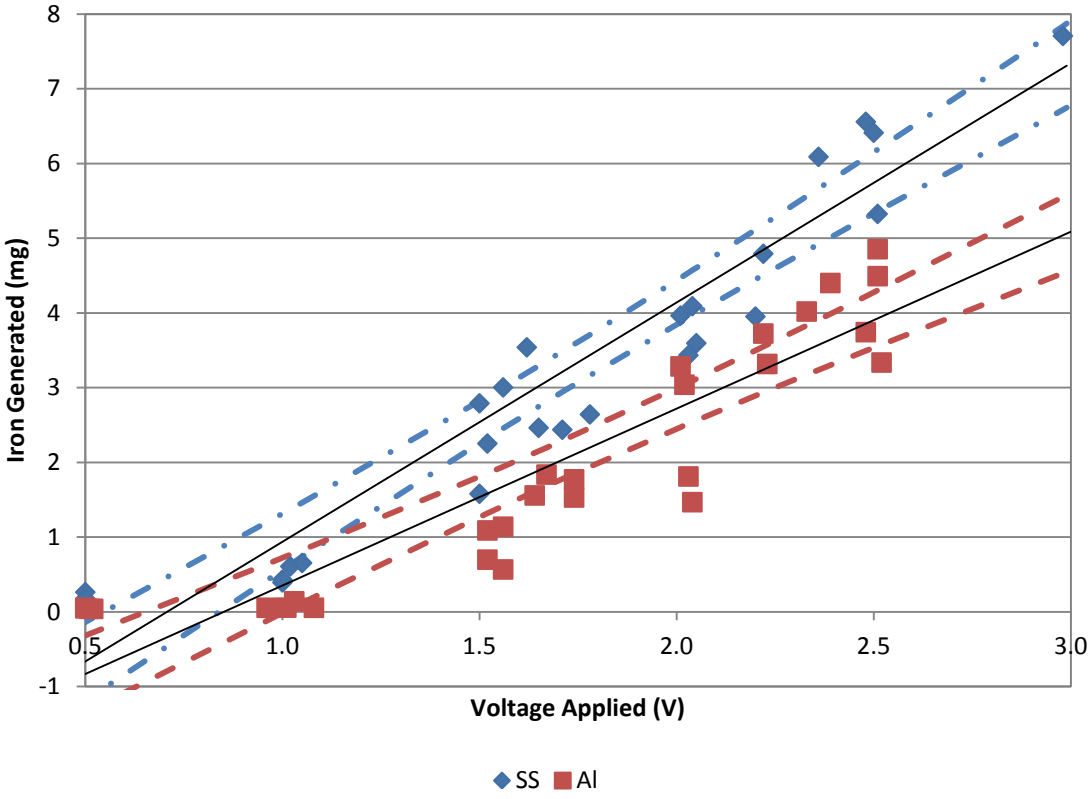

Figure 4.1: Relationship between iron and voltage when using either stainless steel or aluminum cathodes in an electrocoagulation system. The unbroken lines provide the regressions, while the broken lines give the 95% confidence intervals. As given in Table 4.2, F = 3.20V – 2.26 (R^2 = 0.921) for the stainless steel data, and F = 2.37V – 2.01 (R^2 = 0.869) for the aluminum data.

Using a SS cathode was also found to be more efficient. Figure 4.2 plots the amount of iron generated against the power consumed, and shows that the SS cathode generally produced more iron than its aluminum counterpart over the range of power tested. This effect also becomes more pronounced at higher power levels. For example, at 0.5 W, roughly 3.5 mg and 3.2 mg of iron were produced using SS and aluminum cathodes, respectively. In other words, there was a 9% increase in iron production as a result of using the SS cathode. At 1.5 W, this value increased to 34%, corresponding to approximately 7.5 mg of iron produced when using a SS cathode and 5.6 mg when using an aluminum one. Using an aluminum cathode also resulted in higher resistances across the EC cell, particularly at lower voltages (Figure 4.3a).

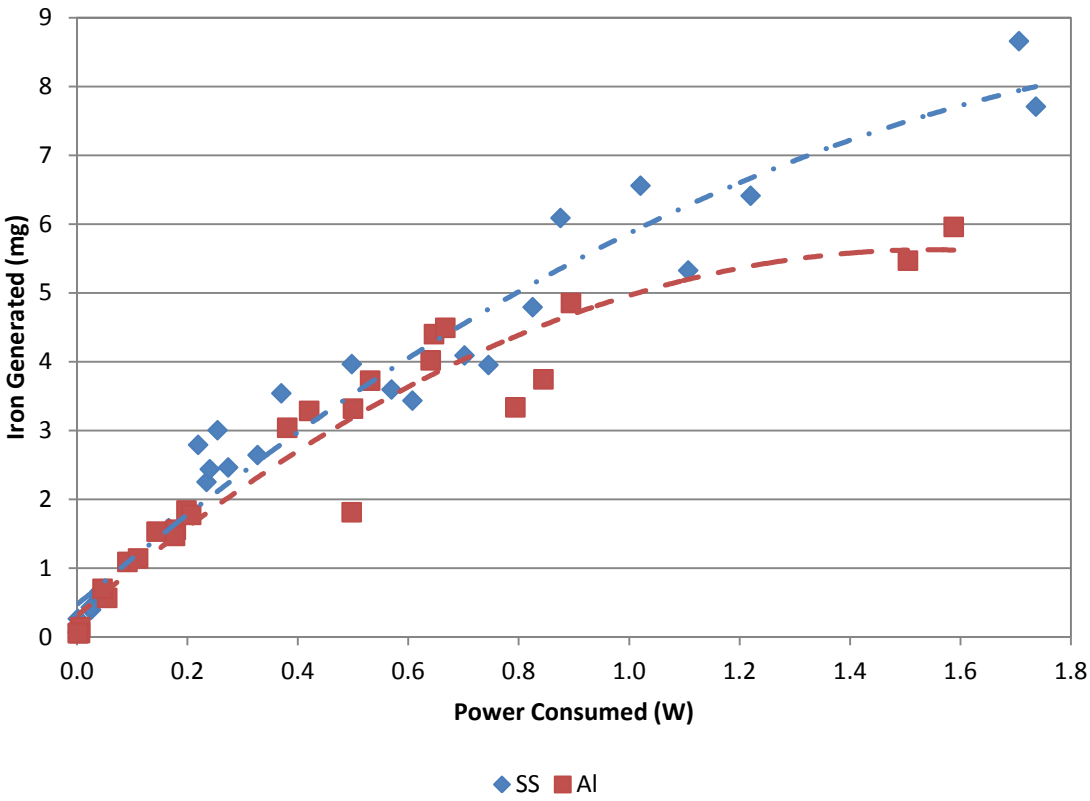

Figure 4.2: Iron generation plotted against power consumption for a bench-scale electrocoagulation system using either stainless steel or aluminum cathodes. The dashed lines indicate the general trends of the data.

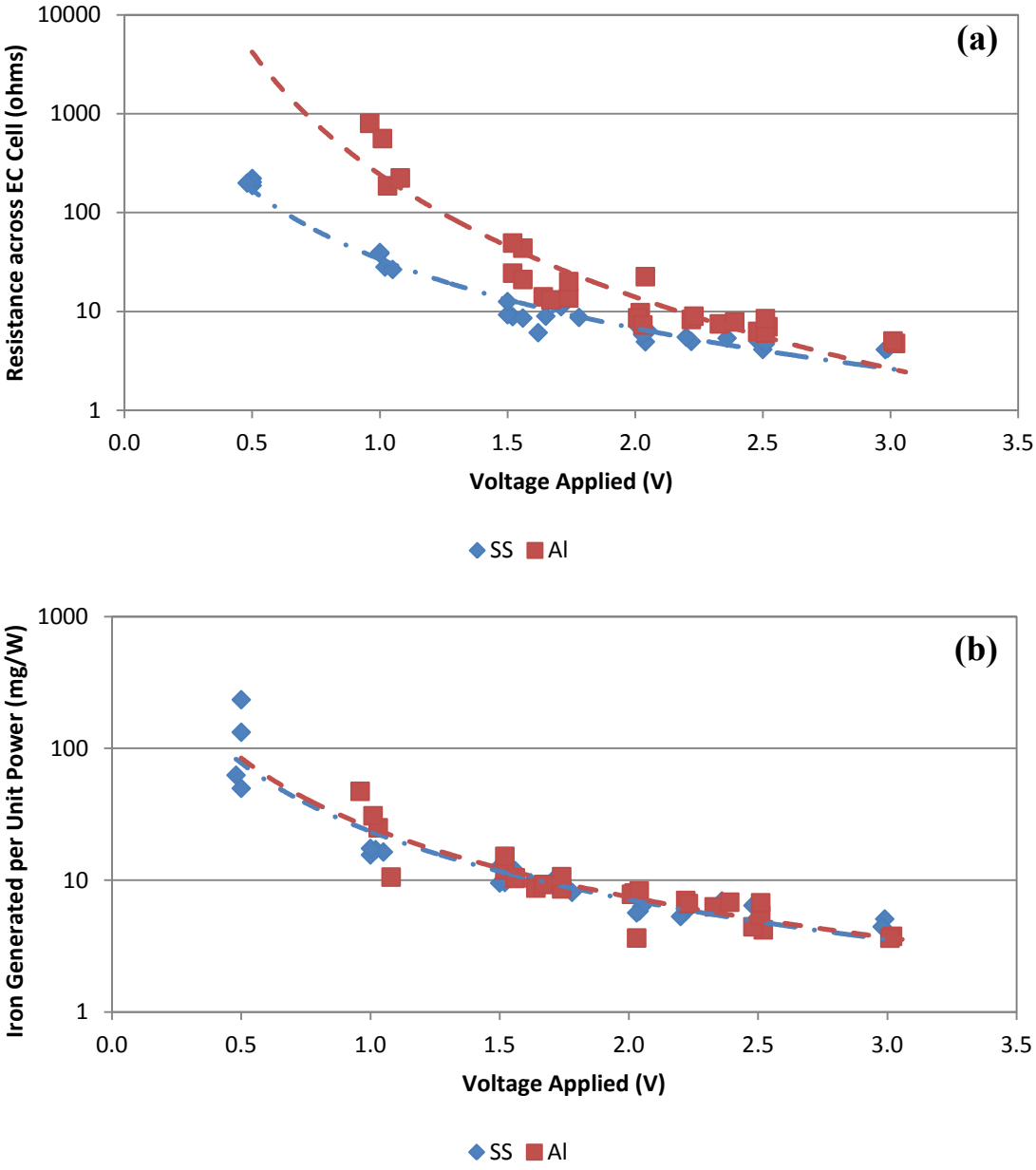

Figure 4.3: Resistance across an electrocoagulation cell (a) and iron generated per unit power (b) in a bench-scale electrocoagulation system at varying voltages when using either stainless steel or aluminum cathodes. The dashed lines indicate the general trends of the data.

4.4.3 Effect of Cathode Material on Solution pH

As a side effect of increased iron cation and hydrogen gas production, using a SS cathode rather than an aluminum one tended to result in greater pH increases. When using a SS cathode, the median pH change was an increase of 0.465, while the mean and standard deviation were 0.531 and 0.533, respectively. When using an aluminum cathode, the median pH change was a decrease of 0.055, while the mean and standard deviation were respectively positive 0.044 and 0.297. From stoichiometry, one would expect the EC process to be neutral as the amount of hydroxide and hydrogen ions produced theoretically balance. In practice, however, most cases underwent a pH increase.

Harif et al. (2012) suggested that pH increases during the operation of an EC cell could be attributed to the hydroxide ion production rate exceeding the metal cation precipitation rate. That is, a metal cation can hydrolyze into a variety of species, not all of which would release the maximum quantity of hydrogen ions. Therefore, the bulk solution would experience a net increase in hydroxide. As using a SS cathode resulted in higher concentrations of iron and hydrogen gas, it follows that a larger pH increase would occur as well.

4.4.4 Effect of Operating Voltage on Iron Generation Efficiency

An objective during EC cell design should be to minimize resistance as much as feasible. It is expected that the resistance of the EC cell is a function of a variety of factors, including operating conditions and cell geometry and materials. From the graph

of EC cell resistance versus applied voltage (Figure 4.3a), resistance increases as voltage decreases. From Ohm's law, one would expect resistance to decrease with decreasing voltage. However, because current is also dropping, the net effect is an increase in resistance; current was observed to have a stronger effect than voltage.

Although Figure 4.3a implies that operating at higher voltages would be more energy efficient, Figure 4.3b shows that the EC system actually produced more iron per unit power when operated at lower voltages. One explanation is that at lower voltages, the corrosion that occurs spontaneously in the absence of any applied current contributes an appreciable portion to the total amount of iron released. This explanation is corroborated by Figure 4.4, which gives the experimental iron concentrations (sorted by cathode material) against the theoretical iron concentration as given by Faraday's law assuming ferrous iron generation. This assumption was made as it gives the highest possible theoretical iron concentration. At higher currents (and therefore voltages) the actual iron concentrations were less than the theoretical values. Conversely, at the lower currents, the experimental data closely mimicked the theoretical data.

In this experiment, the amount of iron generated at these lower voltages was very small and insufficient for coagulation. Nevertheless this suggests that it may be more efficient to design EC systems with more electrodes operating at low power than to have fewer electrodes operating at high power.

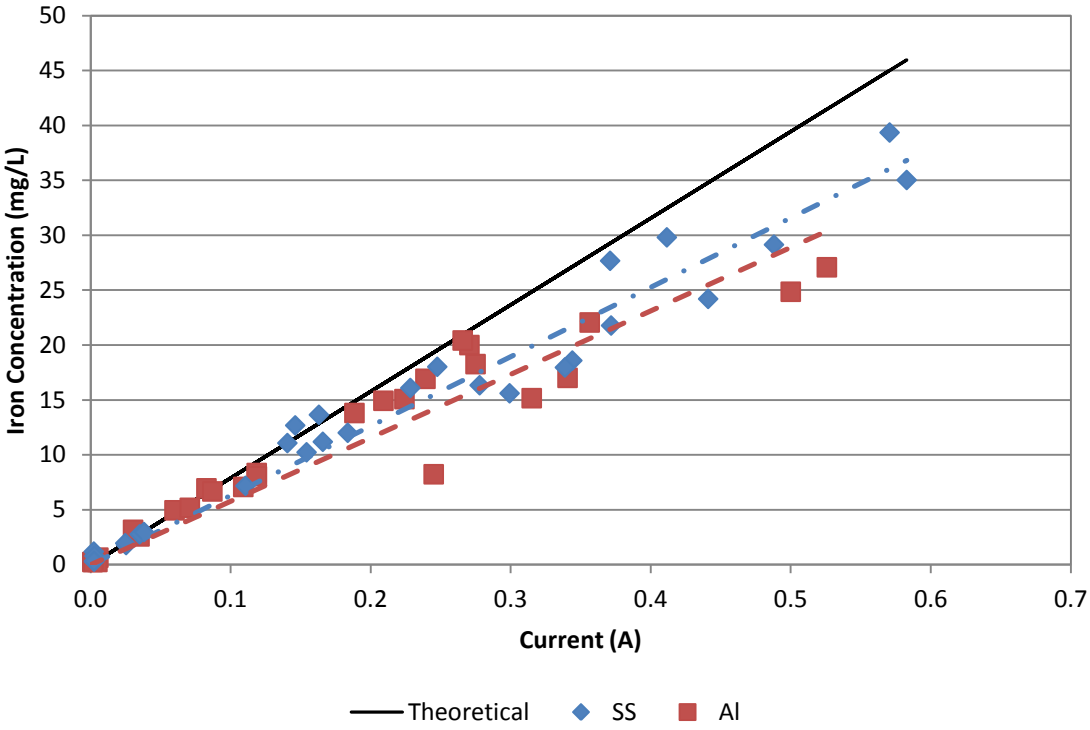

Figure 4.4: Theoretical versus experimental iron concentrations in an electrocoagulation system using stainless steel or aluminum cathodes. The solid line presents the theoretical iron concentration according to Faraday's law, assuming that only ferrous iron was released from the anode. The dashed lines present the linear best-fits for the experimental data using zero intercepts.

4.4.5 Electrocoagulation Efficiency in Practice

The current efficiency of the EC system was determined by comparing the slopes of the experimental iron concentrations (graphed in Figure 4.4) against the slope of the theoretical iron concentration (78.9 mg L^{-1}/A). All best-fit lines were calculated using a zero intercept. When using a SS cathode with an iron generation slope of 63.2 mg L^{-1}/A,

the system operated at 80% of its theoretical current efficiency. When using an aluminum cathode (57.8 mg L^{-1}/A), this value was 73%. Overall, corresponding to a slope of 61.1 mg L^{-1}/A, this value was 77%. Zhu et al. (2005), who treated synthetic fresh waters at the bench-scale, also performed this calculation and reported a current efficiency of 93%.

Current efficiency can also be calculated by dividing the amount of metal cation produced experimentally by the theoretical value. Jiang et al. (2002) regularly achieved greater than 100% current efficiencies (115% to 138%) when operating their EC-flotation system for the treatment of surface water. They argued that electrochemical side reactions (oxygen reduction at both anodes and cathodes, and the HER at the cathodes) caused a discrepancy between the net, measured currents at the electrodes and the currents associated with aluminum electrode dissolution. Chen et al. (2000) calculated a 118.8% current efficiency when treating restaurant wastewater using a bench-scale system with a bipolar electrode configuration. They attributed this to enhanced electrode dissolution caused by localized acidity near the anode due to proton production, and localized alkalinity near the cathode due to hydroxide production. Chen et al. (2000) also operated their system for 33.2 hours, much longer than the 60 second intervals used in this research, which allowed for greater corrosion.

4.5 Conclusions

This research explored the effects of operating voltage, cathode material, and electrolyte composition on iron generation rate and efficiency in an EC system. Bench-scale tests were operated over 60 second periods. The resulting information provides

useful guidance regarding the design of EC systems, and addresses some of the current gaps in EC literature. Given below are the key findings:

- The presence of naphthalene, acenaphthene, and 4-nonylphenol in the electrolyte did not have a significant effect on iron generation rate, efficiency, EC cell resistance, or solution pH. Possible explanations for this result include insufficient organic concentrations, high organic solubility, and experimental run times that were too short to allow for adsorption. Although more comprehensive research is required, this indicates that EC systems will not suffer adverse effects when treating wastewaters associated with oil and gas production.
- Using a SS cathode, in comparison to an aluminum cathode, increased the rate of iron generation at the anode by 0.83 mg/V per minute (i.e., 35% gain). This likely resulted because the hydrogen evolution reaction at the cathode surface occurred more quickly on an iron alloy than on aluminum. Thus, it was the cathode half-reaction rate limiting the overall reaction, rather than the anode half-reaction.
- Using a SS cathode rather than an aluminum one increased the efficiency of iron generation. Equating power consumption, using the SS cathode resulted in greater iron production than its aluminum counterpart, an effect that was enhanced at higher power levels. When operating at 0.5 W, using the SS cathode produced about 9% more iron; at 1.5 W, this value increased to 34%.
- The EC system was more efficient (produced more iron per unit power) when operated at lower voltages. When the voltage was low, the corrosion that occurred spontaneously in the absence of an applied current may have contributed a significant portion to the total iron. Thus, it may be more efficient to design EC

systems to use more electrodes at low power, rather than fewer electrodes at high power.

CHAPTER 5: GROWTH AND STRUCTURE OF FLOCS FOLLOWING ELECTROCOAGULATION

5.1 Abstract

The growth and structure of iron precipitate flocs produced in salt water from a bench-scale electrocoagulation (EC) system was investigated. During floc growth, changes in the scattering exponent, an indicator of a flocs' degree of compaction, were reflected by changes in the particle size (diameter of a volume equivalent sphere). Flocs initially behaved in a manner suggestive of the diffusion limited aggregation (DLA) model, forming loose, open structures that spanned broad size ranges. The initial aggregates reformed into more compact structures, suggesting a shift towards the reaction limited aggregation (RLA) model. Comparing plots of scattering exponent against time, it was found that operating at higher current densities caused this process to occur more quickly. However, the plots were all similar in shape, suggesting that the structural progression of the EC flocs was not affected. The final floc structures had an average scattering exponent of 2.34 (standard deviation 0.02), which is consistent with literature for flocs produced from iron-based chemical coagulants despite differences in electrolyte ionic strength. Analysis via transmission electron microscopy (TEM) suggested that EC flocs also exhibited amorphous, fractal structures. Operating at higher current densities (providing larger iron concentrations) resulted in larger flocs. The average steady-state floc sizes when operating at 27.2, 54.4, and 81.6 mA/cm^2 were 93, 147, and 191 μm, respectively. Floc size distributions also reached steady-state more quickly due to the

higher frequency of particle collisions. Using a stainless steel (SS) cathode rather than an aluminum one resulted in 15% larger flocs (154 μm and 134 μm, respectively). However, given that experimental conditions (mixing and current density) were otherwise equivalent, more research is required to determine the cause of this difference. The results of this work were consistent with literature regarding chemical coagulation (CC) and may have implications for the design of downstream clarification processes.

5.2 Introduction

5.2.1 Electrocoagulation

Electrocoagulation (EC) is a water treatment technology that has been investigated in a variety of bench-scale water treatment scenarios. These include the pretreatment of surface water for microfiltration (Bagga et al. 2008), the removal of silica from brackish water as a pretreatment to membrane filtration (Den and Wang, 2008), and the treatment of high conductivity black liquor resulting from the paper industry (Zaied and Bellakhal, 2009). Like chemical coagulation (CC) using metal salts, EC works by releasing metal cations into solution in order to destabilize small particles in water, thereby making particle collisions more likely to result in aggregation (Gregory, 2006). However, instead of using metal salts such as ferric chloride or alum, EC uses sacrificial electrodes to provide a direct source of cations.

An EC system is an electrolytically operated electrochemical cell. As such, by controlling the current, an operator can control the rate of cation generation. In its

simplest form, an EC system must consist of a power source, an electrolyte, and at least one anode-cathode pair. At the anode, metal cations are released into solution and react with water molecules to form metal hydroxide species. At the cathode, the evolution of hydrogen gas occurs. These electrochemical reactions are discussed in further detail elsewhere (e.g., Lee and Gagnon, 2014; Mollah et al., 2001).

5.2.2 Floc Growth and Structure

Floc growth in coagulation processes occurs over several phases. Initially, aggregation is dominant, and flocs rapidly increase in size, forming large, open structures. Using higher coagulant doses tends to result in large, fast growing flocs, due to the higher concentration of particles available for collision (Duan and Gregory, 2003; Spicer and Pratsinis, 1996). Eventually, floc aggregation and breakage balance to create a steady-state particle size distribution, with flocs reaching a limited size. This occurs because the rate of aggregation decreases as a result of increased floc size (as the number of particles in the system is reduced). Larger flocs are also more vulnerable to breakage. In addition, there is evidence that floc breakage is somewhat irreversible, as flocs do not completely reform after being broken by high shear (Duan and Gregory, 2003; Jarvis et al. 2005a). Operating at higher shear forces increases particle fragmentation and restructuring, thereby producing smaller, more compact aggregates (Bouyer et al. 2005; Chakraborti et al. 2003; Spicer and Pratsinis, 1996; Tang et al., 2000).

Diffusion limited aggregation (DLA) and reaction limited aggregation (RLA) are particle aggregation models designed with the assumption that particle collisions occur

only via Brownian motion (random movement caused by thermal energy). Although most systems apply some form of shear, invalidating this assumption, the models are still useful in illustrating the formation of different floc structures. The DLA model assumes that there is negligible repulsion between particles, such that when they collide, they adhere to each other easily and form loose, open structures. In contrast, the RLA model assumes that there is significant repulsion between particles, such that many collisions are required in order to form an attachment; this allows aggregates to break and reform, resulting in more compact structures (Gregory, 2006; Tang et al. 2000).

5.2.3 Flocs Produced from Electrocoagulation

There is limited research available regarding the characteristics of flocs produced from EC. One study by Harif et al. (2012) found, when comparing CC against EC, that the latter process created more fragile flocs, albeit more quickly and over a broader pH range. Furthermore, based on settling data, Larue and Vorobiev (2003) found that the density of EC flocs (1050.0 ± 2.0 kg/m^3) was very similar to the density of flocs from ferrous sulphate (1053.0 ± 2.0 kg/m^3), but greater than the density of flocs from ferric chloride (1026.4 ± 0.0 kg/m^3). However, ferric chloride produced the largest flocs (213 ± 4 μm), followed by EC (141 ± 4 μm), and finally ferrous sulphate (100 ± 6 μm). In general, more research on this subject is required.

Floc characteristics, such as size and structure, will impact the effectiveness of downstream clarification methods. EC unfortunately does not share the same breadth of research that is available on CC systems. This work attempts to help close this gap by

investigating the effect of cathode material and current density on the growth and structure of EC flocs using particle size distribution data, structural analysis over time, and transmission electron microscopy (TEM). Prior work has suggested that the cathode material affects the power consumption of an EC system (Lee and Gagnon, 2015); however, the effect on the flocs produced was not explored. This research was conducted using salt water, as EC is inherently more efficient when treating a high conductivity solution. Furthermore, for simplicity, no pollutant was added to the solution; in other words, this experiment forms and aggregates only iron hydroxide precipitates.

5.3 Materials and Methods

5.3.1 Bench-Scale EC System

The bench-scale EC system used in this experiment is described in Section 3.1. It used an 1170 mL working volume, and tested both SS and aluminum cathodes.

5.3.2 Electrolyte

The electrolyte was made by dissolving 25 g/L of sodium chloride and 15 g/L of calcium chloride dihydrate (Fisher Scientific, Waltham, MA, USA) into reverse osmosis water. Averaging all tests, the initial conductivity and pH were respectively 60.38 ± 2.05 mS/cm and 5.46 ± 0.05. Likewise, the final conductivity and pH were respectively 59.76 ± 2.32 mS/cm and 5.99 ± 0.08. The solution's ionic strength was 0.73 M, which was

comparable to that of sea water. The approximate ionic strength of sea water was calculated to be 0.7 M, based on a list of major ionic species provided by McLellan (1965). As no target pollutant was added, this experiment studied the formation and characteristics of iron hydroxide precipitates.

5.3.3 Experimental Design and Procedure

This experiment studied the effect of cathode material on particle growth and structure at 3 different current densities. As listed in Table 5.1, this resulted in 6 unique cases (with 1 replicate, 12 total runs). The operating voltage, theoretical current density, and approximate power consumption for each experimental combination are also given in Table 5.1. The operating voltages were calculated using Equations 5.1 and 5.2 for the SS cathode and the aluminum cathode, respectively. These equations, which were determined experimentally and are specific to the bench-scale system and the electrolyte, relate the mass of iron produced in 1 minute to the operating voltage:

$$F = 3.38V - 2.32; \qquad R^2 = 0.944 \tag{5.1}$$

$$F = 2.37V - 1.89; \qquad R^2 = 0.928 \tag{5.2}$$

where F is the mass of iron (mg), and V is the operating voltage (V).

Table 5.1: Electrocoagulation system parameters for experiment investigating floc growth and structure.

Case No.	Cathode	Target Dose ($FeCl_3$ equiv)[a]	Target Dose (pure Fe)	Current Density[b]	Voltage[c]	Power[d]
		mg/L	mg/L	mA/cm^2	V	W
1	SS	25	5.2	27.2	1.0	0.087
2	SS	50	10.3	54.4	1.4	0.244
3	SS	75	15.5	81.6	1.8	0.470
4	Al	25	5.2	27.2	1.3	0.113
5	Al	50	10.3	54.4	1.8	0.313
6	Al	75	15.5	81.6	2.3	0.600

Note: Each test was 11.5 minutes long, with electrolysis occurring during the first 5 minutes.

[a]Ferric chloride hexahydrate

[b]Current was calculated from Faraday's law (assuming z = 2.5), then divided by the surface area of the anode (3.20 cm^2) to determine current density

[c]Voltages calculated from Equations 5.1 and 5.2

[d]Approximate power consumption calculated by multiplying current and voltage

A test jar filled with 1170 mL of salt solution was kept well mixed throughout the duration of the experiment using a stir plate set to 200 rpm. Initial pH and conductivity were measured, and a Malvern Mastersizer 3000 (Malvern Instruments, Worcestershire,

UK) was setup to take particle size and scattering exponent measurements once per minute.

Each experimental trial was operated for 11.5 minutes. Iron was dosed during the first 5 minutes. Throughout this period, voltage was manually adjusted when necessary in order to maintain consistent current levels; adjustments were typically minor, no more than a few tenths of a volt off of the target voltage. At 5 minutes, the electrodes were removed, and the flocs were allowed to develop over the remaining 6.5 minutes of the experiment. At the end of the experiment, the solution's final pH and conductivity were measured, and samples were taken for total iron analysis. A sample was also taken for analysis under a TEM.

5.3.4 Precision of Iron Dosing

While the targeted iron doses were 5.2, 10.3, and 15.5 mg/L for the low, medium, and high doses, respectively, the averaged actual amounts were 5.7, 10.6, and 17.1 mg/L. For each concentration, the standard deviation was less than 5% of the average. As such, the iron dosing was considered to be fairly precise.

A paired t-test conducted using Minitab 17 statistical software confirmed that, when experiments were paired according to current level, the amount of iron cation produced when using the SS cathode was not inadvertently greater than the amount produced when using the aluminum one. At the 95% confidence level, it was determined that there was no significant difference between the amounts of iron dosed when using either material as cathode.

5.4 Results and Discussion

5.4.1 Floc Structure at the Nanoscale

Figure 5.1 gives TEM images of EC flocs at the nanoscale. Figure 5.1a (resulting from case 2) is an extreme close-up of an iron precipitate. The particle was likely amorphous, as there is no visible evidence of a regular or crystalline structure. The darker regions of the TEM image resemble folds in a scrap of fabric, as if the iron precipitate had wrinkled and overlapped on itself. The lighter regions, particularly near the edges of the floc, indicate where the precipitate is not as thick. Neither cathode material nor current density had any visible effect on the particle structure.

Figure 5.1b and Figure 5.1c (both resulting from case 1, the latter provides a higher magnification view of the former) provide evidence for the fractal nature of the flocs. Both images have a similar geometrical resemblance, regardless of magnification. This indicates that repeating, self-similar structures existed, which is essential to the definition of a fractal object (Gregory, 1997; Li and Ganczarczyk, 1989). Furthermore, Figure 5.1c focuses on a point where either two smaller flocs were attaching, or one larger floc was breaking apart. When the fractal dimension is constant (the floc is not compacting), floc aggregates will decrease in density as they increase in size (Chakraborti et al. 2003; Gregory, 1997), as demonstrated by the floc images provided in Figure 5.1c. Assuming that the particles were joining, the overall area of the new floc was significantly increased; however, because a great deal of void space was then included in the new calculation of area, the overall aggregate became less dense.

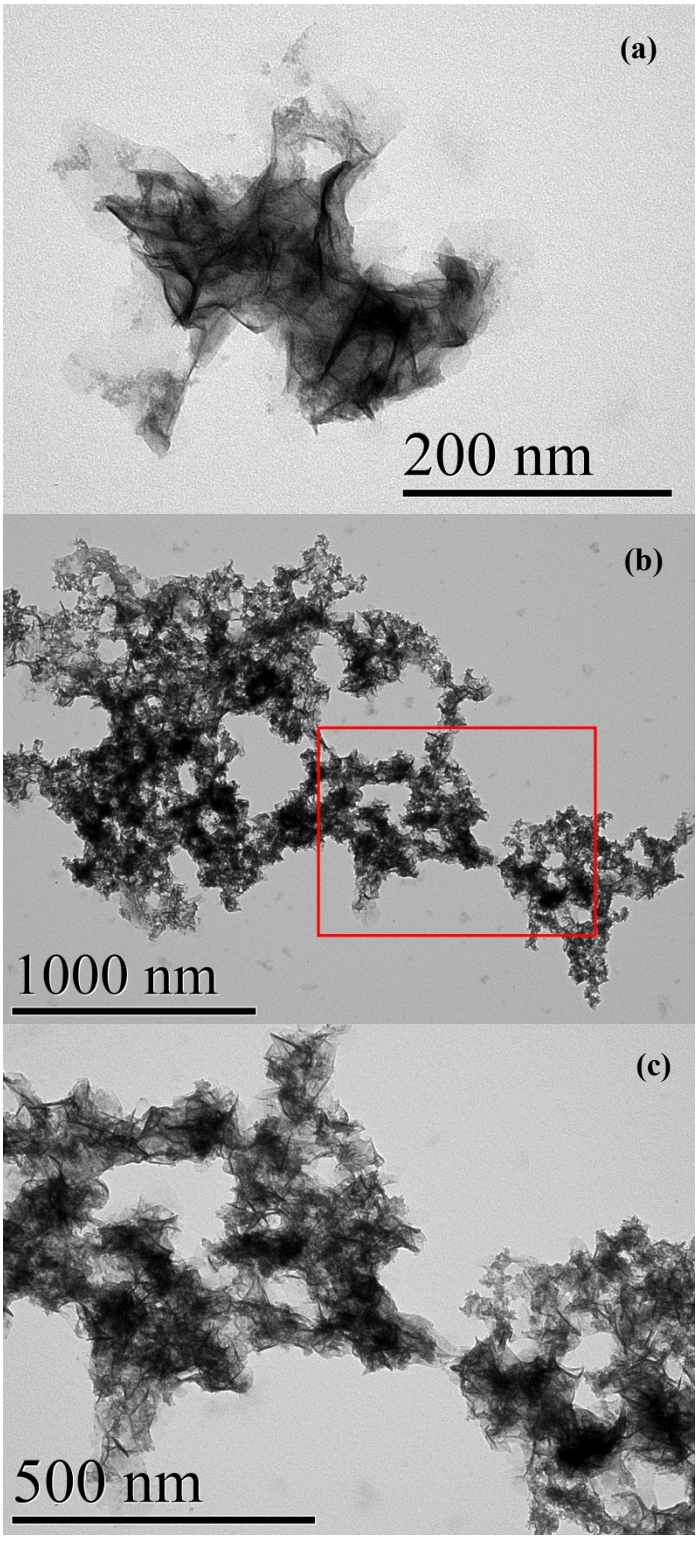
(a)
200 nm
(b)
1000 nm
(c)
500 nm

Figure 5.1: Transmission electron microscopy images of iron precipitate flocs produced via electrocoagulation. Image (a) gives an extreme close-up of a floc. Image (c) provides a magnified view of (b).

5.4.2 Particle Size Distributions over Time

Figure 5.2 gives the particle size distributions over time when using a SS cathode and operating at 27.2 mA/cm^2 (case 1). As all the cases followed similar trends, this figure is used as a representative example. As seen in Figure 5.2a, the distributions were irregular during the initial minutes of the test (with iron dosing ongoing during the first 5 minutes). In Figure 5.2b, the distributions gradually become log-normal in shape before reaching a steady-state. Similar to Spicer and Pratsinis (1996), this paper defines steady-state simply as the point when a floc size distribution no longer changes with time.

While cathode material had no discernible effect on floc growth, operating at higher current densities decreased the time required by the size distributions to reach steady-state. As summarized in Table 5.2, at the low, medium, and high current densities, log-normalization occurred on average at 7.5, 5.5, and 4 minutes, respectively. Likewise, steady-state size distributions were achieved on average at 10.5, 7, and 6 minutes for the low, medium, and high current densities. In all cases, the particle size distributions reached steady-state within 3 minutes of log-normalization. This result is consistent with literature in suggesting that operating at higher currents promotes faster floc aggregation. As particle aggregation requires the collision and then adhesion of smaller particles,

having a higher concentration of particles (and hence a higher frequency of collision) results in faster forming flocs (Duan and Gregory, 2003; Kusters et al. 1997).

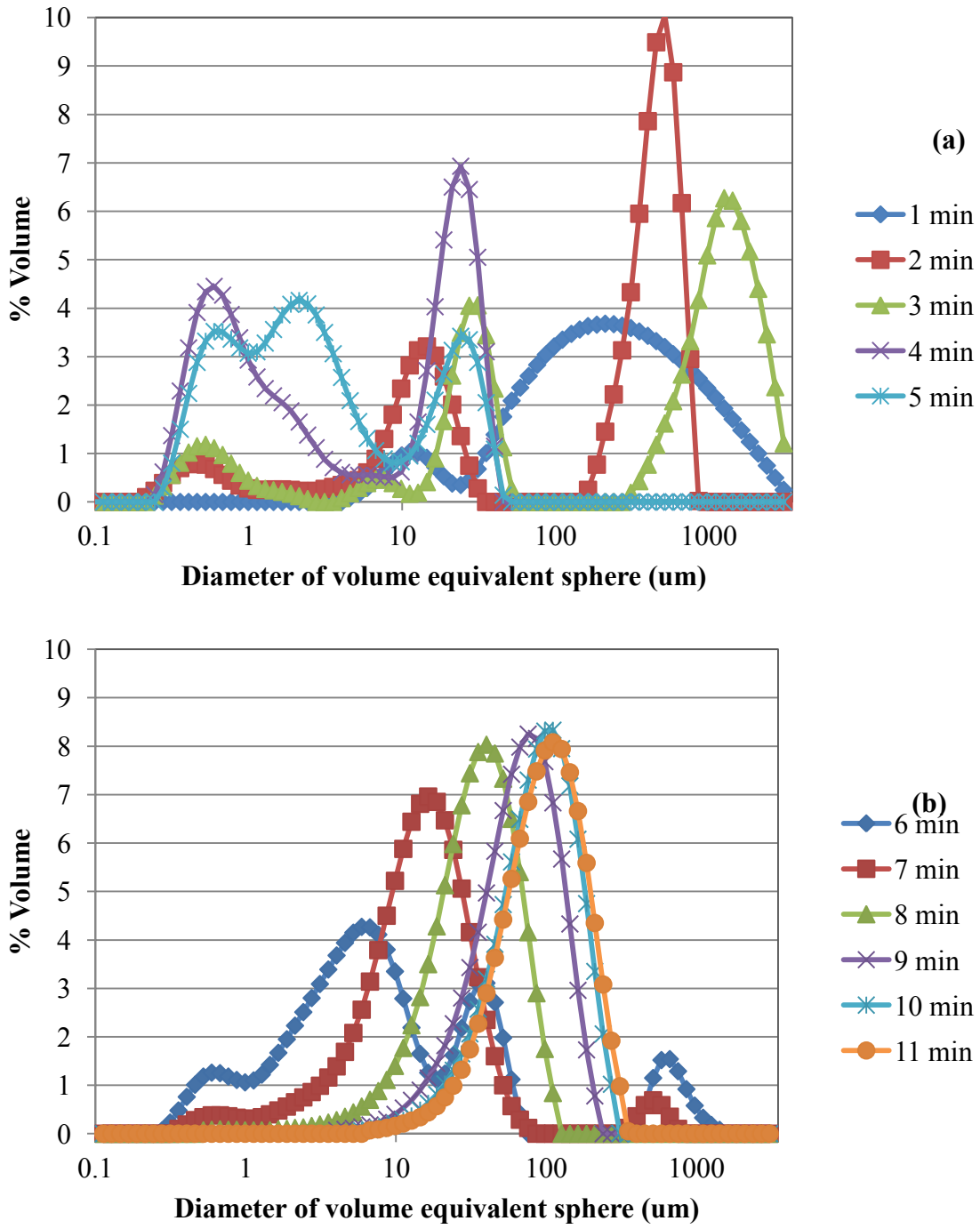

Figure 5.2: Floc size distributions over time generated via electrocoagulation using a stainless steel cathode and operating at 27.2 mA/cm^2. Iron was continuously generated from a sacrificial anode for the first five minutes (a), after which the iron dosing was stopped (b).

Table 5.2: Average times required for floc size distributions generated via electrocoagulation to log-normalize in shape and achieve steady-state, ± one standard deviation.

Case No.	Experimental Conditions	Time to Log-Normalize	Time to Steady-State	Steady-State Floc Size
		min	min	μm
1	SS, 27.2 mA/cm^2	7.0 ± 0.0	10.0 ± 0.0	104.0 ± 1.4
2	SS, 54.4 mA/cm^2	5.5 ± 0.7	7.0 ± 0.0	161.5 ± 2.1
3	SS, 81.6 mA/cm^2	4.0 ± 0.0	6.0 ± 0.0	196.0 ± 1.4
4	Al, 27.2 mA/cm^2	8.0 ± 0.0	11.0 ± 0.0	82.0 ± 0.2
5	Al, 54.4 mA/cm^2	5.5 ± 0.7	7.0 ± 0.0	133.0 ± 7.1
6	Al, 81.6 mA/cm^2	4.0 ± 0.0	6.0 ± 0.0	185.5 ± 29.0
Averages by Current Density				
	27.2 mA/cm^2	7.5 ± 0.6	10.5 ± 0.6	93.0 ± 12.8
	54.4 mA/cm^2	5.5 ± 0.6	7.0 ± 0.0	147.3 ± 17.0
	81.6 mA/cm^2	4.0 ± 0.0	6.0 ± 0.0	190.8 ± 17.8
Averages by Cathode Material				
	SS	5.5 ± 1.4	7.7 ± 1.9	153.8 ± 41.6
	Al	5.8 ± 1.8	8.0 ± 2.4	133.5 ± 48.2

Note: Steady-state was noted when the shape of the distributions stopped changing. Steady-state floc size was estimated as the median floc size at 11 minutes.

5.4.3 Floc Structure over Time

Changes in scattering exponent were reflected by changes in particle size. Figure 5.3 gives the 10^{th}, 50^{th}, and 90^{th} percentile particle size data along with the scattering exponent data over time when using a SS cathode and operating at 27.2 mA/cm^2 (Case 1). Figure 5.3 was derived from the same data set that produced Figure 5.2, and likewise serves as a representative example. During the initial minutes of the test while aggregation was dominant, the particles spanned a broad size range and the scattering exponent was low (close to 1.0). This behaviour was reminiscent of DLA, where, due to low particle repulsion, particles adhere easily and form loose, open structures (Gregory, 2006; Tang et al. 2000). After 3 minutes, the largest particles broke, shifting the particle size distribution towards smaller sizes (see Figure 5.2). At around 4 minutes, the scattering exponent began increasing, indicating that the flocs were slowly beginning to reform, albeit into structures that were significantly more compact. Floc size gradually increased from approximately 4 minutes onwards. The phase is comparable to the slow mixing phase in chemical jar tests, where floc size increases steadily over time before reaching some plateau value, typically within 10 to 15 minutes (Gregory, 2004; Jarvis et al. 2006; Yu et al. 2010). Due to the floc size limitations inherent in the calculation of scattering exponent (Section 3.2.4), it is the smallest flocs (10^{th} percentile) that best mimic the progression of the scattering exponent. The final scattering exponent at 11 minutes was 2.34, which is comparable to reported fractal dimension values for flocs formed under RLA conditions (around 2.2 to 2.3) (Waite, 1999).

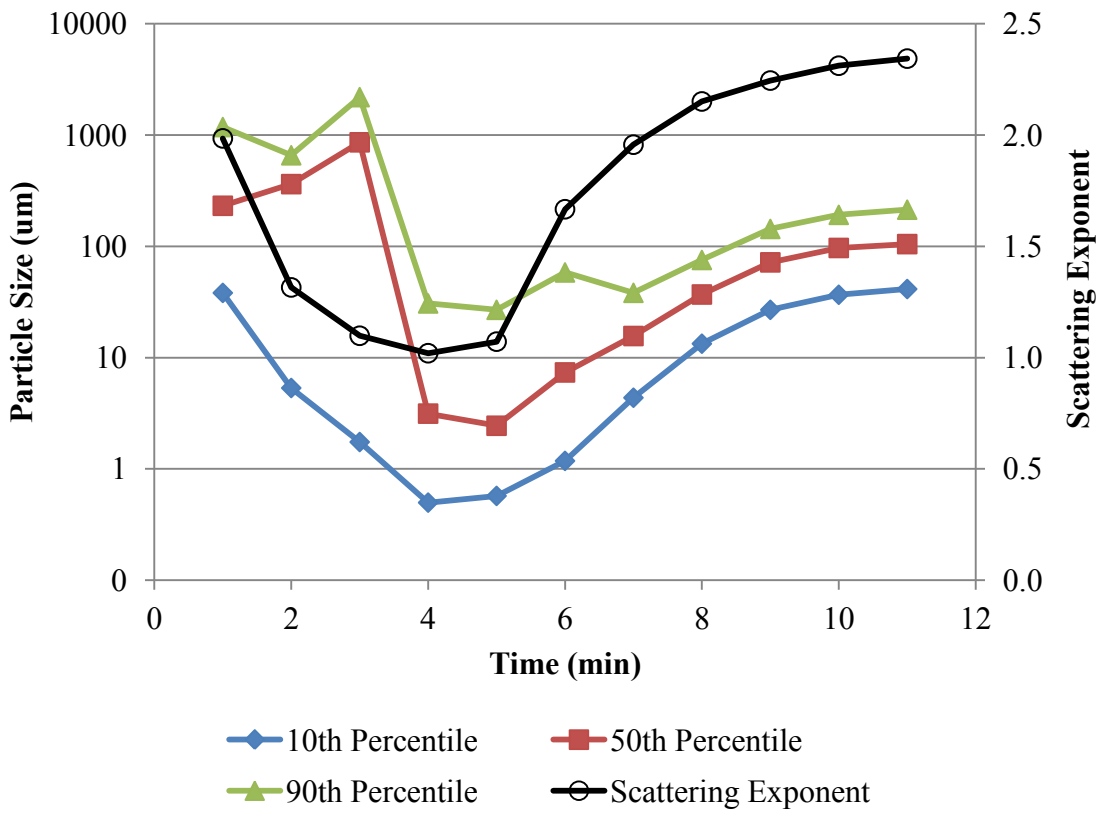

Figure 5.3: Scattering exponent and percentile particle size data presented over time for flocs generated via electrocoagulation using a stainless steel cathode and operating at 27.2 mA/cm^2. Iron was continuously generated from a sacrificial anode for the first five minutes, after which the iron dosing was stopped.

Figure 5.4 gives the average scattering exponent data for the 3 current densities tested (cathode material did not have a confirmed effect). The shape of the data is approximately the same for all cases, except shifted along the time axis. This suggests that while the dose of iron affected the rate of floc growth (as discussed in Section 5.4.2), it did not affect the structural progression. The flocs in the high current density cases began compacting more quickly than those in the low current density cases. The average

minimum scattering exponents (when the flocs were least compact) were reached at 4, 3, and 2 minutes for the low, medium, and high current densities, respectively. Compared against the times noted in Table 5.2, these minimums occurred before log-normalization was observed. This result is consistent with the observation that larger coagulant doses result in faster floc growth (Duan and Gregory, 2003; Spicer and Pratsinis, 1996).

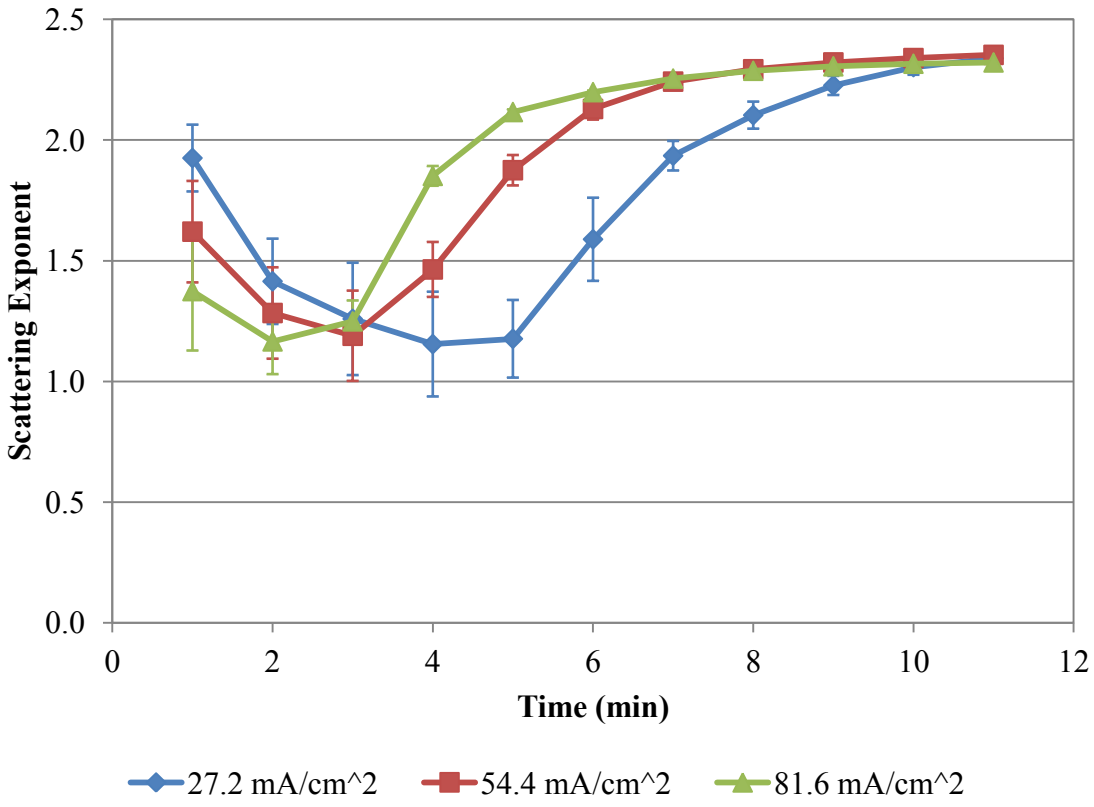

Figure 5.4: Scattering exponent data presented over time for flocs generated via electrocoagulation while operating at 27.2, 54.4, and 81.6 mA/cm^2. Iron was continuously generated from a sacrificial anode for the first five minutes, after which the iron dosing was stopped. The error bars mark ± one standard deviation.

The final floc structures (regardless of either cathode material or current density) were very similar in their level of compaction as this experiment did not vary mixing intensity. Averaging all cases, the scattering exponent at 11 minutes was 2.34, with a standard deviation of 0.02. When using ferric chloride coagulant and a t-bar stirrer set to 60 rpm, Jung et al. (1996) found that iron hydroxide flocs at pH 7 had a steady-state fractal dimension of 2.25 ± 0.05. Furthermore, Jarvis et al. (2005b) determined a fractal dimension of 2.15 for flocs formed from ferric sulphate in a solution of natural organic matter after rapid mixing at 200 rpm and slow mixing at 30 rpm. These examples and this research have comparable fractal dimension/scattering exponent values, despite the former using low ionic strength solutions, and the latter using a high ionic strength solution (0.73 M). A solution with significant ionic strength can destabilize particles via compression of the electrical double layer (Duan and Gregory, 2003), suggesting the formation of open-structured flocs. However, in this case the effect of ionic strength was likely negated, as continuous mixing ensured that the flocs would break and re-collide.

5.4.4 Steady-State Floc Size

An ANOVA analysis conducted using Minitab 17 statistical software determined that, at the 95% confidence level, both the factors cathode material and current density were significant to the steady-state floc size (estimated as the median floc size at 11 minutes). In general, operating at higher current densities and using a SS cathode tended to result in larger flocs. The cathode-current density interaction was not determined to be significant.

As given in Table 5.2, when using the aluminum cathode, the mean steady-state floc size was 134 μm; when using the SS cathode, the floc size was 15% larger (154 μm). Because floc size is dependent on particle concentration and mixing intensity (Duan and Gregory, 2003), operating currents were controlled such that comparable levels of iron were dosed when using either cathode. Furthermore, the mixing speed and electrode and container shapes were the same in both cases. The authors thus recommend further investigation in order to explain the differences in floc size resulting from the use of different cathode materials.

The average steady-state floc sizes were 191, 147, and 93 μm for the high, medium, and low current densities, respectively. In other words, doubling the low current density resulted in a 58% increase in floc size, while tripling it resulted in a 105% increase. This outcome is consistent with the findings of Chakraborti et al. (2000), who experimented with alum in lake water. When comparing alum doses of approximately 3.5 and 13.5 mg/L, they observed that the higher concentration shifted their distribution of flocs towards larger sizes.

5.5 Conclusions

This study investigated the growth and structure of iron-hydroxide flocs generated in salt water from a bench-scale electrocoagulation (EC) system. Considered were the factors cathode material and current density. The results were consistent with literature regarding chemical coagulation (CC), and may aid with the design downstream clarification processes. The key findings are summarized below:

- Changes in scattering exponent were reflected by changes in particle size. Initially, flocs spanned a broad size range and formed loose, open structures, in a manner suggestive of the diffusion limited aggregation (DLA) model. These initial aggregates then broke and formed into more compact structures, indicating a shift towards the reaction limited aggregation (RLA) model. Comparing plots of scattering exponent against time revealed that operating at higher current densities increased the rate of this process; however, the structural progression of the EC flocs was likely unaffected, as the plots were all similar in shape.
- EC flocs produced from an iron anode were found to have structural similarities with those produced from iron-based chemical coagulants. Transmission electron microscopy (TEM) revealed that EC flocs were irregular, likely amorphous, and fractal. Furthermore, the average final scattering exponent was 2.34, with a small standard deviation of 0.02 likely because the applied mixing was the same in all cases; despite differences in solution ionic strength, this value is consistent with CC literature for iron-based flocs.
- Operating at higher current densities resulted in larger flocs and floc size distributions reaching steady-state more quickly. When operating at 27.2, 54.4, and 81.6 mA/cm^2, the average steady-state floc sizes were respectively 93, 147, and 191 μm. At the highest current density tested (81.6 mA/cm^2), on average steady-state was reached 1 minute after iron dosing was stopped. This was likely due to the increased rate of particle collision, and thus aggregation.
- Using a stainless steel cathode (SS) rather than an aluminum one resulted in larger flocs. The mean steady-state floc size was 154 μm when using SS and 134 μm

when using aluminum. As both the mixing and the iron dosing were equivalently applied, more research is required to determine the cause of this difference.

CHAPTER 6: COMPARING THE GROWTH AND STRUCTURE OF FLOCS FROM ELECTROCOAGULATION AND CHEMICAL COAGULATION

6.1 Abstract

This study compares the growth and structure of flocs from chemical coagulation (CC) and EC. Flocs were more compact and larger when using CC rather than EC (on average, scattering exponents were 2.60 versus 2.31, while floc sizes were 254 versus 144 μm), and in low rather than high salt (2.51 versus 2.40, 222 versus 181 μm). They were also more compact at final pH 8.3 rather than pH 6.0 (2.53 versus 2.38). Transmission electron microscopy (TEM) revealed that CC and EC flocs were structurally distinct, possibly affecting the scattering exponent. In low salt and at pH 8.3, flocs were more stable and likely required more collisions to form, producing denser structures. Compact flocs tend to be more resistant to breakage, allowing them to grow to larger sizes. The time required for a floc size distribution to stabilize depended strongly upon the interaction between method of dosing and final pH. The CC-pH 6.0 and EC-pH 8.3 cases stabilized fastest (averaging 8.0 and 7.8 minutes), as they were always in the appropriate pH range for iron precipitation. The CC-pH 8.3 cases were initially adjusted close to pH 9 to counter coagulant acidity, while the EC-pH 6.0 cases possibly suffered from localized acidity near the anode, making precipitation less successful.

6.2 Introduction

6.2.1 Electrocoagulation

In water treatment, coagulation is a process wherein additives are used to destabilize particles in solution, thus making them more likely to aggregate upon collision (Gregory, 2006). Coagulation can be induced using chemical salts (such as ferric chloride or alum), or via electrocoagulation (EC), which uses sacrificial electrodes to provide a pure source of cations. Unlike chemical coagulation (CC), EC is not a commonly used water treatment technology. Nevertheless, EC has successfully treated a diverse variety of water types at the bench-scale, including municipal, textile dye, and petroleum refinery wastewaters (Bukhari, 2008; Zodi et al. 2013; El-Naas et al. 2009).

An EC system includes an electrochemical cell; it must contain at least one anode-cathode pair, along with an electrolyte and power source. While hydrogen gas is produced at the cathode surface, metal cations are released at the anode surface and react with water to form a variety of metal-hydroxide complexes. The rate of cation generation can be controlled by adjusting the applied current, according to Faraday's law. Mollah et al. (2001) have described these electrochemical reactions in greater detail.

EC has certain advantages over CC. For example, EC typically consumes less alkalinity and requires fewer chemical additives for pH adjustment. Solid metal electrodes are also easier to store and move than corrosive chemical salts. These qualities potentially make EC an option for use in remote areas or in emergency situations (Bagga et al. 2008; Zhu et al. 2005).

6.2.2 Floc Development

Floc growth begins with the aggregation of primary particles (which are simply the "original," unbound particles (Gregory, 2006)). Initial floc growth is rapid, forming large, porous structures. As the process continues, floc breakage becomes more prominent. The rates of aggregation and breakage eventually equalize, creating stable particle size distributions (Duan and Gregory, 2003; Jarvis et al. 2005a; Spicer and Pratsinis, 1996). Floc growth is affected by a number of factors, such as coagulant concentration and applied shear. Higher coagulant doses tend to increase both floc size and growth rate, as there are more particles available for aggregation (Duan and Gregory, 2003; Spicer and Pratsinis, 1996). Furthermore, mixing at greater intensities (higher shear) tends increase breakage, thereby reducing floc size and creating more compact structures (Chakraborti et al. 2003; Spicer and Pratsinis, 1996)

6.2.3 Comparing Chemical Coagulation and Electrocoagulation

Previous research has compared CC and EC. Perhaps unsurprisingly, their results are widely varied as the experimental systems and/or the solutions under treatment are all unique. For example, Bagga et al. (2008) used EC as a pretreatment step for surface water microfiltration, but found that CC with $FeCl_3$ was better at reducing membrane fouling. They found that EC produced soluble ferrous iron, which was less effective than ferric iron. Zhu et al. (2005) experimented with the removal of viruses from a synthetic freshwater using CC or EC, followed by microfiltration. The authors found that EC

outperformed CC, and proposed that virus adsorption and/or enmeshment was improved due to localized regions near the anodes having lower pH levels, as well as higher iron and virus concentrations. Cañizares et al. (2008) compared EC with aluminum electrodes against CC with alum for the break-up of oil-in-water emulsions. Unlike either Bagga et al. (2008) or Zhu et al. (2005), they found that the process efficiency depended on the pH and the aluminum concentration, but not the technology itself. As a final example, Harif et al. (2012) studied floc formation in a suspension of kaolin, comparing CC with alum and EC with aluminum electrodes. They determined that, when compared to CC flocs, EC flocs were more fragile, but formed faster and over a wider pH range.

Studies regarding EC flocs are limited, particularly in salt water. This Chapter compares the growth and structure of CC and EC flocs in low and high salt solutions at two pH levels, analyzing differences in zeta potential, scattering exponent (an approximation of fractal dimension), particle size distributions, and transmission electron microscopy (TEM) images. Floc characteristics are relevant to the effectiveness of downstream processes in a water treatment train, such as settling or filtration.

6.3 Materials and Methods

6.3.1 Bench-Scale EC System

The bench-scale EC system used in this experiment is described in Section 3.1. It used an 1170 mL working volume, and the cathode material was stainless steel (SS).

6.3.2 Electrolyte

This research varied two electrolyte parameters: the salt concentration, and the final pH. Regarding salt concentration, the low salt electrolyte consisted of 0.25 g/L NaCl and 0.50 g/L $NaHCO_3$ dissolved together in RO water. This resulted in an ionic strength of 10^{-2} M and an average initial conductivity of 1.12 mS/cm (standard deviation 0.04 mS/cm). The high salt solution used 25 g/L NaCl and 0.50 g/L $NaHCO_3$, resulting in an ionic strength of 0.43 M and an average initial conductivity of 42.2 mS/cm (1.6 mS/cm). For comparison, the ionic strength of seawater is approximately 0.7 mol/kg, while the ionic strength of freshwater ranges from 5×10^{-4} to 10^{-2} M (Edzwald and Haarhoff, 2011). The solution alkalinity was 298 mg/L as $CaCO_3$. Note that oceans can have alkalinity levels in the ballpark of 2300 μmol/kg, or 230 mg/kg as $CaCO_3$ after conversion (Lee et al. 2006).

Furthermore, the solutions were pH adjusted such that the final pH after coagulant addition would be either 6.0 or 8.3. pH adjustments were made using dilute solutions of HCl and/or NaOH, as necessary. The average final pH values for each group were 6.00 (standard deviation 0.07) and 8.30 (0.07). All chemicals used in this experiment were purchased from Fisher Scientific (Waltham, MA, USA).

6.3.3 Experimental Design and Procedure

The experimental design for this project was a 2^3 factorial design. The experimental factors studied were final pH (6.0 and 8.3), salt concentration (0.25 and 25

g/L NaCl), and method of coagulant dosing (CC and EC). This resulted in 8 combinations, which were run in duplicate. The factors and levels are listed in Table 6.1.

Table 6.1: Experimental factors and levels

Factor	(-)	(+)
Final pH	6.0	8.3
Salt concentration	0.25 g/L NaCl, 0.50 g/L $NaHCO_3$	25 g/L NaCl, 0.50 g/L $NaHCO_3$
Method of dosing	Chemical coagulation	Electrocoagulation

Each test began by filling a jar with 1170 mL of salt solution. The solution was pH adjusted such that the final pH after CC or EC would target either 6.0 or 8.3. A stir bar was set to continuously mix the solution at a speed of 200 rpm. Initial pH, conductivity, and zeta potential measurements were taken. The particle sizer was primed with the test solution and setup to take measurements once every minute.

Coagulant was added continuously over 5 minutes using either CC or EC. With the former, 25 mg/L $FeCl_3$ hexahydrate was dosed from a 5 g/L stock solution at a rate of 1.2 mL/min using a 7543-12 Masterflex pump (Cole-Parmer, Vernon Hills, IL, USA). With the latter, a targeted concentration of 5.2 mg/L of pure iron was generated from a sacrificial anode using 7.3 V and 1.3 V for the low and high salt concentrations, respectively. The relationship between voltage and per-minute iron output was

established experimentally before the start of the tests for both the low salt (Equation 6.1) and high salt (Equation 6.2) solutions:

$$F = 0.171V - 0.201; \quad R^2 = 0.903 \tag{6.1}$$

$$F = 3.087V - 2.947; \quad R^2 = 0.978 \tag{6.2}$$

where F is the iron concentration (mg/L), and V is the operating voltage (V).

At 0.5, 2.5 and 5 minutes after the beginning of coagulant addition, pH, conductivity, and zeta potential were again measured. Coagulant addition was halted at 5 minutes. The test continued until minute 11.5, when pH, conductivity, and zeta potential were measured for the final time. Samples were also collected for total iron determination and analysis via TEM.

6.3.4 Data Analysis

All statistical tests were conducted using Minitab 17 Statistical Software (Minitab Inc., State College, PA, USA) at the 99% confidence level.

The amount of iron dosed was inconsistent between the CC and EC cases. For reference, the targeted iron dose was 5.2 mg/L of iron, or 25 mg/L $FeCl_3$ hexahydrate. On average, the CC tests were given 4.7 mg/L of iron (standard deviation 0.3 mg/L), equivalent to 22.7 mg/L $FeCl_3$ hexahydrate. Likewise, the EC tests were given 6.4 mg/L of iron (0.3 mg/L), equivalent to 31.0 mg/L $FeCl_3$ hexahdyrate. Using a two-sample t-

test, the sample means were found to be statistically different at the 99% confidence level. Comparing averages, the EC jar tests dosed 36% more iron.

6.4 Results

6.4.1 pH Changes over Time

One advantage of EC is that it does not deplete/depletes less solution alkalinity than CC, as the hydrogen evolution reaction at the cathode consumes protons (Lee and Gagnon, 2014). In order to have equivalent final pH levels, pH adjustments were made such that the CC cases had higher initial pH values than their EC counterparts. In addition, electrolytes with high alkalinity were used (298 mg/L as $CaCO_3$).

Figure 6.1 shows pH over time for each of the 8 experimental conditions. The EC cases were fairly stable in pH from start to finish. For the EC-pH 6.0 cases, the average initial and final pH values were respectively 5.99 (standard deviation 0.11) and 6.00 (0.05). For the EC-pH 8.3 cases, these values were 8.23 (0.07) and 8.28 (0.04). For the CC cases, the initial pH was adjusted high in order to compensate for the addition of the acidic coagulant. The average initial and final pH values were respectively 8.92 (0.14) and 8.33 (0.09) for the CC-pH 8.3 cases. In comparison, the CC-pH 6.0 cases experienced a much less significant pH change; the average initial and final pH values were 6.13 (0.07) and 6.00 (0.10).

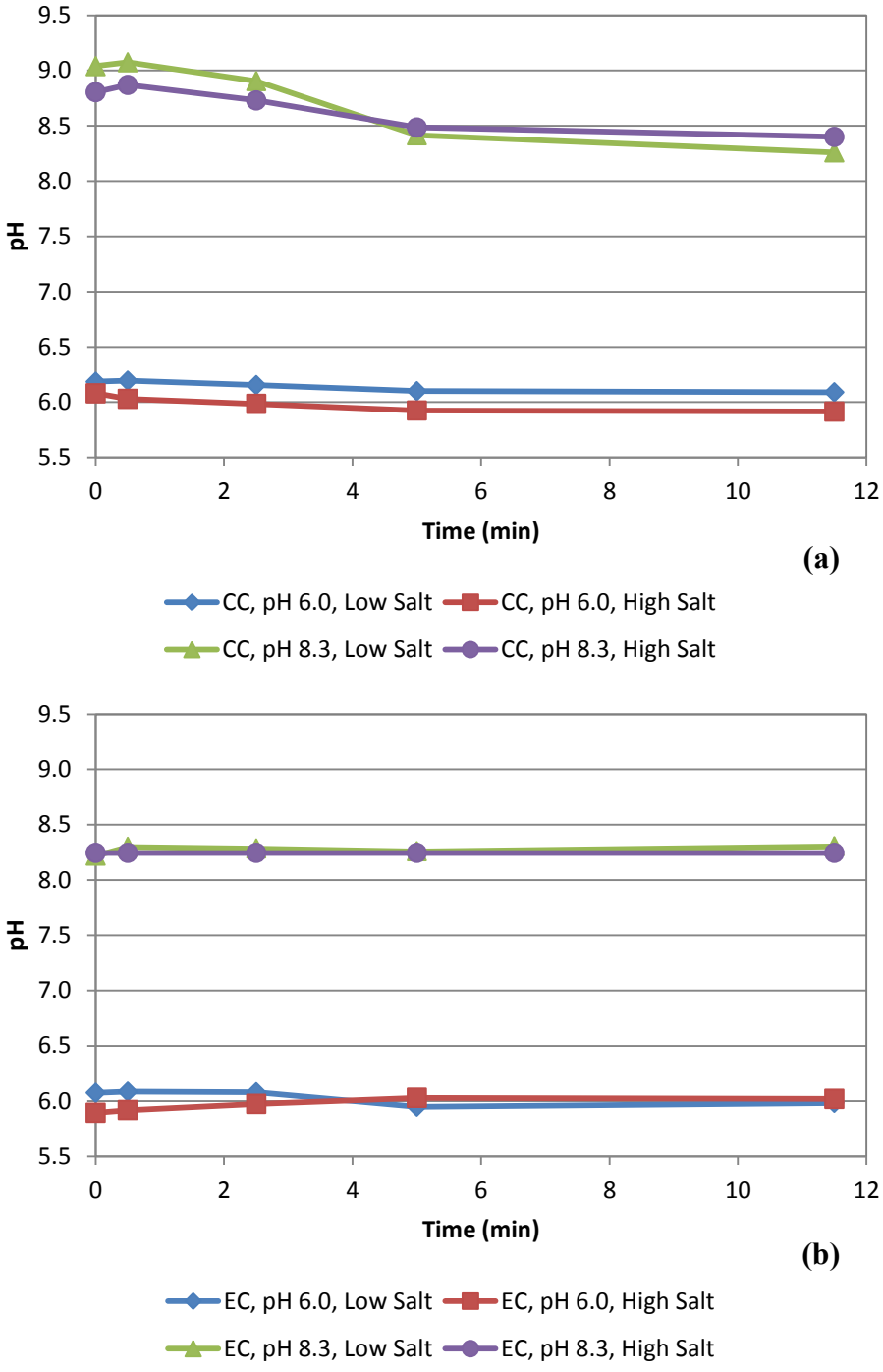

Figure 6.1: pH profiles over time for (a) chemical coagulation and (b) electrocoagulation jar tests. For both cases, coagulant dosing occurred continuously during the first 5 minutes. Error bars were not included as standard deviations were small.

6.4.2 Zeta Potential

The steady-state zeta potential was calculated as the average zeta potential at 11.5 minutes, and is reported in Table 6.2 for each of the 8 experimental conditions. ANOVA analysis determined that, at the 99% confidence level, the salt concentration ($p = 0.000$), final pH ($p = 0.000$), and the interactions method of dosing-final pH ($p = 0.009$) and salt concentration-final pH ($p = 0.001$) were all significant to the steady-state zeta potential (Table 6.3). Method of dosing was not found to be a significant factor, as evidenced by the relatively similar profiles of zeta potential over time for CC and EC (Figure 6.2a and Figure 6.2b, respectively). Note that zeta potential, which is strongly pH dependent (Gregory, 2006), was fairly stable during the experiments as pH did not fluctuate much during operation (discussed in Section 6.4.1).

Both targeting a final pH of 6.0 and operating in the high salt solution resulted in zeta potential values settling closer to 0 mV. At the final pH values of 6.0 and 8.3, the average steady-state zeta potentials were respectively -5.9 mV and -17.7 mV. Using the low and high salt solutions, these values were -20.4 mV and -3.2 mV, respectively (Table 6.3). It is well known that a solution with high ionic strength can cause double layer compression, wherein the repulsive energy barrier between particles is compressed, resulting in particle destabilization (Duan and Gregory, 2003; Rattanakawin and Hogg, 2001). The two significant interactions, salt concentration-final pH and method of dosing-final pH, were found to be in-line with the trends of the main factors.

Table 6.2: Steady-state characteristics of flocs produced from chemical coagulation and electrocoagulation jar tests. Steady-state was noted when the floc size distributions stopped changing, and a clear log-normal shape was established. The floc size and scattering exponent were considered to be at steady-state at 11 minutes; the zeta potential was considered to be at steady-state at 11.5 minutes.

	Time Required to Reach Steady-State (min)		**Median Floc Size (μm)**		**Zeta Potential (mV)**		**Scattering Exponent**	
	Avg.	Std. Dev.	Avg.	Std. Dev.	Avg.	Std. Dev.	Avg.	Std. Dev.
CC, pH 6.0, Low Salt	7.5	0.7	272	25	-8.5	0.7	2.71	0.03
CC, pH 8.3, Low Salt	9.5	0.7	274	13	-32.0	2.0	2.67	0.04
CC, pH 6.0, High Salt	8.5	0.7	216	25	3.2	4.6	2.53	0.05
CC, pH 8.3, High Salt	8.5	0.7	254	28	-4.5	5.0	2.50	0.01
EC, pH 6.0, Low Salt	11.0	0.0	159	47	-14.7	2.7	2.23	0.02
EC, pH 8.3, Low Salt	7.5	0.7	183	16	-26.2	2.5	2.44	0.02
EC, pH 6.0, High Salt	11.0	n. a.	77	n. a.	-3.6	1.7	2.05	0.12

	Time Required to Reach Steady-State (min)		Median Floc Size (µm)		Zeta Potential (mV)		Scattering Exponent	
	Avg.	Std. Dev.	Avg.	Std. Dev.	Avg.	Std. Dev.	Avg.	Std. Dev.
EC, pH 8.3, High Salt	8.0	0.0	125	6	-8.0	6.5	2.53	0.01

n. a. = no replicate available

Table 6.3: Averages and p-values for various floc characteristics at steady-state, given for the factors method of dosing, salt concentration, and final pH. Steady-state was noted when the floc size distributions stopped changing, and a clear log-normal shape was established. The floc size and scattering exponent were considered to be at steady-state at 11 minutes; the zeta potential was considered to be at steady-state at 11.5 minutes.

	Time Required to Reach Steady-State (min)			**Median Floc Size (µm)**			**Zeta Potential (mV)**			**Scattering Exponent**		
Factor	**Avg.**	**Std. Dev.**	**p-value**	**Avg.**	**Std. Dev.**	**p-value**	**Avg.**	**Std. Dev.**	**p-value**	**Avg.**	**Std. Dev.**	**p-value**
CC	8.5	0.9		254	31		-10.5	14.1		2.60	0.10	
			> 0.01			0.000			> 0.01			0.000
EC	9.1	1.8		144	43		-13.1	9.4		2.31	0.20	
Low Salt	8.9	1.6		222	60		-20.4	10.0		2.51	0.21	
			> 0.01			0.006			0.000			0.003
High Salt	8.7	1.1		181	73		-3.2	4.7		2.40	0.22	
pH 6.0	9.3	1.7		196	74		-5.9	7.2		2.38	0.28	
			0.009			> 0.01			0.000			0.000
pH 8.3	8.4	0.9		209	65		-17.7	12.6		2.53	0.09	

	Time Required to Reach Steady-State (min)			Median Floc Size (µm)			Zeta Potential (mV)			Scattering Exponent		
Factor	**Avg.**	**Std. Dev.**	**p-value**	**Avg.**	**Std. Dev.**	**p-value**	**Avg.**	**Std. Dev.**	**p-value**	**Avg.**	**Std. Dev.**	**p-value**
Significant 2-way interactions												
CC, pH 6.0	8.0	0.8					-2.7	6.8		2.62	0.11	
CC, pH 8.3	9.0	0.8					-18.3	16.0		2.58	0.11	0.000
			0.000						0.009			
EC, pH 6.0	11.0	0.0					-9.1	6.8		2.14	0.13	
EC, pH 8.3	7.8	0.5					-17.1	10.7		2.48	0.05	
Low Salt, pH 6.0							-11.6	4.1				
Low Salt, pH 8.3							-29.1	3.5				
									0.001			
High Salt, pH 6.0							-0.2	4.2				
High Salt, pH 8.3							-6.2	3.1				

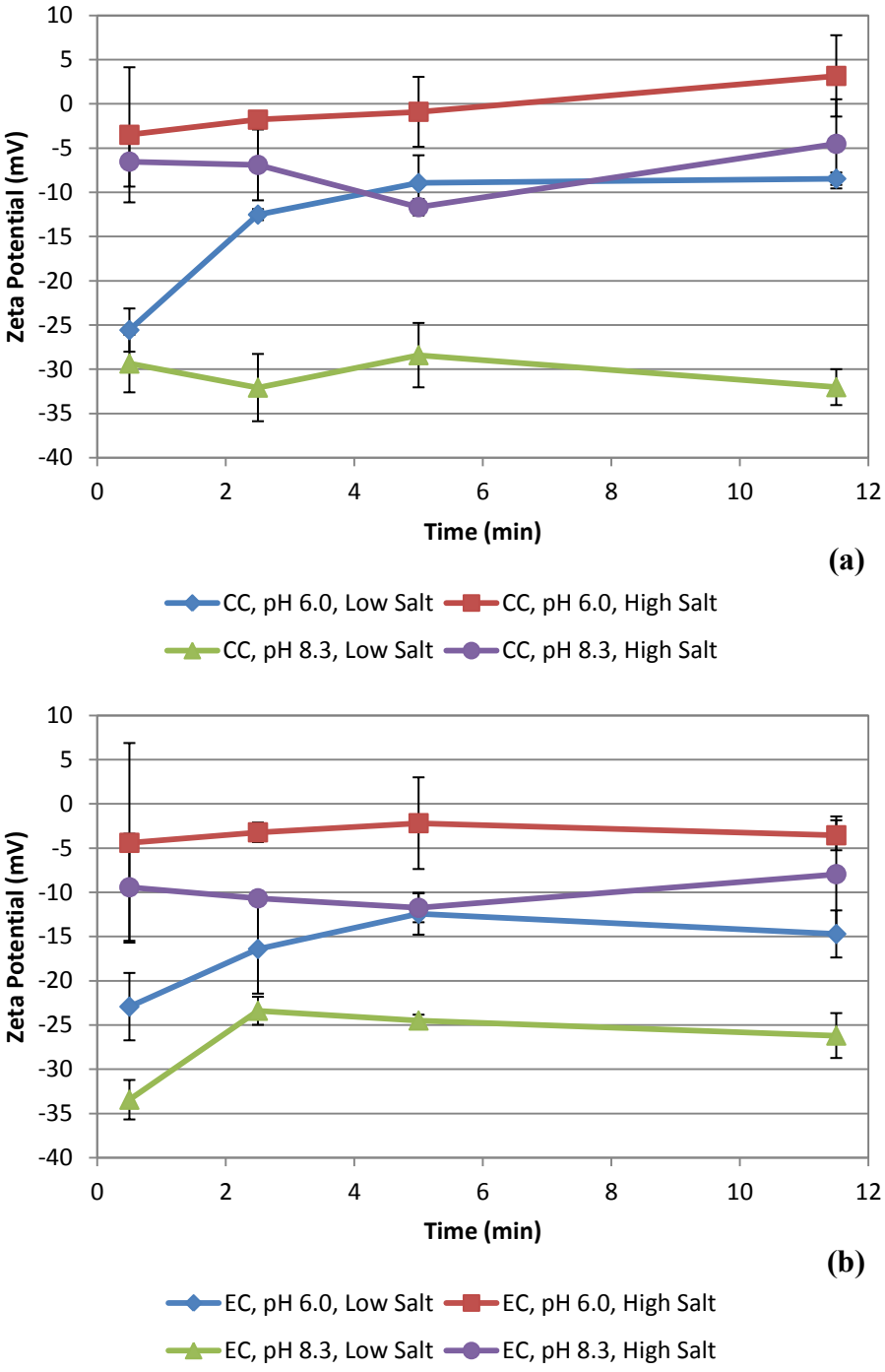

Figure 6.2: Zeta potential profiles over time for (a) chemical coagulation and (b) electrocoagulation jar tests. For both cases, coagulant dosing occurred continuously during the first 5 minutes. Error bars denote ± one standard deviation.

6.4.3 Scattering Exponent

The steady-state scattering exponent was calculated as the average scattering exponent at 11 minutes, and is reported in Table 6.2 for each of the 8 experimental conditions. At the 99% confidence level, ANOVA analysis determined that all 3 factors, method of dosing ($p = 0.000$), salt concentration ($p = 0.003$), and final pH ($p = 0.000$), had a significant effect on the steady-state scattering exponent. The interaction method of dosing-final pH ($p = 0.000$) was also found to be significant (Table 6.3). On average, flocs were more compact when produced using CC rather than EC (the scattering exponents were 2.60 versus 2.31), in low salt rather than high salt (2.51 versus 2.40), and at pH 8.3 rather than pH 6.0 (2.53 versus 2.38). Regarding the significant interaction method of dosing-final pH, the scattering exponents for CC flocs at both pH levels were fairly consistent (2.62 at pH 6.0, and 2.58 at pH 8.3). However, there was a notable difference between the EC-pH 6.0 and EC-pH 8.3 cases, which had scattering exponents of 2.14 and 2.48, respectively.

As seen in Figure 6.3, the profiles of scattering exponent over time tended to start low before climbing to a stable maximum level. The profiles for the CC cases all finished higher than or equivalent to their EC counterparts. Of the CC cases, the flocs that were most compact over the duration of the experiment were formed in the low salt solution at pH 6.0. Of the EC cases, compact flocs were most consistently formed in the high salt solution at pH 8.3. The EC-pH 6.0 cases show a large decrease in scattering exponent from approximately 4 to 7 minutes, indicating that the particles were slow to begin

compacting. Incidentally, the floc size distributions for the EC-pH 6.0 cases were also the slowest to reach steady-state (discussed in Section 6.4.5).

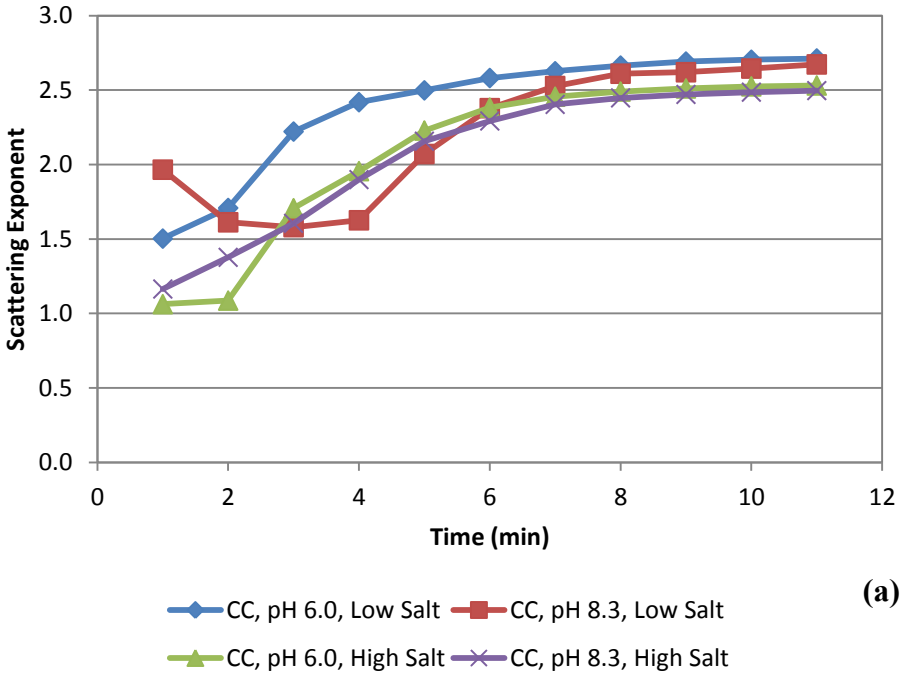

(a)

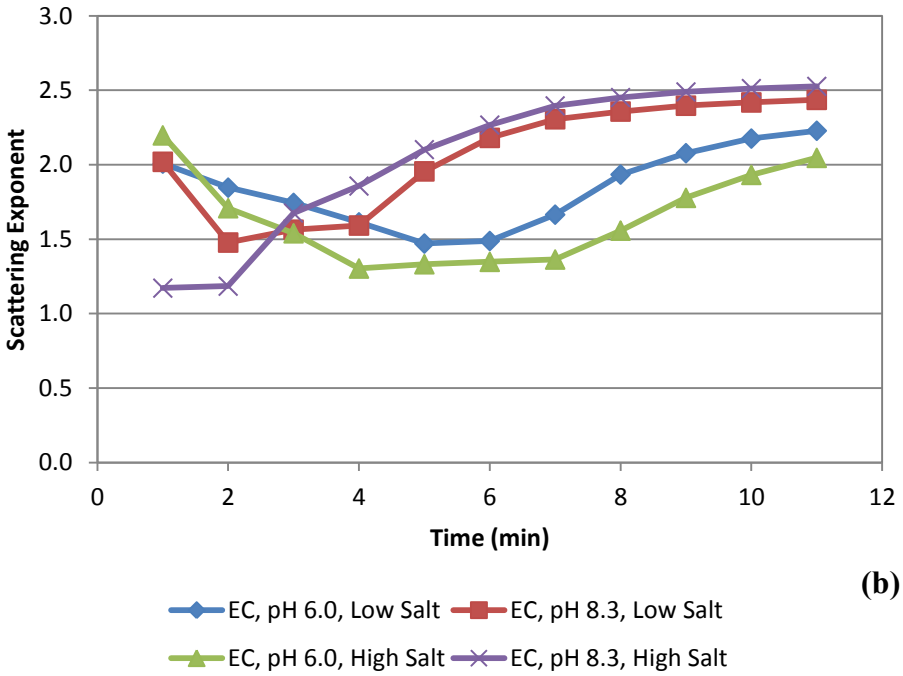

(b)

Figure 6.3: Scattering exponent profiles over time for (a) chemical coagulation and (b) electrocoagulation jar tests. For both cases, coagulant dosing occurred continuously during the first 5 minutes. Error bars were not included as standard deviations were small.

6.4.4 TEM Imaging

Using TEM to investigate floc structure at the nanoscale revealed that both method of dosing and salt concentration had a visible effect. Figure 6.4a gives a TEM image of the "basic" floc structure common to all CC cases, while Figure 6.4b does the same for all EC cases. Figure 6.4c and Figure 6.4d respectively give TEM images of CC and EC flocs that were found only in solutions with high salt concentrations. Although they share the same inherent structures as the "basic" flocs, these flocs are more densely packed. It is clear that CC and EC flocs are structurally very distinct, likely due to their means of formation. Using EC, iron cations were shed from a solid surface in situ. Using CC, ferric ions were dissolved in an acidic solution before being released into a far more alkaline bulk solution. The EC flocs appear comprised of spine-like formations that unfold into more nebulous structures with "fuzzy" edges. The CC flocs look "bubblier," with more rounded aspects.

For the most part, neither the CC nor the EC flocs appear to have any organized or crystalline structures. The exceptions are the dark, rectangular particles seen in Figure 6.4a. These particles are possibly goethite, as the chemical coagulant was a source of ferric ions that was well aged and stored in the correct pH range for goethite formation via the dissolution-crystallization process (Jolivet et al. 2004). The particles also resemble the image of goethite provided by Jolivet et al. (2004).

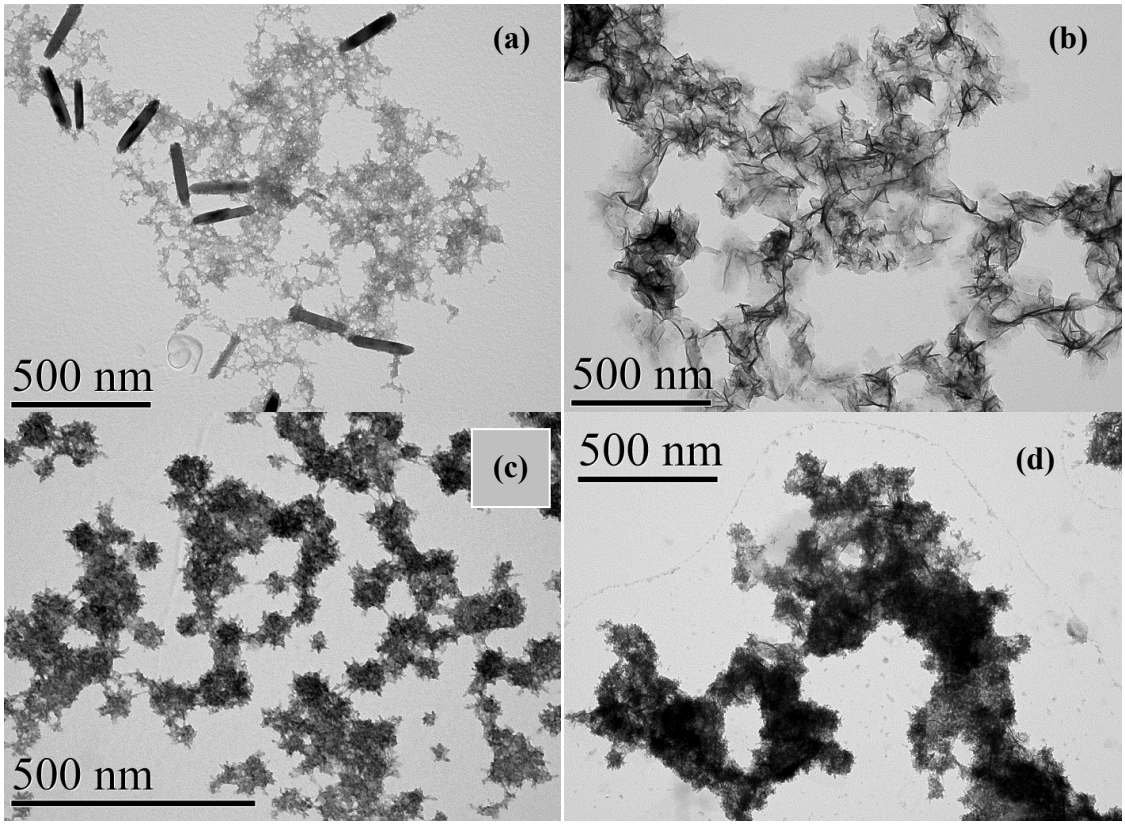

Figure 6.4: Transmission electron microscopy images. (a) Basic floc structure found in all chemical coagulation cases. (b) Basic floc structure found in all electrocoagulation cases. (c) Floc structure found only when using chemical coagulation in a solution with a high salt concentration. (d) Floc structure found only when using electrocoagulation in a solution with a high salt concentration.

6.4.5 Particle Size Distributions

Serving as representative examples for the CC and EC cases, respectively, Figure 6.5a and Figure 6.5b are floc size distributions that were generated in the low salt electrolyte at pH 6.0. For both methods of dosing, the size distributions were erratic in shape during the initial minutes of the tests, but gradually became log-normal. For each

of the 8 experimental conditions, the average steady-state floc sizes and times required to achieve steady-state are reported in Table 6.2.

Steady-state was noted when the floc size distributions stopped changing, and a clear log-normal shape was established. For the EC-pH 6.0 cases, it was assumed that steady-state was reached by the final minute of the experiment; while it could not be confirmed that their size distributions had stopped changing, the shape of their distributions at 11 minutes suggested that steady-state was either achieved or close at hand. At the 99% confidence level, ANOVA analysis indicated that the time required to reach steady-state was dependent on the factor final pH ($p = 0.009$), as well as the method of dosing-final pH interaction ($p = 0.000$). As given in Table 6.3, the pH 8.3 cases averaged 8.4 minutes, while the pH 6.0 cases averaged 9.3 minutes, although the latter had a fairly large standard deviation. The significant interaction is far more revealing. While the CC-pH 6.0 and the EC-pH 8.3 cases had similar average times (respectively 8.0 and 7.8 minutes), the CC-pH 8.3 cases averaged 9.0 minutes, while the EC-pH 6.0 cases averaged 11.0 minutes.

The steady-state floc size was taken as the median floc size at 11 minutes. At the 99% confidence level, ANOVA analysis indicated that the factors method of dosing ($p = 0.000$) and salt concentration ($p = 0.006$) were significant to the steady-state floc size. On average, flocs were larger when produced via CC rather than EC (254 μm versus 144 μm), and in low salt rather than high salt (222 μm versus 181 μm).

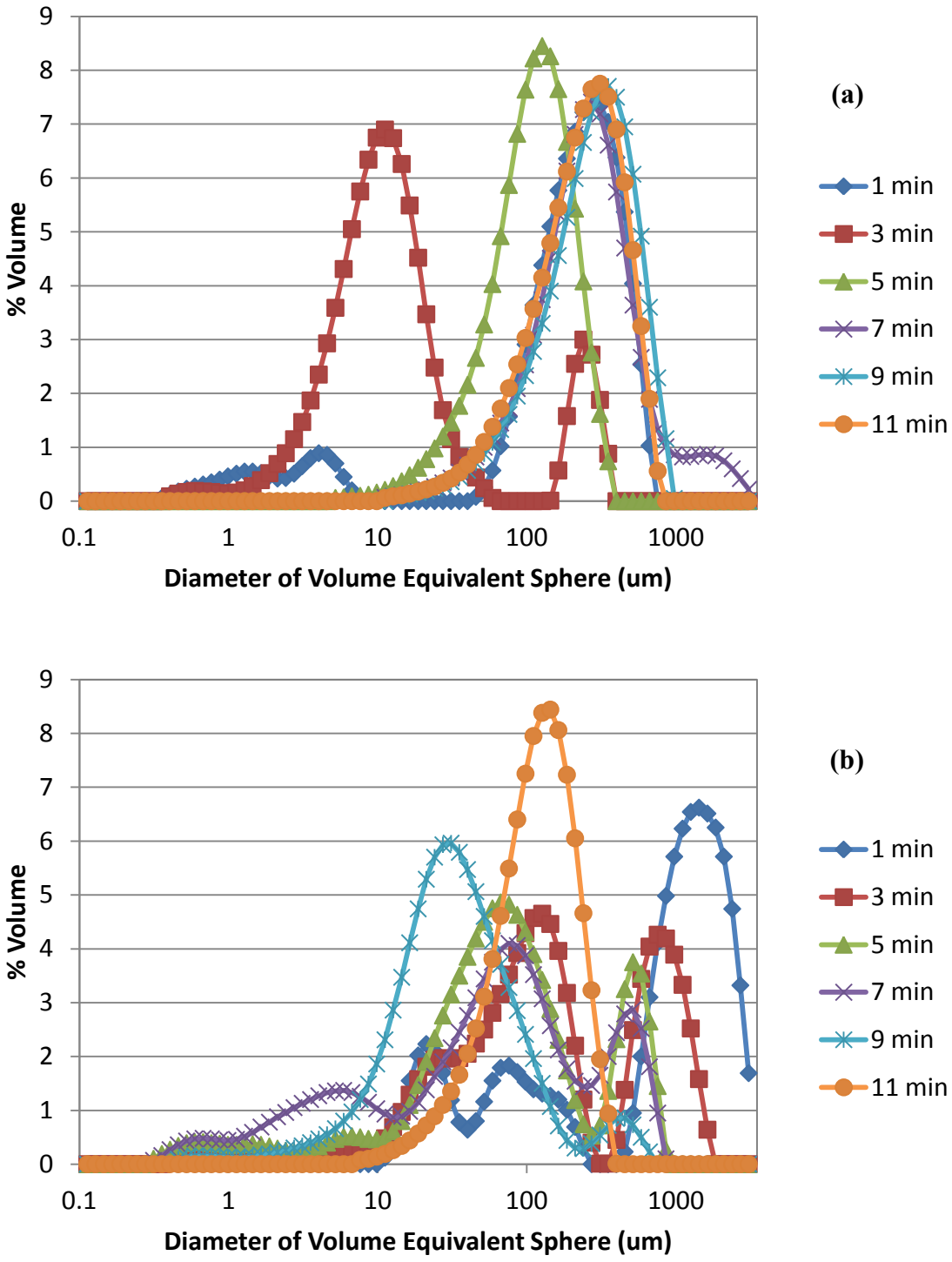

Figure 6.5: Floc size distributions generated over time at pH 6.0 and in low salt solutions using both (a) chemical coagulation and (b) electrocoagulation. For both cases, coagulant dosing occurred continuously during the first 5 minutes.

6.5 Discussion

6.5.1 Floc Structure

Judging from the average scattering exponents, flocs were typically more compact when created using CC rather than EC, in the low salt rather than high salt solution, and at pH 8.3 rather than pH 6.0 (Section 6.4.3). Flocs in the low salt electrolyte and at pH 8.3 were more stable in solution than their counterparts; in other words, these particles had zeta potentials farther from 0 mV (Section 6.4.2). These particles required more collisions to form, resulting in more compact structures. However, the CC flocs were more compact than EC flocs, despite having no significant difference in zeta potential. From the TEM images given in Figure 6.4, it is clear that CC and EC flocs are structurally very distinct. It is possible that the CC flocs have a structure that is better at binding with itself.

Figure 6.4c and Figure 6.4d give TEM images of CC and EC flocs that were found only when working in the high salt solution. These images show dense structures, which is contradictory to the scattering exponent result indicating that flocs were more compact when formed in the low salt solution. This can be explained by the absence of a slow mixing phase in this experiment. Double layer compression, which reduces the electrical repulsion between particles (Edzwald and Haarhoff, 2011), combined with this experiment's relatively high mixing intensity likely created the dense structures observed via TEM. However, the mixing also sheared apart these structures, which is likely why the flocs seen in Figure 6.4c and Figure 6.4d are not more prevalent.

6.5.2 Floc Size

Flocs were largest when produced using CC in the low salt solution (Section 6.4.5). This occurred despite the EC jar tests dosing 36% more iron (discussed in Section 6.3.4), as using larger quantities of coagulant tends to result in larger flocs due to increased particle concentrations (Duan and Gregory, 2003; Spicer and Pratsinis, 1996). When electrocoagulating lake water, Bagga et al. (2008) found that ferrous iron was produced in significant portions when operating at pH 6.4, resulting in smaller flocs. However, iron speciation was likely irrelevant to floc size in this experiment given that pH was not a significant factor (ferric iron almost certainly would have been dominant at pH 8.3). This is also in contrast to the findings of Harif et al. (2012); they observed that, at an aluminum dose of 2.4 mg/L, flocs from both CC and EC jar tests with an a final pH between roughly 6 and 7 had modal diameters around 380 μm. Furthermore, one might expect larger flocs to form in the solution with the higher ionic strength, as double layer compression reduces the repulsion between particles.

One explanation is that because EC flocs and high salt flocs were both less compact than their counterparts (Section 6.4.3), they were more prone to breakage. Compact flocs are thought to be stronger, as there are more bonds holding the aggregate together (Jarvis et al. 2005a). This is particularly relevant in the absence of a slow mixing phase, which prevented the formation of loosely-bound, open-structured flocs. The CC cases had consistently higher scattering exponents throughout the test duration (Figure 6.3). Furthermore, as illustrated by Figure 6.5, the floc size distributions for the EC cases tended to span broader size ranges, possibly indicating the presence of fragmented flocs.

6.5.3 Floc Growth

The times required for the floc size distributions to reach steady-state were heavily dependent upon the interaction method of dosing-final pH (Section 6.4.5). While the CC-pH 6.0 and EC-pH 8.3 cases performed similarly (averaging 8.0 and 7.8 minutes, respectively), the CC-pH 8.3 cases averaged 9.0 minutes, and EC-pH 6.0 cases 11.0 minutes. Thus, if stabilization times can be taken as a performance metric, EC performed better at pH 8.3, while CC performed better at pH 6.0. This can be attributed to pH levels over time (Section 6.4.1), as well as localized pH zones near the electrode surfaces.

Iron-hydroxides tend to be fairly insoluble over a broad pH range. Their minimum solubility occurs between approximately pH 6.5 and 9, assuming a solution with zero ionic strength at 25 °C (Duan and Gregory, 2003). Furthermore, Edzwald and Haarhoff (2011) calculated that the minimum solubility of amorphous ferric hydroxide in seawater is around pH 7 or 8, depending on the temperature. The CC-pH 8.3 tests started at an average pH of 8.92, which is somewhat high for effective iron precipitation, making them slower to stabilize. In contrast, the CC-pH 6.0 cases were at an effective pH for the entire experimental duration. For the EC cases, the bulk solutions were all stable in pH during the tests. As such, the EC-pH 8.3 cases remained well within the optimum pH range for iron precipitation, resulting in comparatively fast stabilization times. In contrast, the EC-pH 6.0 cases were slow to reach steady-state; while the bulk solution was within the appropriate pH range, localized acidity near the anode due to the hydrolysis of iron cations may have prevented effective precipitation (Chen et al. 2002; Zhu et al. 2005). The EC cases also benefited from coagulant overdose (discussed in Section 6.3.4), as

aggregation rate increases as a result of particle availability (Duan and Gregory, 2003; Kusters et al. 1997).

6.6 Conclusions

This research compared the growth and structure of flocs produced from chemical coagulation (CC) and electrocoagulation (EC). Three factors were considered: method of dosing, salt concentration, and final pH. In a water treatment train, floc characteristics are pertinent to the operation of downstream processes. This work adds to the limited body of literature available regarding EC flocs, both in general and in salt water. The key findings are summarized below:

- Flocs were typically more compact when formed from CC rather than EC (with average scattering exponents of 2.60 versus 2.31), in low rather than high salt solution (2.51 versus 2.40), and at pH 8.3 rather than pH 6.0 (2.53 versus 2.38). From transmission electron microscopy (TEM), it was clear that CC and EC flocs were structurally different, possibly affecting the scattering exponent. Flocs formed in low salt and at pH 8.3 were more stable in solution than their counterparts, and likely required more collisions to form, producing denser structures.
- Flocs were larger when produced via CC rather than EC (on average, 254 μm versus 144 μm) and in low rather than high salt solution (222 μm versus 181 μm). Under these conditions, the flocs formed were more compact than their

counterparts, and therefore less likely to break. Floc strength was particularly relevant to floc size in this experiment, as no slow mixing phase was employed.

- The time needed for a floc size distribution to achieve steady-state was strongly dependent upon the interaction method of dosing-final pH. The CC-pH 6.0 and EC-pH 8.3 cases had similarly fast stabilization times (respectively averaging 8.0 and 7.8 minutes), as they were both at an appropriate pH for iron precipitation throughout the experiments. The CC-pH 8.3 cases (9.0 minutes) were initially adjusted close to pH 9 in order to account for the acidity of the coagulant, while the EC-pH 6.0 cases (11.0 minutes) may have suffered from localized acidity near the anode. At such pH levels, precipitation was less successful.

CHAPTER 7: SUMMARY

EC is not currently a well established water treatment technology, largely because of a lack of systematic research. Although many studies have proved that EC is effective at the bench-scale for the treatment of a wide variety of water types, the technology suffers from a lack of standardized design and operational procedures, as well as a lack of research regarding the mechanisms of how it functions. To become a viable technology, EC requires more research regarding its design, operation, and resultant effects. This work attempted to address a narrow portion of this broad research gap.

The objective of this thesis was to investigate the production efficiency, growth and structure of flocs from EC. Because this research used a bench-scale system and synthetic solutions, more testing is required before definite conclusions can be drawn regarding full-scale EC performance. Nevertheless, as many of the experimental parameters (e.g., cathode material, electrolyte composition) and studied outcomes (e.g., floc characteristics) were chosen because of their invariance to scale, many of the results found are relevant to the design or operation of EC systems, or to the study of EC floc characteristics. Table 7.1 summarizes the conclusions found in this thesis.

Table 7.1: Summary of conclusions

Chapter	Conclusion	Relevance
2	There is very little in the literature regarding the effects of electrode configuration, which would be a significant issue for scale-up from laboratory to full-scale operation.	EC system design or operation
2	It was observed that the operational procedures reported in the literature were largely dependent upon the characteristics of the wastewater under treatment.	EC system design or operation
4	Using a SS cathode rather than an Al one resulted in faster and more efficient iron generation. This was likely because the hydrogen evolution half-reaction at the cathode surface occurs more quickly on SS than on Al.	EC system design or operation
4	The EC system produced more iron per unit power when operated at lower voltages. This suggests that it may be more efficient to design EC systems to use more electrodes at low power, rather than fewer electrodes at high power.	EC system design or operation
5	Operating at higher currents resulted in larger flocs and floc size distributions reaching steady-state more quickly. However, comparing plots of scattering exponent against time revealed that the structural progression of the flocs was unaffected.	EC system design or operation/floc characteristic

Chapter	Conclusion	Relevance
5	During floc growth, changes in scattering exponent were reflected by changes in particle size. Flocs initially spanned a broad size range and formed loose, open structures. These initial aggregates then broke and formed into more compact structures.	Floc characteristic
6	The time needed for a floc size distribution to achieve steady-state was strongly dependent upon the method of dosing (CC or EC) and the final pH. CC-pH 6.0 and EC-pH 8.3 cases had similar stabilization times, likely because they were both at an appropriate pH for iron precipitation throughout the experiments.	EC system design or operation/floc characteristic
6	Flocs were typically more compact when formed from CC rather than EC, in low rather than high salt solution, and at pH 8.3 rather than pH 6.0. TEM imaging revealed that CC and EC flocs were structurally different, which possibly affected the scattering exponent. Flocs formed in low salt and at pH 8.3 were more stable in solution than their counterparts, and likely required more collisions to form, producing denser structures.	Floc characteristic

Chapter	Conclusion	Relevance
6	Flocs were larger when produced via CC rather than EC and in low rather than high salt solution. Under these conditions, the flocs formed were more compact than their counterparts and therefore likely less prone to breakage. Floc strength was particularly relevant to floc size in this experiment, as no slow mixing phase was employed.	Floc characteristic

CHAPTER 8: CONCLUSIONS

Chapter 4 found that the cathode material affected the rate and efficiency of iron generation at the anode. This was likely due an inherent property of the material—that is, the magnitude of the exchange current density for the HER on the cathode surface. As such, one would expect to find differences in both rate and efficiency when comparing the materials tested (SS316 and aluminum) at any scale of operation. Nevertheless, tests at the pilot-scale could determine how the magnitudes of these effects alter with scale. At the bench-scale, future experiments should consider a greater variety of materials; the various grades of steel may be of particular interest, given their widespread use. Furthermore, additional experiments using genuine wastewaters (rather than a synthetic formula) would provide a greater understanding of EC performance in practice. In addition, the conclusion that it may be more efficient to operate an EC system using more electrodes at low power rather than vice versa should be tested directly.

Chapters 5 and 6 explored the growth and structure of EC flocs. As with Chapter 4, additional experiments should be conducted using genuine wastewaters. This is particularly relevant given that the solutions used in Chapters 5 and 6 did not include a target pollutant. Future tests should also incorporate rapid and slow mixing phases, unlike the single mixing intensity used in this research. Such experiments could also be expanded to test floc strength. Finally, the analysis of floc structure should be expanded. For example, X-ray diffraction could provide definite information regarding the amorphous or crystalline nature of EC flocs.

REFERENCES

Adhoum, N., & Monser, L. (2004). Decolourization and removal of phenolic compounds from olive mill wastewater by electrocoagulation. *Chemical Engineering and Processing, 43*(10), 1281-1287. doi:10.1016/j.cep.2003.12.001

Ahmad, Z. (2006). Corrosion Kinetics. *Principles of corrosion engineering and corrosion control* (pp. 57-119). Jordan Hill, Oxford, UK: Butterworth-Heinemann.

Ahmadun, F., Pendashteh, A., Abdullah, L. C., Biak, D. R. A., Madaeni, S. S., & Abidin, Z. Z. (2009). Review of technologies for oil and gas produced water treatment. *Journal of Hazardous Materials, 170*(2), 530-551.

Bagga, A., Chellam, S., & Clifford, D. A. (2008). Evaluation of iron chemical coagulation and electrocoagulation pretreatment for surface water microfiltration. *Journal of Membrane Science, 309*(1-2), 82-93.

Bard, A. J., & Faulkner, L. R. (2001). Electrochemical instrumentation. *Electrochemical methods: Fundamentals and applications* (pp. 647). New York, New York: John Wiley & Sons, Inc.

Baudequin, C., Couallier, E., Rakib, M., Deguerry, I., Severac, R., & Pabon, M. (2011). Purification of firefighting water containing a fluorinated surfactant by reverse osmosis coupled to electrocoagulation–filtration. *Separation and Purification Technology, 76*(3), 275-282. doi:10.1016/j.seppur.2010.10.016

Biggs, S., Habgood, M., Jameson, G. J., & Yan, Y. (2000). Aggregate structures formed via a bridging flocculation mechanism. *Chemical Engineering Journal, 80*(1-3), 13-22. doi:10.1016/S1383-5866(00)00072-1

Bockris, J. O., & Reddy, A. K. N. (2000). Electrochemistry in materials science. *Modern electrochemistry 2B: Electrodics in chemistry, engineering, biology, and environmental science* (2nd ed., pp. 1693-1726). New York, New York: Kluwer Academic/Plenum Publishers.

Bockris, J. O., Reddy, A. K. N., & Gamboa-Aldeco, M. (2000). Electrodics. *Modern electrochemistry 2A: Fundamentals of electrodics* (2nd ed., pp. 1166-1169). New York, New York: Kluwer Academic/Plenum Publishers.

Bouyer, D., Coufort, C., Liné, A., & Do-Quang, Z. (2005). Experimental analysis of floc size distributions in a 1-L jar under different hydrodynamics and physicochemical conditions. *Journal of Colloid and Interface Science, 292*(2), 413-428. doi:10.1016/j.jcis.2005.06.011

Bukhari, A. A. (2008). Investigation of the electro-coagulation treatment process for the removal of total suspended solids and turbidity from municipal wastewater. *Bioresource Technology, 99*(5), 914-921. doi:10.1016/j.biortech.2007.03.015

Cañizares, P., Jiménez, C., Martínez, F., Rodrigo, M. A., & Sáez, C. (2009). The pH as a key parameter in the choice between coagulation and electrocoagulation for the treatment of wastewaters. *Journal of Hazardous Materials, 163*(1), 158-164. doi:10.1016/j.jhazmat.2008.06.073

Cañizares, P., Martínez, F., Jiménez, C., Sáez, C., & Rodrigo, M. A. (2008). Coagulation and electrocoagulation of oil-in-water emulsions. *Journal of Hazardous Materials, 151*(1), 44-51. doi:10.1016/j.jhazmat.2007.05.043

Carmona, M., Khemis, M., Leclerc, J., & Lapicque, F. (2006). A simple model to predict the removal of oil suspensions from water using the electrocoagulation technique. *Chemical Engineering Science, 61*(4), 1237-1246. doi:10.1016/j.ces.2005.08.030

Canadian Council of Ministers of the Environment. (2007). Summary of Canadian water quality guidelines for the protection of aquatic life. Retrieved from http://www.ccme.ca/en/resources/canadian_environmental_quality_guidelines/

Chakraborti, R. K., Atkinson, J. F., & Van Benschoten, J. E. (2000). Characterization of alum floc by image analysis. *Environmental Science & Technology, 34*(18), 3969-3976.

Chakraborti, R. K., Gardner, K. H., Atkinson, J. F., & Van Benschoten, J. E. (2003). Changes in fractal dimension during aggregation. *Water Research, 37*(4), 873-883.

Chavalparit, O., & Ongwandee, M. (2009). Optimizing electrocoagulation process for the treatment of biodiesel wastewater using response surface methodology. *Journal of Environmental Sciences, 21*(11), 1491-1496. doi:10.1016/S1001-0742(08)62445-6

Chen, X., Chen, G., & Yue, P. L. (2000). Separation of pollutants from restaurant wastewater by electrocoagulation. *Separation and Purification Technology, 19*(1-2), 65-76.

Chen, X., Chen, G., & Yue, P. L. (2002). Investigation on the electrolysis voltage of electrocoagulation. *Chemical Engineering Science, 57*(13), 2449-2455.

Cornelissen, A., Burnett, M. G., McCall, R. D., & Goddard, D. T. (1997). The structure of hydrous flocs prepared by batch and continuous flow water treatment systems and obtained by optical, electron and atomic force microscopy. *Water Science and Technology, 36*(4), 41-48.

Den, W., & Wang, C. (2008). Removal of silica from brackish water by electrocoagulation pretreatment to prevent fouling of reverse osmosis membranes. *Separation and Purification Technology, 59*, 318-325. doi:10.1016/j.seppur.2007.07.025

Duan, J., & Gregory, J. (2003). Coagulation by hydrolysing metal salts. *Advances in Colloid and Interface Science, 100-102*, 475-502.

Dubrawski, K. L., & Mohseni, M. (2013). Standardizing electrocoagulation reactor design: Iron electrodes for NOM removal. *Chemosphere, 91*(1), 55-60. doi:10.1016/j.chemosphere.2012.11.075

Edzwald, J. K., & Haarhoff, J. (2011). Seawater pretreatment for reverse osmosis: Chemistry, contaminants, and coagulation. *Water Research, 45*(17), 5428-5440. doi:10.1016/j.watres.2011.08.014

El-Naas, M. H., Al-Zuhair, S., Al-Lobaney, A., & Makhlouf, S. (2009). Assessment of electrocoagulation for the treatment of petroleum refinery wastewater. *Journal of Environmental Management, 91*(1), 180-185.

Gamage, N. P., & Chellam, S. (2014). Mechanisms of physically irreversible fouling during surface water microfiltration and mitigation by aluminum electroflotation pretreatment. *Environmental Science & Technology, 48,* 1148-1157.

Gao, S., Du, M., Tian, J., Yang, J., Yang, J., Ma, F., & Nan, J. (2010). Effects of chloride ions on electro-coagulation-flotation process with aluminum electrodes for algae removal. *Journal of Hazardous Materials, 182,* 827-834.

Gomes, J., Cocke, D., Das, K., Guttula, M., Tran, D., & Beckman, J. (2009). Treatment of produced water by electrocoagulation. *EPD Congress 2009: Proceedings of Sessions and Symposia Held during TMS 2009 Annual Meeting & Exhibition,* San Francisco, California. 459-456.

Gregory, J. (1997). The density of particle aggregates. *Water Science and Technology, 36*(4), 1-13.

Gregory, J. (2004). Monitoring floc formation and breakage. *Water Science and Technology, 50*(12), 163-170.

Gregory, J. (2006). *Particles in water: Properties and processes*. Boca Raton, Florida, US: CRC Press.

Harif, T., Khai, M., & Adin, A. (2012). Electrocoagulation versus chemical coagulation: Coagulation/flocculation mechanisms and resulting floc characteristics. *Water Research, 46*(10), 3177-3188. doi:10.1016/j.watres.2012.03.034

Holt, P. K., Barton, G. W., & Mitchell, C. A. (2005). The future for electrocoagulation as a localised water treatment technology. *Chemosphere, 59*(3), 355-367. doi:10.1016/j.chemosphere.2004.10.023

Inan, H., Dimoglo, A., Şimşek, H., & Karpuzcu, M. (2004). Olive oil mill wastewater treatment by means of electro-coagulation. *Separation and Purification Technology, 36*(1), 23-31. doi:10.1016/S1383-5866(03)00148-5

Jarvis, P., Jefferson, B., & Parsons, S. A. (2005b). Breakage, regrowth, and fractal nature of natural organic matter flocs. *Environmental Science & Technology, 39*(7), 2307-2314. doi:10.1021/es048854x

Jarvis, P., Jefferson, B., & Parsons, S. A. (2006). Floc structural characteristics using conventional coagulation for a high doc, low alkalinity surface water source. *Water Research, 40*(14), 2727-2737.

Jarvis, P., Jefferson, B., Gregory, J., & Parsons, S. A. (2005a). A review of floc strength and breakage. *Water Research, 39*(14), 3121-3137. doi:10.1016/j.watres.2005.05.022

Jiang, J., Graham, N., André, C., Kelsall, G. H., & Brandon, N. (2002). Laboratory study of electro-coagulation–flotation for water treatment. *Water Research, 36*(16), 4064-4078.

Jolivet, J., Chanéac, C., & Tronc, E. (2004). Iron oxide chemistry. from molecular clusters to extended solid networks. *Chemical Communications,* (5), 481-487. doi:10.1039/b304532n

Jung, S. J., Amal, R., & Raper, J. A. (1996). Monitoring effects of shearing on floc structure using small-angle light scattering. *Powder Technology, 88*(1), 51-54. doi:10.1016/0032-5910(96)03102-6

Khosla, N. K., Venkatachalam, S., & Somasundaran, P. (1991). Pulsed electrogeneration of bubbles for electroflotation. *Journal of Applied Electrochemistry, 21*(11), 986-990. doi:10.1007/BF01077584

Kusters, K. A., Wijers, J. G., & Thoenes, D. (1997). Aggregation kinetics of small particles in agitated vessels. *Chemical Engineering Science, 52*(1), 107-121.

Larue, O., & Vorobiev, E. (2003). Floc size estimation in iron induced electrocoagulation and coagulation using sedimentation data. *International Journal of Mineral Processing, 71*, 1-15. doi:10.1016/S0301-7516(03)00026-7

Lee, K., Tong, L. T., Millero, F. J., Sabine, C. L., Dickson, A. G., Goyet, C., . . . Key, R. M. (2006). Global relationships of total alkalinity with salinity and temperature in surface waters of the world's oceans. *Geophysical Research Letters, 33*(19), L19605. doi:10.1029/2006GL027207

Lee, S. Y., & Gagnon, G. A. (2014). Review of the factors relevant to the design and operation of an electrocoagulation system for wastewater treatment. *Environmental Reviews, 22*(4), 421-429.

Lee, S. Y., & Gagnon, G. A. (2015). The rate and efficiency of iron generation in an electrocoagulation system. *Environmental Technology, 36*(19), 2419-2427. doi:10.1080/09593330.2015.1032367

Li, D., & Ganczarczyk, J. (1989). Fractal geometry of particle aggregates generated in water and wastewater treatment processes. *Environmental Science & Technology, 23*(11), 1385-1389.

Li, T., Zhu, Z., Wang, D., Yao, C., & Tang, H. (2006). Characterization of floc size, strength and structure under various coagulation mechanisms. *Powder Technology, 168*(2), 104-110. doi:10.1016/j.powtec.2006.07.003

Malakootian, M., Mansoorian, H. J., & Moosazadeh, M. (2010). Performance evaluation of electrocoagulation process using iron-rod electrodes for removing hardness from drinking water. *Desalination, 255*(1), 67-71. doi:10.1016/j.desal. 2010.01.015

McLellan, H. J. (1965). The chemical nature of the ocean. *Elements of physical oceanography* (pp. 16-24). Oxford, UK: Pergamon Press.

Mollah, M. Y. A., Schennach, R., Parga, J. R., & Cocke, D. L. (2001). Electrocoagulation (EC) — science and applications. *Journal of Hazardous Materials, B84*, 29-41.

Moreno, C. H. A., Cocke, D. L., Gomes, J. A. G., Morkovsky, P., Parga, J. R., Peterson, E., & Garcia, C. (2009). Electrochemical reactions for electrocoagulation using iron electrodes. *Industrial & Engineering Chemistry Research, 48*(4), 2275-2282. doi:10.1021/ie8013007

Morgan, B., & Lahav, O. (2007). The effect of pH on the kinetics of spontaneous Fe(II) oxidation by O_2 in aqueous solution - basic principles and a simple heuristic description. *Chemosphere, 68*(11), 2080-2084.

MWH, Crittenden, J. C., Trussell, R. R., Hand, D. W., Howe, K. J., & Tchobanoglous, G. (2005). Coagulation, mixing, and flocculation. *Water treatment: Principles and design* (2nd ed., pp. 643-777). Hoboken, New Jersey: John Wiley & Sons, Inc.

Nørskov, J. K., Bligaard, T., Logadottir, A., Kitchin, J. R., Chen, J. G., Pandelov, S., & Stimming, U. (2005). Trends in the exchange current for hydrogen evolution. *Journal of the Electrochemical Society, 152*(3), J23-J26. doi:10.1149/1.1856988

Picard, T., Cathalifaud-Feuillade, G., Mazet, M., & Vandensteendam, C. (2000). Cathodic dissolution in the electrocoagulation process using aluminium electrodes. *Journal of Environmental Monitoring, 2*, 77-80. doi:10.1039/A908248D

Rattanakawin, C., & Hogg, R. (2001). Aggregate size distributions in flocculation. *Colloids and Surfaces A: Physicochemical and Engineering Aspects, 177*(2-3), 87-98.

Roberge, P. R. (2008). Corrosion Kinetics and Applications of Electrochemistry to Corrosion. *Corrosion Engineering: Principles and Practice* (pp. 85-144). New York, New York: McGraw-Hill.

Sari, M. A., & Chellam, S. (2015). Mechanisms of boron removal from hydraulic fracturing wastewater by aluminum electrocoagulation. *Journal of Colloid and Interface Science, 458,* 103-111.

Spicer, P. T., & Pratsinis, S., E. (1996). Shear-induced flocculation: The evolution of floc structure and the shape of the size distribution at steady state. *Water Research, 30*(5), 1049-1056.

Stumm, W., & Lee, G. F. (1961). Oxygenation of ferrous iron. *Industrial & Engineering Chemistry, 53*(2), 143-146. doi:10.1021/ie50614a030

Tang, S., Preece, J. M., McFarlane, C. M., & Zhang, Z. (2000). Fractal morphology and breakage of DLCA and RLCA aggregates. *Journal of Colloid and Interface Science, 221*(1), 114-123.

Tanneru, C.T., & Chellam, S. (2012). Mechanisms of virus control during iron electrocoagulation – Microfiltration of surface water. *Water Research, 46,* 2111-2120.

Timmes, T. C., Kim, H., & Dempsey, B. A. (2010). Electrocoagulation pretreatment of seawater prior to ultrafiltration: Pilot-scale applications for military water purification systems. *Desalination, 250*(1), 6-13.

Un, U. T., Koparal, A. S., & Ogutveren, U. B. (2009). Electrocoagulation of vegetable oil refinery wastewater using aluminum electrodes. *Journal of Environmental Management, 90*(1), 428-433. doi:10.1016/j.jenvman.2007.11.007

Vasudevan, S., Lakshmi, J., & Sozhan, G. (2009). Studies on a Mg-Al-Zn alloy as an anode for the removal of fluoride from drinking water in an electrocoagulation process. *Clean – Soil, Air, Water, 37*(4-5), 372-378. doi:10.1002/clen.200900031

Waite, T. D. (1999). Measurement and implications of floc structure in water and wastewater treatment. *Colloids and Surfaces A: Physicochemical and Engineering Aspects, 151*(1), 27-41.

Wan, W., Pepping, T. J., Banerji, T., Chaudhari, S., & Giammar, D. E. (2011). Effects of water chemistry on arsenic removal from drinking water by electrocoagulation. *Water Research, 45*(1), 384-392. doi:10.1016/j.watres.2010.08.016

Wang, C., Chou, W., & Kuo, Y. (2009). Removal of COD from laundry wastewater by electrocoagulation/electroflotation. *Journal of Hazardous Materials, 164*(1), 81-86.

Wei, M., Wang, K., Huang, C., Chiang, C., Chang, T., Lee, S., & Chang, S. (2012). Improvement of textile dye removal by electrocoagulation with low-cost steel wool cathode reactor. *Chemical Engineering Journal, 192*, 37-44.

Wilén, B., Jin, B., & Lant, P. (2003). Impacts of structural characteristics on activated sludge floc stability. *Water Research, 37*(15), 3632-3645. doi:10.1016/S0043-1354(03)00291-4

Yu, W., Gregory, J., & Campos, L. (2010). Breakage and regrowth of al-humic flocs - effect of additional coagulant dosage. *Environmental Science & Technology, 44*(16), 6371-6376.

Zaied, M., & Bellakhal, N. (2009). Electrocoagulation treatment of black liquor from paper industry. *Journal of Hazardous Materials, 163*, 995-1000. doi:10.1016/j.jhazmat.2008.07.115

Zhu, B., Clifford, D. A., & Chellam, S. (2005). Comparison of electrocoagulation and chemical coagulation pretreatment for enhanced virus removal using microfiltration membranes. *Water Research, 39*(13), 3098-3108.

Zodi, S., Merzouk, B., Potier, O., Lapicque, F., & Leclerc, J. (2013). Direct red 81 dye removal by a continuous flow electrocoagulation/flotation reactor. *Separation and Purification Technology, 108*, 215-222. doi:10.1016/j.seppur.2013.01.052

APPENDIX A: CHAPTER 4 DATA

Table A.1: Known or directly measured parameters

Config. No.	Replicate No.	Cathode	Electrolyte	Test Order*	Initial pH	Final pH	Applied Voltage (V)	System Current (A)	Iron Conc. (mg/L)	Iron (mg)
1	1	SS	Salts	3	5.78	6.53	0.50	0.0023	1.20	0.26
1	1	SS	Salts	7	5.78	6.25	1.02	0.0350	2.77	0.61
1	1	SS	Salts	1	5.78	5.88	1.52	0.1542	10.24	2.25
1	1	SS	Salts	6	5.78	6.40	1.62	0.2283	16.09	3.54
1	1	SS	Salts	4	5.78	6.24	2.04	0.3440	18.59	4.09
1	1	SS	Salts	5	5.78	5.87	2.28	-	-	-
1	1	SS	Salts	2	5.78	6.03	2.50	0.4880	29.14	6.41
1	1	SS	Salts	8	5.78	7.48	2.99	-	-	-
1	2	SS	Salts	4	6.04	5.91	0.50	0.0027	0.80	0.18
1	2	SS	Salts	8	6.04	6.26	1.05	0.0381	2.97	0.65
1	2	SS	Salts	2	6.04	7.05	1.50	0.1461	12.68	2.79
1	2	SS	Salts	5	6.04	6.95	1.65	0.1658	11.19	2.46
1	2	SS	Salts	3	6.04	6.16	2.01	0.2476	18.02	3.96
1	2	SS	Salts	7	6.04	7.36	2.22	0.3717	21.78	4.79
1	2	SS	Salts	1	6.04	6.46	2.48	0.4115	29.81	6.56
1	2	SS	Salts	6	6.04	6.04	2.99	0.5706	39.35	8.66

Config. No.	Replicate No.	Cathode	Electrolyte	Test Order*	Initial pH	Final pH	Applied Voltage (V)	System Current (A)	Iron Conc. (mg/L)	Iron (mg)
2	1	SS	Salts+Org	5	6.16	6.75	0.50	0.0025	0.28	0.06
2	1	SS	Salts+Org	1	6.16	6.09	1.00	0.0253	1.79	0.39
2	1	SS	Salts+Org	6	6.16	6.00	1.50	0.1106	7.18	1.58
2	1	SS	Salts+Org	7	6.16	6.37	1.78	0.1836	12.01	2.64
2	1	SS	Salts+Org	4	6.16	8.38	2.05	0.2778	16.34	3.59
2	1	SS	Salts+Org	2	6.16	7.33	2.20	0.3387	17.96	3.95
2	1	SS	Salts+Org	8	6.16	6.41	2.51	0.4410	24.20	5.32
2	1	SS	Salts+Org	3	6.16	7.32	2.98	0.5828	35.03	7.71
2	2	SS	Salts+Org	3	6.02	6.13	0.48	0.0024	0.33	0.07
2	2	SS	Salts+Org	6	6.02	6.54	1.00	0.0247	1.96	0.43
2	2	SS	Salts+Org	7	6.02	7.05	1.56	0.1630	13.65	3.00
2	2	SS	Salts+Org	1	6.02	6.10	1.71	0.1405	11.08	2.44
2	2	SS	Salts+Org	4	6.02	6.72	2.03	0.2992	15.61	3.43
2	2	SS	Salts+Org	2	6.02	6.55	2.36	0.3710	27.67	6.09
2	2	SS	Salts+Org	8	6.02	7.25	2.50	-	-	-
2	2	SS	Salts+Org	5	6.02	6.86	3.04	-	-	-
3	1	Al	Salts	7	6.14	6.27	0.51	-0.0009	0.19	0.04

Config. No.	Replicate No.	Cathode	Electrolyte	Test Order*	Initial pH	Final pH	Applied Voltage (V)	System Current (A)	Iron Conc. (mg/L)	Iron (mg)
3	1	Al	Salts	3	6.14	6.21	1.03	0.0055	0.64	0.14
3	1	Al	Salts	5	6.14	6.33	1.52	0.0599	4.95	1.09
3	1	Al	Salts	2	6.14	6.20	1.64	0.1090	7.08	1.56
3	1	Al	Salts	1	6.14	6.16	2.02	0.1884	13.81	3.04
3	1	Al	Salts	6	6.14	5.99	2.22	0.2391	16.93	3.72
3	1	Al	Salts	8	6.14	6.20	2.52	0.3150	15.16	3.34
3	1	Al	Salts	4	6.14	7.54	3.02	0.5258	27.08	5.96
3	2	Al	Salts	3	6.20	6.04	0.50	-0.0003	0.22	0.05
3	2	Al	Salts	2	6.20	6.09	0.96	0.0012	0.25	0.05
3	2	Al	Salts	7	6.20	6.10	1.56	0.0708	5.18	1.14
3	2	Al	Salts	6	6.20	6.16	1.67	0.1186	8.35	1.84
3	2	Al	Salts	5	6.20	6.10	2.01	0.2091	14.93	3.28
3	2	Al	Salts	8	6.20	6.11	2.33	0.2749	18.27	4.02
3	2	Al	Salts	1	6.20	6.11	2.48	0.3406	17.01	3.74
3	2	Al	Salts	4	6.20	6.13	3.01	0.5000	24.85	5.47
4	1	Al	Salts+Org	2	6.09	6.06	0.52	-0.0021	0.18	0.04
4	1	Al	Salts+Org	3	6.09	5.93	1.08	0.0048	0.25	0.05

Config. No.	Replicate No.	Cathode	Electrolyte	Test Order*	Initial pH	Final pH	Applied Voltage (V)	System Current (A)	Iron Conc. (mg/L)	Iron (mg)
4	1	Al	Salts+Org	7	6.09	6.01	1.56	0.0349	2.58	0.57
4	1	Al	Salts+Org	5	6.09	5.94	1.74	0.1187	8.06	1.77
4	1	Al	Salts+Org	1	6.09	6.01	2.03	0.2450	8.23	1.81
4	1	Al	Salts+Org	4	6.09	6.00	2.23	0.2241	15.08	3.32
4	1	Al	Salts+Org	6	6.09	6.23	2.51	0.3564	22.06	4.85
4	1	Al	Salts+Org	8	6.09	6.25	3.06	-	-	-
4	2	Al	Salts+Org	4	6.14	6.24	0.50	-0.0004	0.24	0.05
4	2	Al	Salts+Org	8	6.14	6.04	1.01	0.0018	0.25	0.06
4	2	Al	Salts+Org	6	6.14	6.15	1.52	0.0303	3.18	0.70
4	2	Al	Salts+Org	3	6.14	6.15	1.74	0.0827	6.95	1.53
4	2	Al	Salts+Org	2	6.14	6.03	2.04	0.0869	6.67	1.47
4	2	Al	Salts+Org	5	6.14	6.46	2.39	0.2705	20.00	4.40
4	2	Al	Salts+Org	7	6.14	6.66	2.51	0.2657	20.42	4.49
4	2	Al	Salts+Org	1	6.14	6.46	3.05	-	-	-

*For each of the 8 unique combination of Config. No. and Replicate No., Test Order spans 1 through 8

Note: Removed outliers are indicated with "-"

Table A.2: Calculated parameters

Config. No.	Replicate No.	Voltage across Cell[a] (V)	Resistance across Cell[b] (Ω)	Cell Power[c] (W)	System Power[d] (W)	Efficiency[e] (mg/W)
1	1	0.50	221.2	0.00	0.00	234.9
1	1	0.99	28.1	0.03	0.04	17.7
1	1	1.37	8.9	0.21	0.23	10.7
1	1	1.39	6.1	0.32	0.37	11.1
1	1	1.70	4.9	0.58	0.70	7.0
1	1	-	-	-	-	-
1	1	2.01	4.1	0.98	1.22	6.5
1	1	-	-	-	-	-
1	2	0.50	187.7	0.00	0.00	133.2
1	2	1.01	26.6	0.04	0.04	17.0
1	2	1.35	9.3	0.20	0.22	14.1
1	2	1.48	9.0	0.25	0.27	10.0
1	2	1.76	7.1	0.44	0.50	9.1
1	2	1.85	5.0	0.69	0.83	7.0
1	2	2.07	5.0	0.85	1.02	7.7
1	2	2.42	4.2	1.38	1.71	6.3
2	1	0.50	203.1	0.00	0.00	50.0
2	1	0.97	38.5	0.02	0.03	16.0
2	1	1.39	12.6	0.15	0.17	10.3
2	1	1.60	8.7	0.29	0.33	9.0
2	1	1.77	6.4	0.49	0.57	7.3
2	1	1.86	5.5	0.63	0.75	6.3
2	1	2.07	4.7	0.91	1.11	5.8
2	1	2.40	4.1	1.40	1.74	5.5
2	2	0.48	199.0	0.00	0.00	62.9
2	2	0.98	39.5	0.02	0.02	17.9
2	2	1.40	8.6	0.23	0.25	13.2
2	2	1.57	11.2	0.22	0.24	11.1
2	2	1.73	5.8	0.52	0.61	6.6
2	2	1.99	5.4	0.74	0.88	8.3
2	2	-	-	-	-	-
2	2	-	-	-	-	-
3	1	0.51	-	-	-	-
3	1	1.02	186.3	0.01	0.01	25.1

Config. No.	Replicate No.	Voltage across Cell[a] (V)	Resistance across Cell[b] (Ω)	Cell Power[c] (W)	System Power[d] (W)	Efficiency[e] (mg/W)
3	1	1.46	24.4	0.09	0.09	12.5
3	1	1.53	14.0	0.17	0.18	9.3
3	1	1.83	9.7	0.35	0.38	8.8
3	1	1.98	8.3	0.47	0.53	7.9
3	1	2.21	7.0	0.69	0.79	4.8
3	1	2.49	4.7	1.31	1.59	4.5
3	2	0.50	-	-	-	-
3	2	0.96	799.0	0.00	0.00	47.3
3	2	1.49	21.0	0.11	0.11	10.8
3	2	1.55	13.1	0.18	0.20	10.0
3	2	1.80	8.6	0.38	0.42	8.7
3	2	2.06	7.5	0.56	0.64	7.1
3	2	2.14	6.3	0.73	0.84	5.1
3	2	2.51	5.0	1.26	1.51	4.4
4	1	0.52	-	-	-	-
4	1	1.08	224.0	0.01	0.01	10.6
4	1	1.53	43.7	0.05	0.05	10.7
4	1	1.62	13.7	0.19	0.21	9.2
4	1	1.79	7.3	0.44	0.50	4.1
4	1	2.01	9.0	0.45	0.50	7.4
4	1	2.15	6.0	0.77	0.89	6.3
4	1	-	-	-	-	-
4	2	0.50	-	-	-	-
4	2	1.01	560.1	0.00	0.00	30.8
4	2	1.49	49.2	0.05	0.05	15.5
4	2	1.66	20.0	0.14	0.14	11.2
4	2	1.95	22.5	0.17	0.18	8.6
4	2	2.12	7.8	0.57	0.65	7.7
4	2	2.24	8.4	0.60	0.67	7.5
4	2	-	-	-	-	-

[a] $V_{Cell} = V_{Sys} - I_{Sys}$, as described in Section 3.1

[b] R_{Cell} is calculated from Equation 3.1

[c] $Power_{Cell} = V_{Cell} * I_{Sys}$

[d] $Power_{Sys} = V_{Sys} * I_{Sys}$

[e] $Efficiency = (Iron\ Generated)/Power_{Cell}$

Note: Removed outliers are indicated with "-"

APPENDIX B: CHAPTER 5 DATA

Table B.1: General Data

Case No.	Replicate No.	Test Order	pH Initial	pH Final	Conductivity Initial (mS/cm)	Conductivity Final (mS/cm)	Median Current (A)	Iron Concentration (mg/L)
1	1	5	5.48	6.01	60.16	59.47	0.091	5.58
1	2	10	5.47	6.05	58.35	59.13	n/a	5.78
2	1	1	5.37	5.99	63.88	63.00	0.178	9.90
2	2	8	5.42	n/a	58.67	n/a	n/a	10.85
3	1	2	5.41	6.01	63.48	63.69	0.272	17.43
3	2	12	5.54	6.00	59.03	58.22	n/a	17.14
4	1	4	5.44	6.10	61.02	60.09	0.093	6.03
4	2	7	5.45	6.05	62.01	58.21	n/a	5.59
5	1	6	5.44	5.94	58.08	56.50	0.175	10.68
5	2	9	5.47	5.97	58.86	57.94	0.174	11.12
6	1	3	5.47	5.80	62.04	62.46	0.268	17.13
6	2	11	5.54	5.96	59.03	58.61	0.266	16.62

Table B.2: Scattering exponent and percentile particle size (μm) data over time

Case No.	Replicate No.	Time (min)	D_x (10)	D_x (50)	D_x (90)	Scattering Exponent	R^2 *
1	1	1	4.8	21.5	30.9	1.92	0.99
1	1	2	0.8	26.7	40.9	1.22	0.99
1	1	3	0.5	16.7	33.6	1.16	0.98
1	1	4	0.5	3.4	30.4	1.04	0.97
1	1	5	25.1	386.0	549.3	1.09	0.97
1	1	6	1.1	6.0	21.1	1.76	1.00
1	1	7	5.1	16.9	35.1	2.00	1.00
1	1	8	16.3	44.1	89.3	2.15	1.00
1	1	9	29.3	77.7	155.2	2.26	1.00
1	1	10	36.3	95.7	190.3	2.34	1.00
1	1	11	40.2	102.9	215.8	2.37	1.00
1	2	1	38.1	231.3	1179.1	1.98	0.96
1	2	2	5.3	362.0	657.6	1.32	0.98
1	2	3	1.7	860.1	2190.0	1.10	0.95
1	2	4	0.5	3.1	30.7	1.02	0.96
1	2	5	0.6	2.4	26.9	1.07	0.95
1	2	6	1.2	7.4	58.2	1.67	0.99
1	2	7	4.4	15.6	38.2	1.96	1.00
1	2	8	13.3	36.9	75.4	2.15	1.00
1	2	9	26.9	71.8	143.3	2.24	1.00
1	2	10	36.7	96.6	191.7	2.31	1.00
1	2	11	41.3	104.7	213.4	2.34	1.00
2	1	1	623.2	1338.9	2397.8	1.67	0.99
2	1	2	17.2	1321.3	2457.4	1.13	0.99
2	1	3	0.5	5.1	272.4	1.00	0.97
2	1	4	1.0	9.6	1618.3	1.51	0.99
2	1	5	5.1	21.5	1058.1	1.87	1.00
2	1	6	31.0	85.6	164.4	2.14	1.00
2	1	7	51.9	140.8	279.4	2.23	1.00
2	1	8	55.8	152.8	311.4	2.28	1.00
2	1	9	54.8	155.5	316.7	2.32	1.00
2	1	10	57.7	164.1	340.4	2.33	1.00
2	1	11	55.9	162.5	332.8	2.35	1.00
2	2	1	9.0	155.2	264.6	1.31	0.97

Case No.	Replicate No.	Time (min)	D_x (10)	D_x (50)	D_x (90)	Scattering Exponent	R^2 *
2	2	2	0.6	26.9	162.3	1.11	0.99
2	2	3	0.6	17.9	179.9	1.06	0.98
2	2	4	0.9	7.1	1058.8	1.55	0.99
2	2	5	5.6	22.4	48.4	1.88	1.00
2	2	6	32.2	90.5	177.4	2.14	1.00
2	2	7	49.4	136.2	272.1	2.24	1.00
2	2	8	53.4	149.2	308.0	2.29	1.00
2	2	9	54.5	156.3	315.9	2.32	1.00
2	2	10	54.2	160.8	330.1	2.34	1.00
2	2	11	54.2	159.7	325.2	2.35	1.00
3	1	1	0.8	33.6	448.9	1.24	0.97
3	1	2	0.6	23.5	496.1	1.07	0.97
3	1	3	0.7	5.7	58.7	1.26	0.97
3	1	4	6.9	26.8	57.1	1.89	1.00
3	1	5	44.4	123.4	242.2	2.12	1.00
3	1	6	64.2	179.9	371.0	2.19	1.00
3	1	7	69.3	189.5	382.4	2.24	1.00
3	1	8	67.2	191.7	377.0	2.27	1.00
3	1	9	65.7	191.9	382.6	2.29	1.00
3	1	10	67.9	199.2	394.1	2.30	1.00
3	1	11	66.6	197.1	397.1	2.31	1.00
3	2	1	4.4	54.7	161.2	1.39	0.99
3	2	2	1.1	62.3	1996.7	1.17	0.98
3	2	3	0.8	6.4	46.0	1.27	0.98
3	2	4	6.0	24.0	53.1	1.88	1.00
3	2	5	40.7	115.5	227.2	2.13	1.00
3	2	6	62.7	176.8	341.9	2.20	1.00
3	2	7	66.3	189.6	368.2	2.25	1.00
3	2	8	65.8	189.0	372.2	2.28	1.00
3	2	9	65.8	192.0	377.8	2.30	1.00
3	2	10	66.0	194.5	393.9	2.31	1.00
3	2	11	64.9	195.2	397.8	2.31	1.00
4	1	1	5.1	17.6	28.0	2.06	0.95
4	1	2	8.0	38.7	75.0	1.55	0.98
4	1	3	37.6	166.1	300.3	1.60	0.98
4	1	4	18.5	104.7	201.3	1.48	0.98

Case No.	Replicate No.	Time (min)	D_x (10)	D_x (50)	D_x (90)	Scattering Exponent	R^2 *
4	1	5	5.3	152.0	321.1	1.42	0.99
4	1	6	3.1	126.3	308.7	1.36	0.99
4	1	7	3.3	12.6	57.2	1.93	1.00
4	1	8	8.5	24.5	57.4	2.08	1.00
4	1	9	17.3	46.3	95.3	2.22	1.00
4	1	10	26.9	68.6	137.0	2.30	1.00
4	1	11	32.7	81.8	156.0	2.34	1.00
4	2	1	32.4	657.9	952.2	1.73	0.94
4	2	2	21.8	180.0	480.1	1.58	0.95
4	2	3	20.6	1114.5	2297.7	1.17	0.96
4	2	4	4.1	997.1	2245.9	1.08	0.97
4	2	5	1.3	577.9	2065.7	1.13	0.97
4	2	6	1.0	7.3	522.6	1.56	0.99
4	2	7	3.1	15.2	490.0	1.85	1.00
4	2	8	6.8	20.7	51.7	2.03	1.00
4	2	9	14.5	39.7	87.9	2.17	1.00
4	2	10	23.9	61.9	123.2	2.26	1.00
4	2	11	32.4	82.1	165.4	2.31	1.00
5	1	1	22.8	340.5	526.1	1.75	0.99
5	1	2	3.1	32.8	79.7	1.40	0.97
5	1	3	1.5	50.9	214.2	1.31	0.99
5	1	4	1.2	31.7	120.5	1.30	0.99
5	1	5	3.6	20.4	126.7	1.80	1.00
5	1	6	19.4	56.1	115.0	2.07	1.00
5	1	7	39.0	106.9	210.6	2.23	1.00
5	1	8	46.9	125.4	253.0	2.29	1.00
5	1	9	48.3	134.2	261.5	2.32	1.00
5	1	10	50.1	140.0	279.4	2.34	1.00
5	1	11	49.5	138.3	274.0	2.35	1.00
5	2	1	3.5	29.8	173.4	1.75	0.99
5	2	2	3.5	38.0	1269.1	1.49	1.00
5	2	3	1.4	30.2	83.0	1.38	0.99
5	2	4	1.8	23.7	65.7	1.51	0.99
5	2	5	8.0	28.1	62.5	1.95	1.00
5	2	6	30.4	86.9	175.4	2.17	1.00
5	2	7	40.3	111.5	224.0	2.27	1.00

Case No.	Replicate No.	Time (min)	D_x (10)	D_x (50)	D_x (90)	Scattering Exponent	R^2 *
5	2	8	42.6	120.5	252.2	2.31	1.00
5	2	9	43.7	126.8	257.6	2.33	1.00
5	2	10	43.3	127.1	255.1	2.35	1.00
5	2	11	43.6	128.3	255.1	2.36	1.00
6	1	1	0.4	2.2	14.2	1.15	0.98
6	1	2	0.5	4.8	30.6	1.07	0.98
6	1	3	0.7	6.2	75.7	1.13	0.98
6	1	4	3.0	14.8	37.4	1.81	1.00
6	1	5	30.5	85.8	169.7	2.11	1.00
6	1	6	60.9	164.7	326.1	2.20	1.00
6	1	7	69.1	192.0	398.2	2.27	1.00
6	1	8	70.8	197.8	405.5	2.30	1.00
6	1	9	71.2	198.0	395.8	2.32	1.00
6	1	10	68.4	195.3	371.4	2.34	1.00
6	1	11	70.5	206.3	408.9	2.34	1.00
6	2	1	21.9	36.1	59.8	1.71	0.95
6	2	2	2.5	34.9	70.7	1.36	0.95
6	2	3	1.2	31.0	133.7	1.33	0.99
6	2	4	4.2	20.5	61.4	1.83	1.00
6	2	5	34.3	98.2	192.9	2.11	1.00
6	2	6	53.3	148.5	292.4	2.20	1.00
6	2	7	56.2	160.1	315.5	2.26	1.00
6	2	8	56.8	165.6	323.7	2.29	1.00
6	2	9	57.1	166.3	327.7	2.31	1.00
6	2	10	56.7	167.3	328.6	2.32	1.00
6	2	11	54.8	164.8	320.3	2.33	1.00

*R^2 is the coefficient of determination calculated for the linear relationship between *log(I)* and *log(Q)*. The calculation of scattering exponent is described in Section 3.2.4.

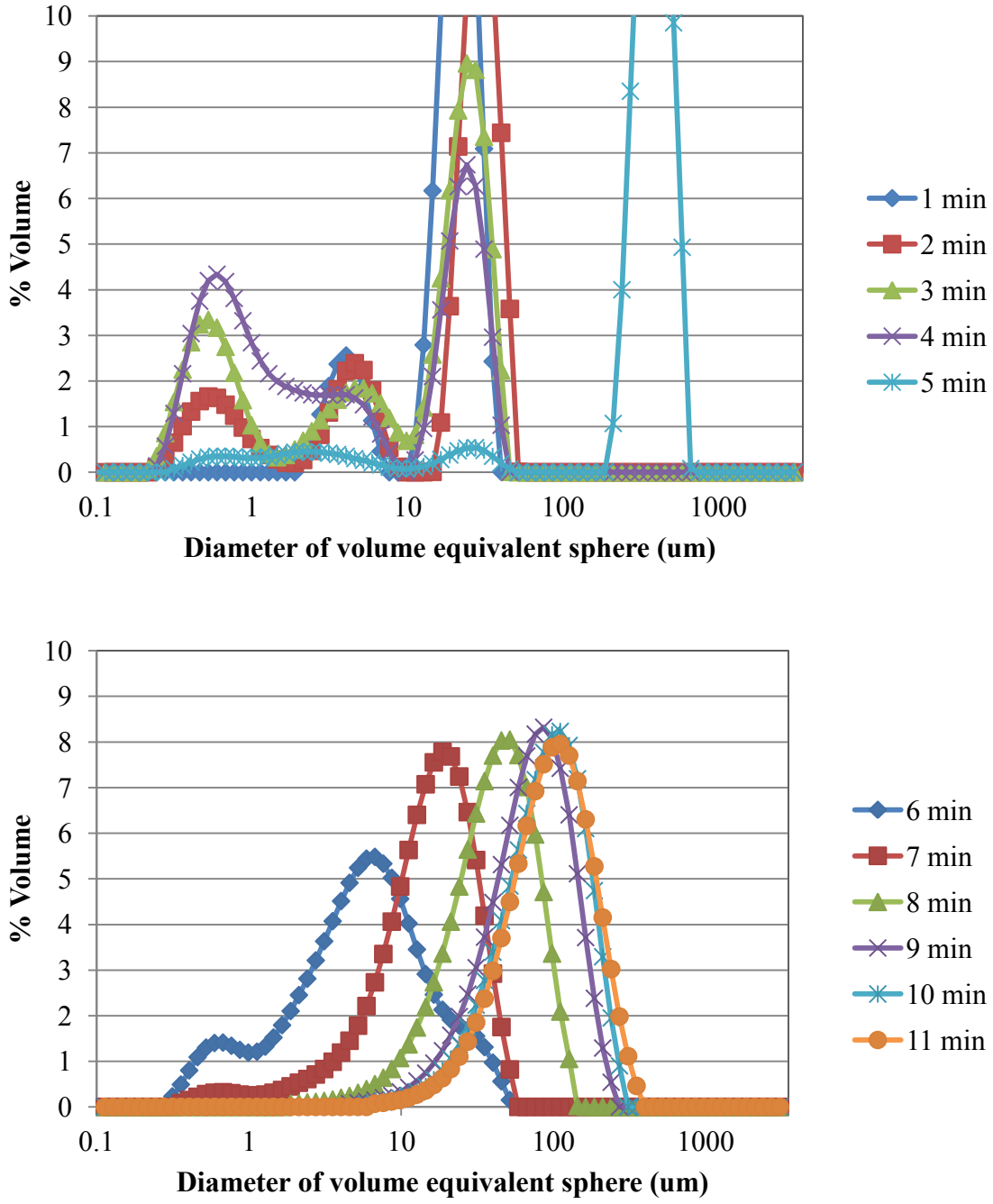

Figure B.1: Floc size distributions generated over time for Case No. 1 (Replicate No. 1). Iron was continuously generated from a sacrificial anode for the first five minutes, after which the iron dosing was stopped.

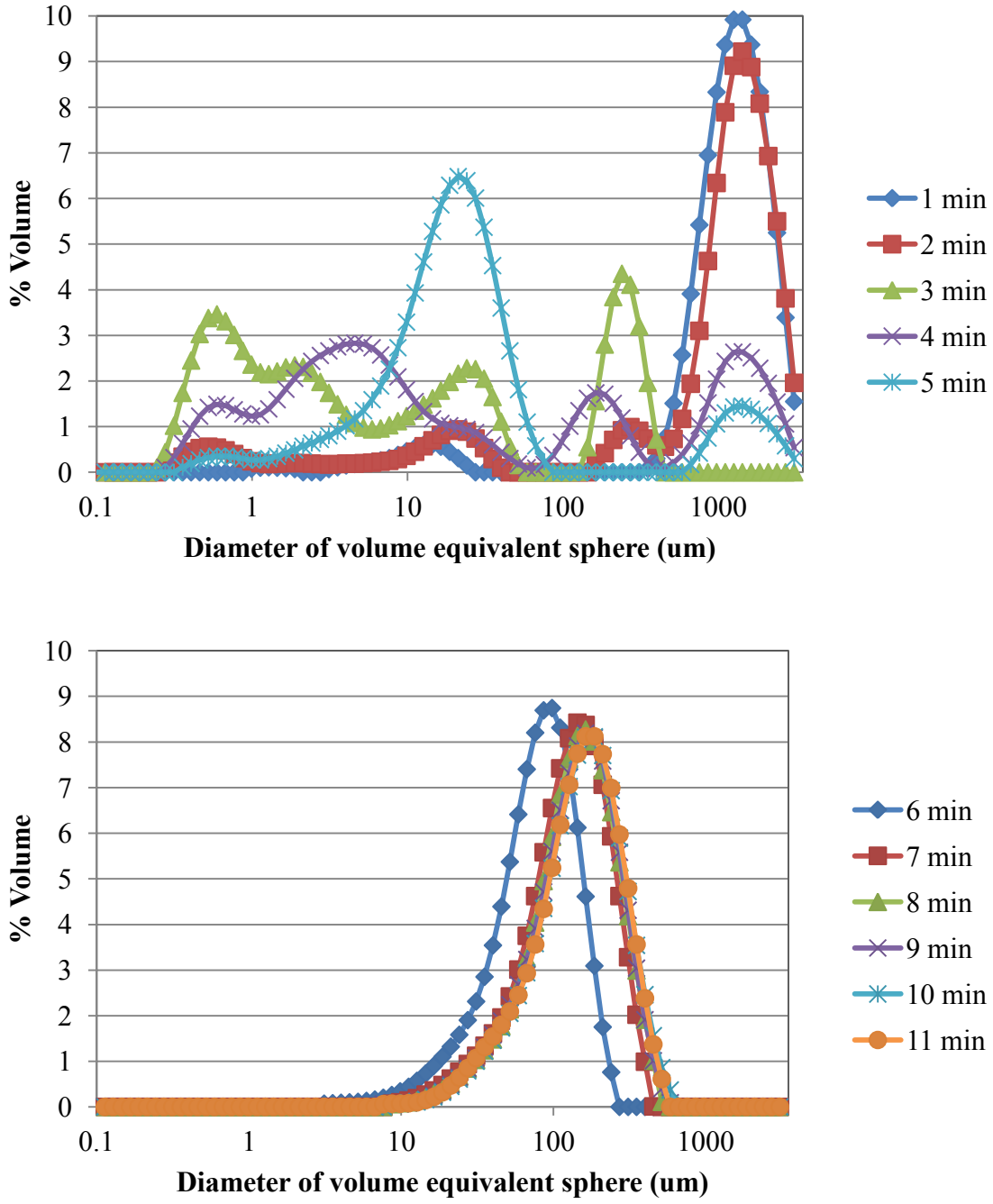

Figure B.2: Floc size distributions generated over time for Case No. 2 (Replicate No. 1). Iron was continuously generated from a sacrificial anode for the first five minutes, after which the iron dosing was stopped.

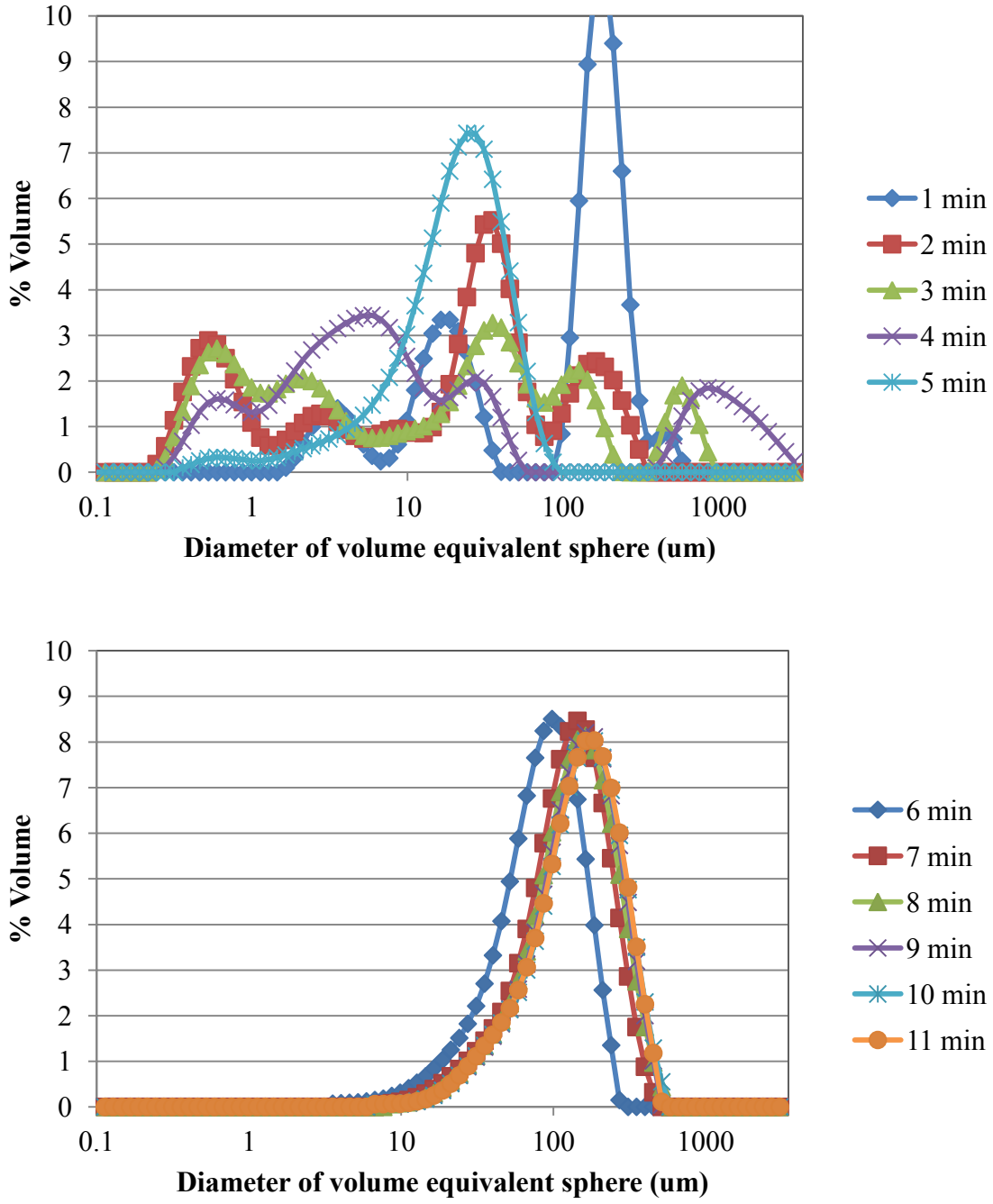

Figure B.3: Floc size distributions generated over time for Case No. 2 (Replicate No. 2). Iron was continuously generated from a sacrificial anode for the first five minutes, after which the iron dosing was stopped.

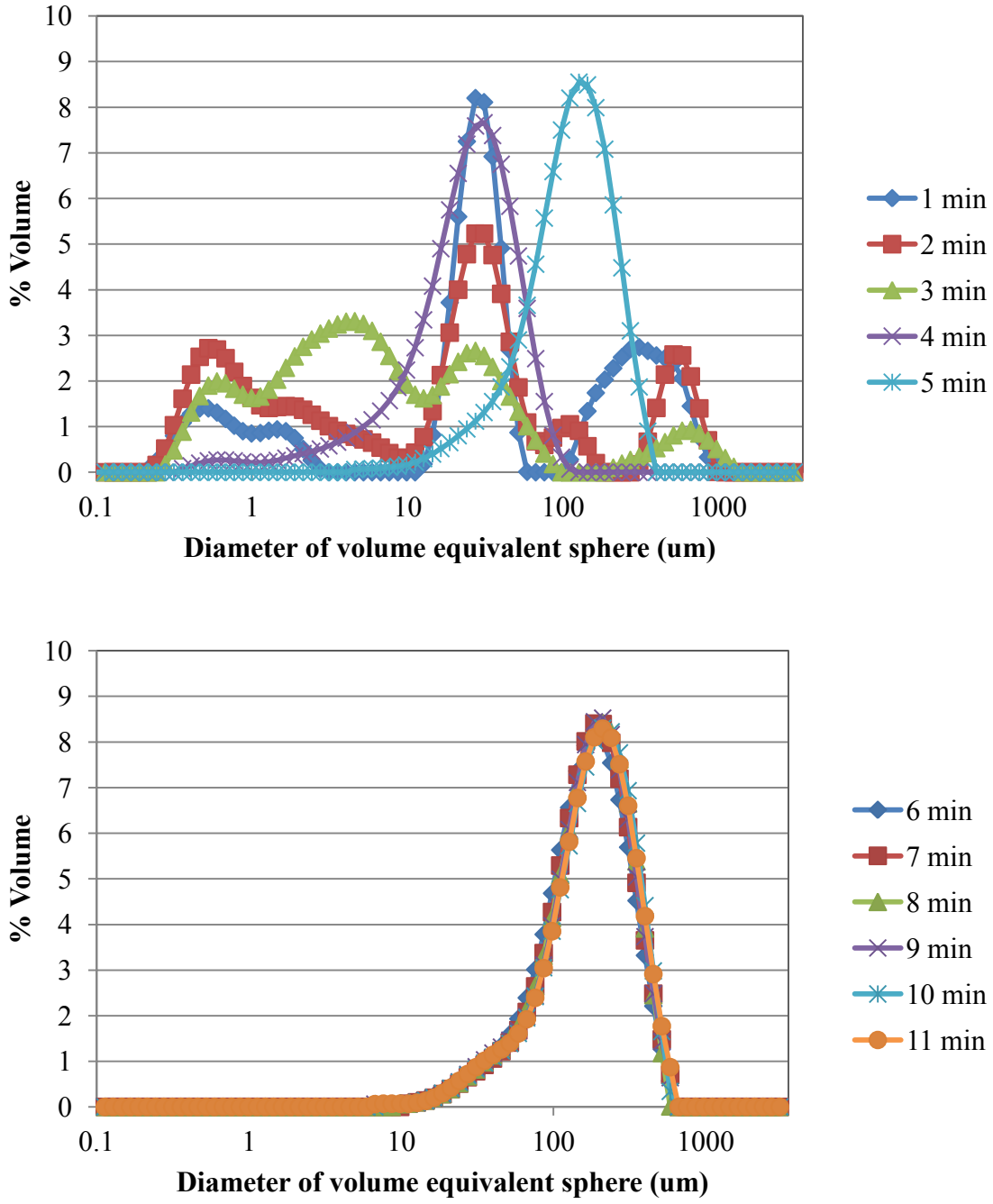

Figure B.4: Floc size distributions generated over time for Case No. 3 (Replicate No. 1). Iron was continuously generated from a sacrificial anode for the first five minutes, after which the iron dosing was stopped.

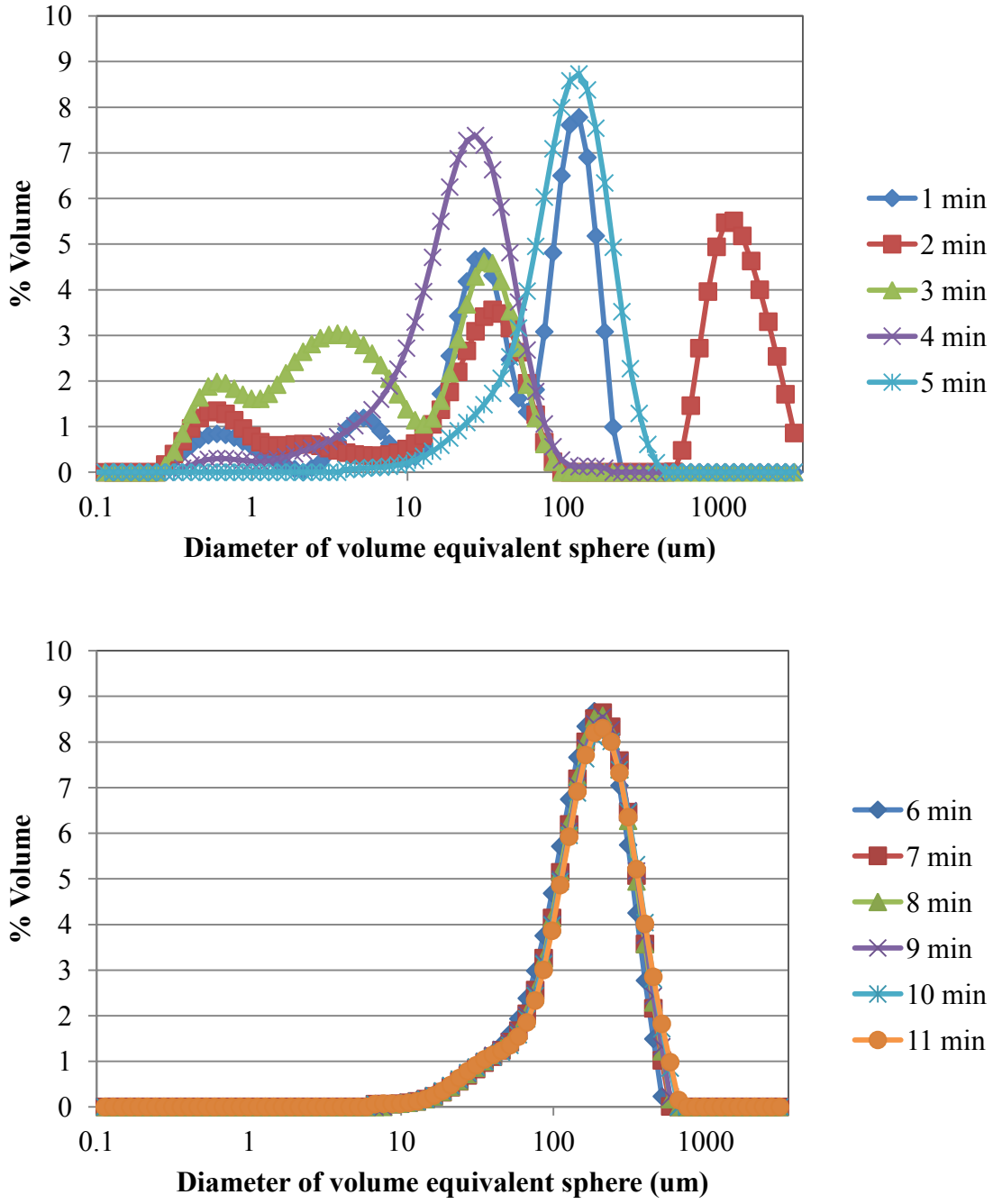

Figure B.5: Floc size distributions generated over time for Case No. 3 (Replicate No. 2). Iron was continuously generated from a sacrificial anode for the first five minutes, after which the iron dosing was stopped.

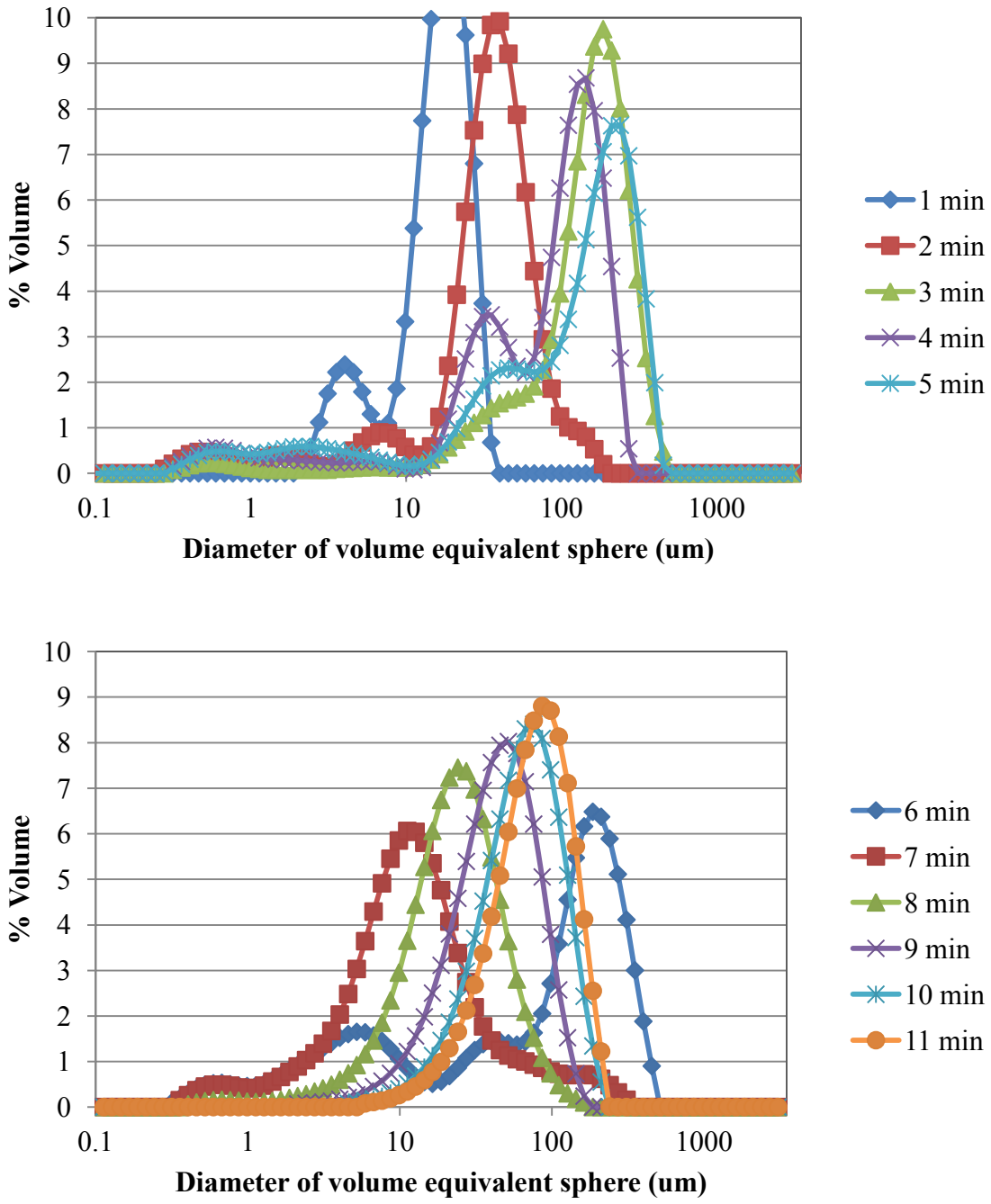

Figure B.6: Floc size distributions generated over time for Case No. 4 (Replicate No. 1). Iron was continuously generated from a sacrificial anode for the first five minutes, after which the iron dosing was stopped.

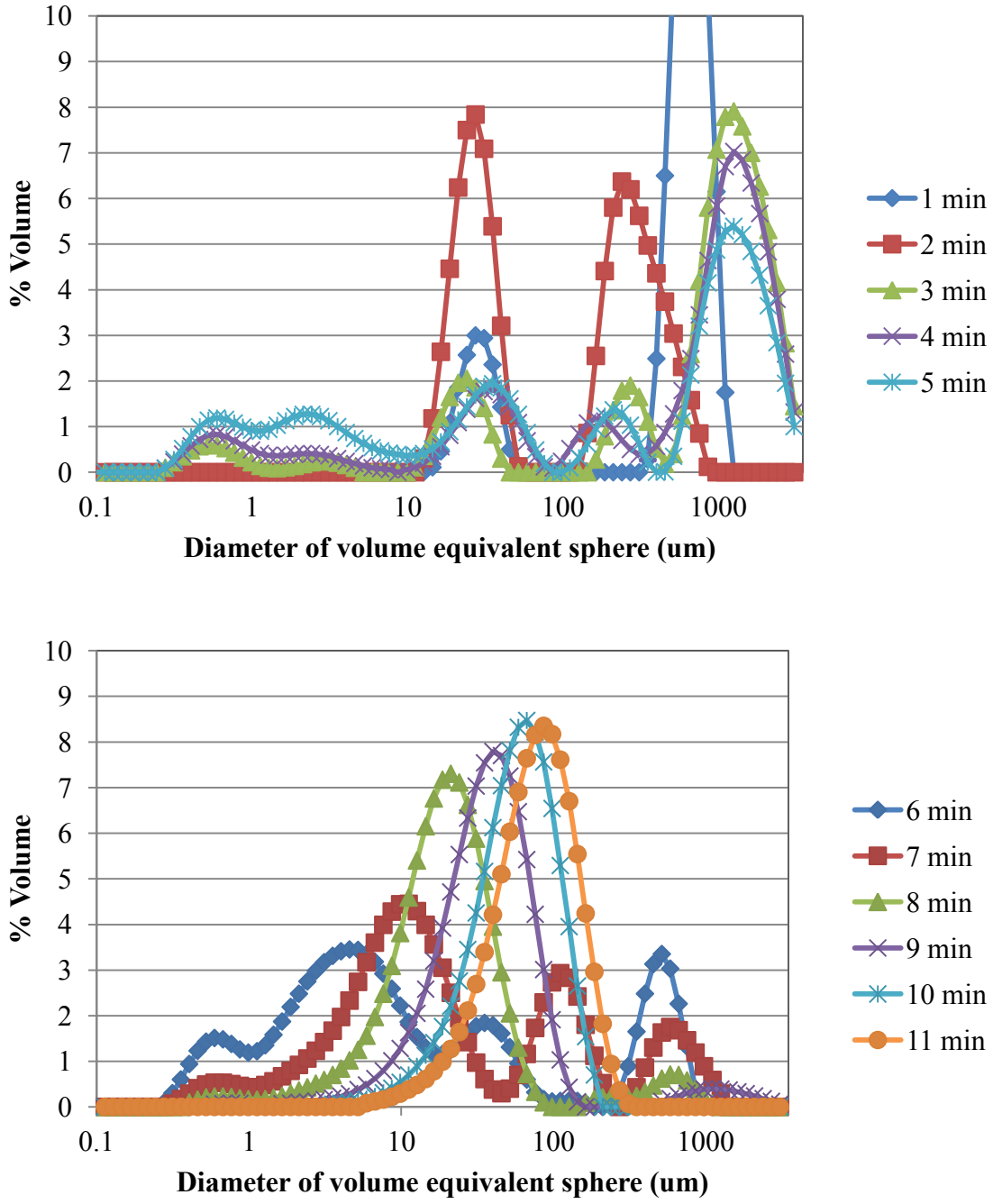

Figure B.7: Floc size distributions generated over time for Case No. 4 (Replicate No. 2). Iron was continuously generated from a sacrificial anode for the first five minutes, after which the iron dosing was stopped.

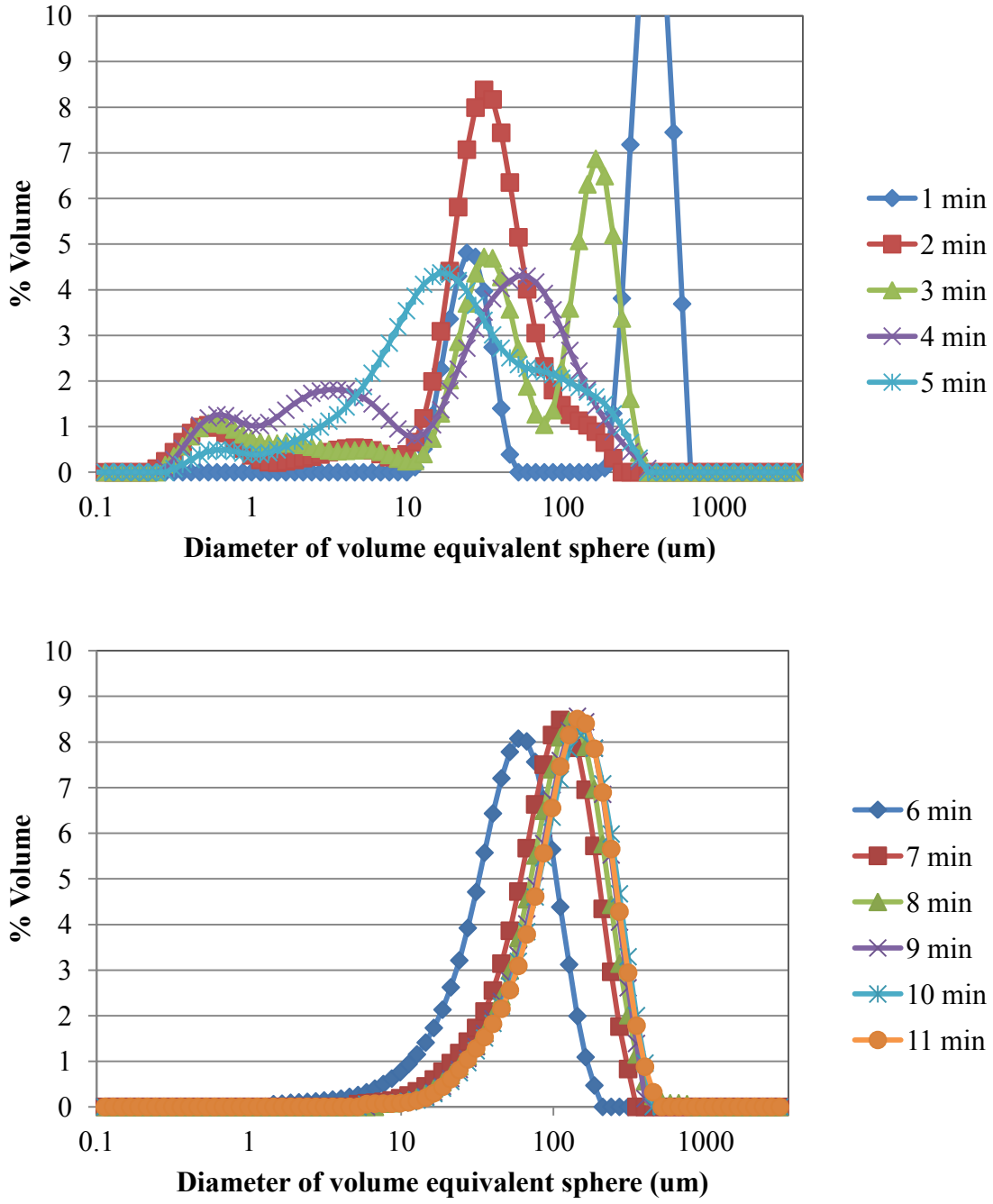

Figure B.8: Floc size distributions generated over time for Case No. 5 (Replicate No. 1). Iron was continuously generated from a sacrificial anode for the first five minutes, after which the iron dosing was stopped.

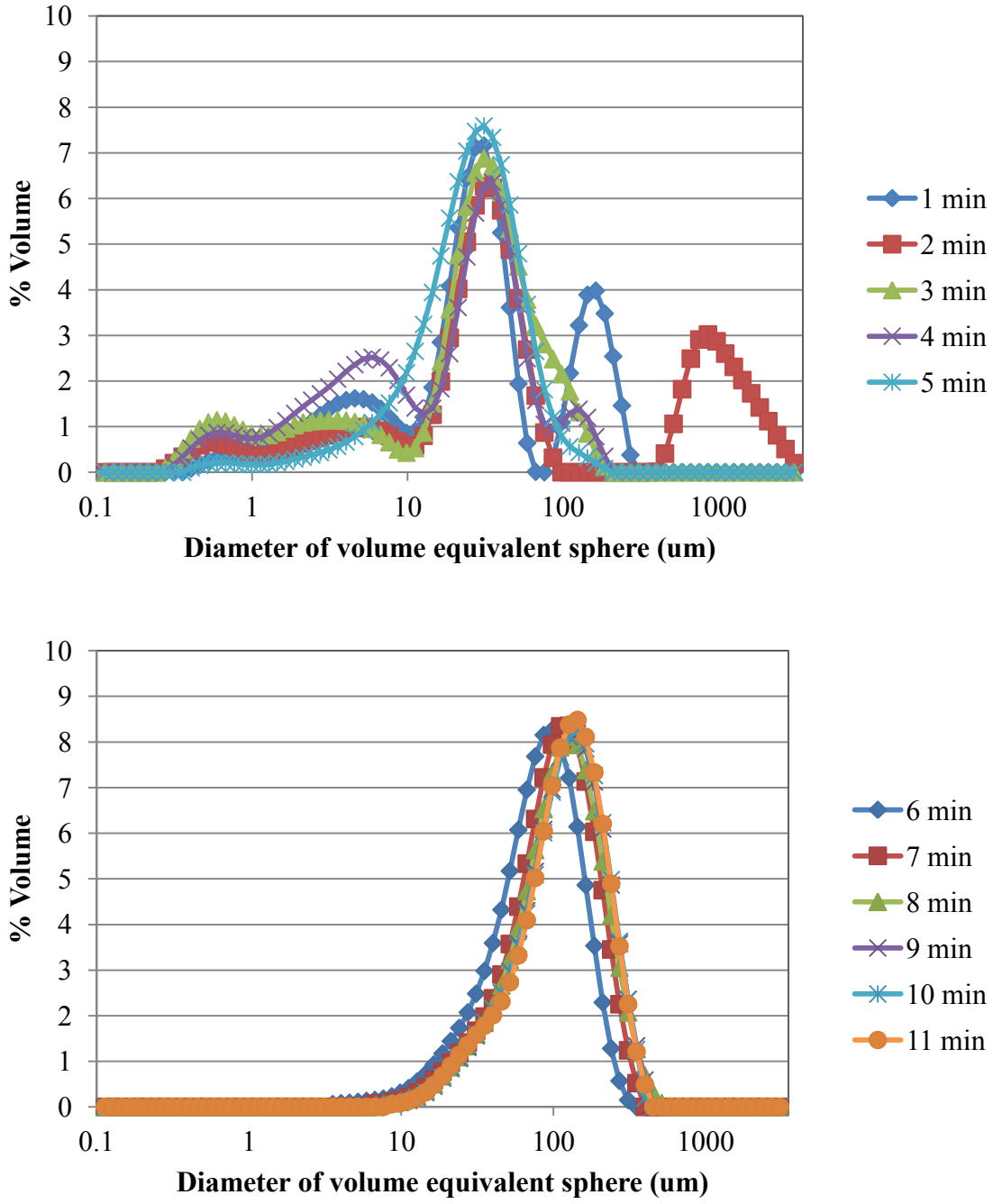

Figure B.9: Floc size distributions generated over time for Case No. 5 (Replicate No. 2). Iron was continuously generated from a sacrificial anode for the first five minutes, after which the iron dosing was stopped.

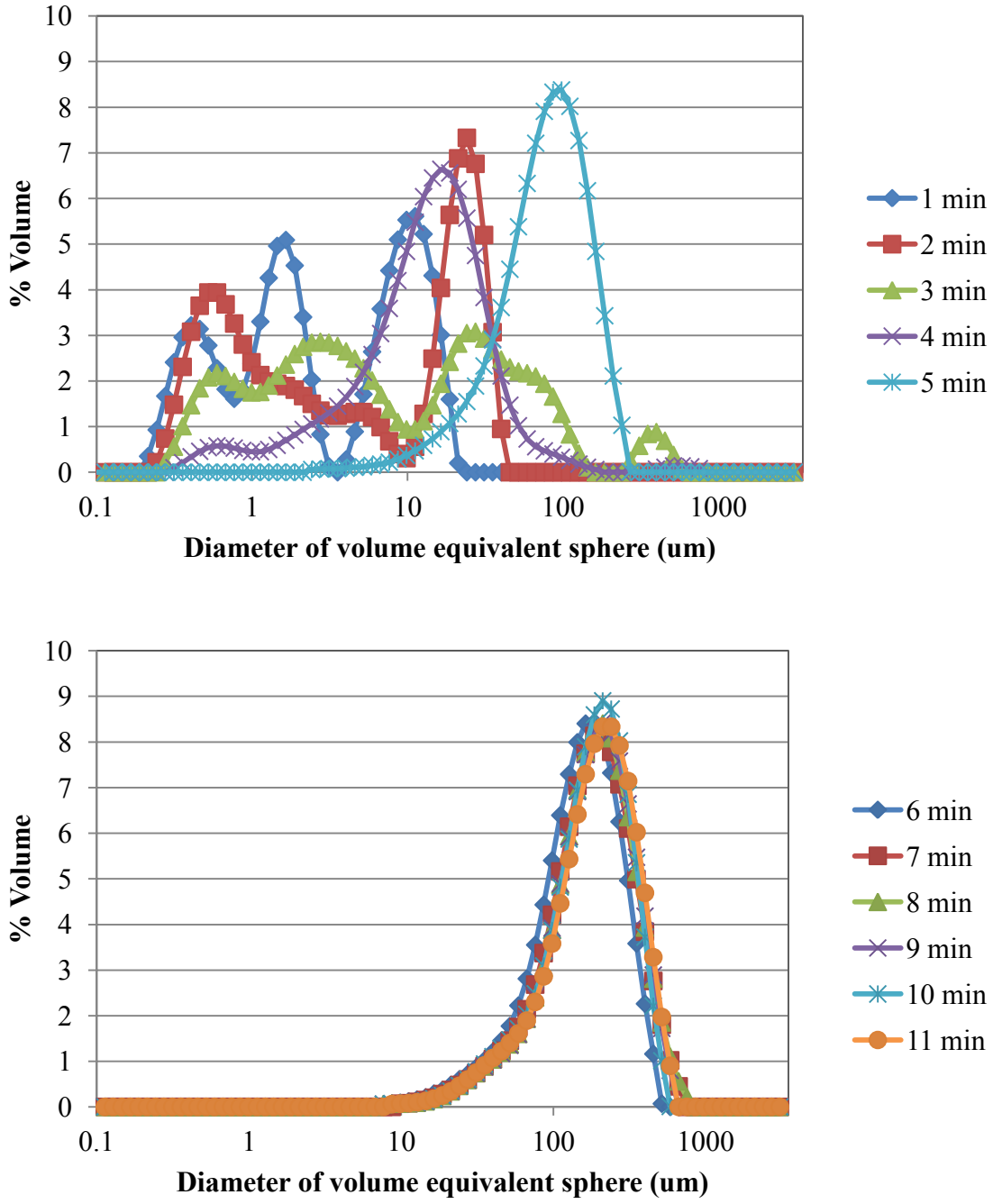

Figure B.10: Floc size distributions generated over time for Case No. 6 (Replicate No. 1). Iron was continuously generated from a sacrificial anode for the first five minutes, after which the iron dosing was stopped.

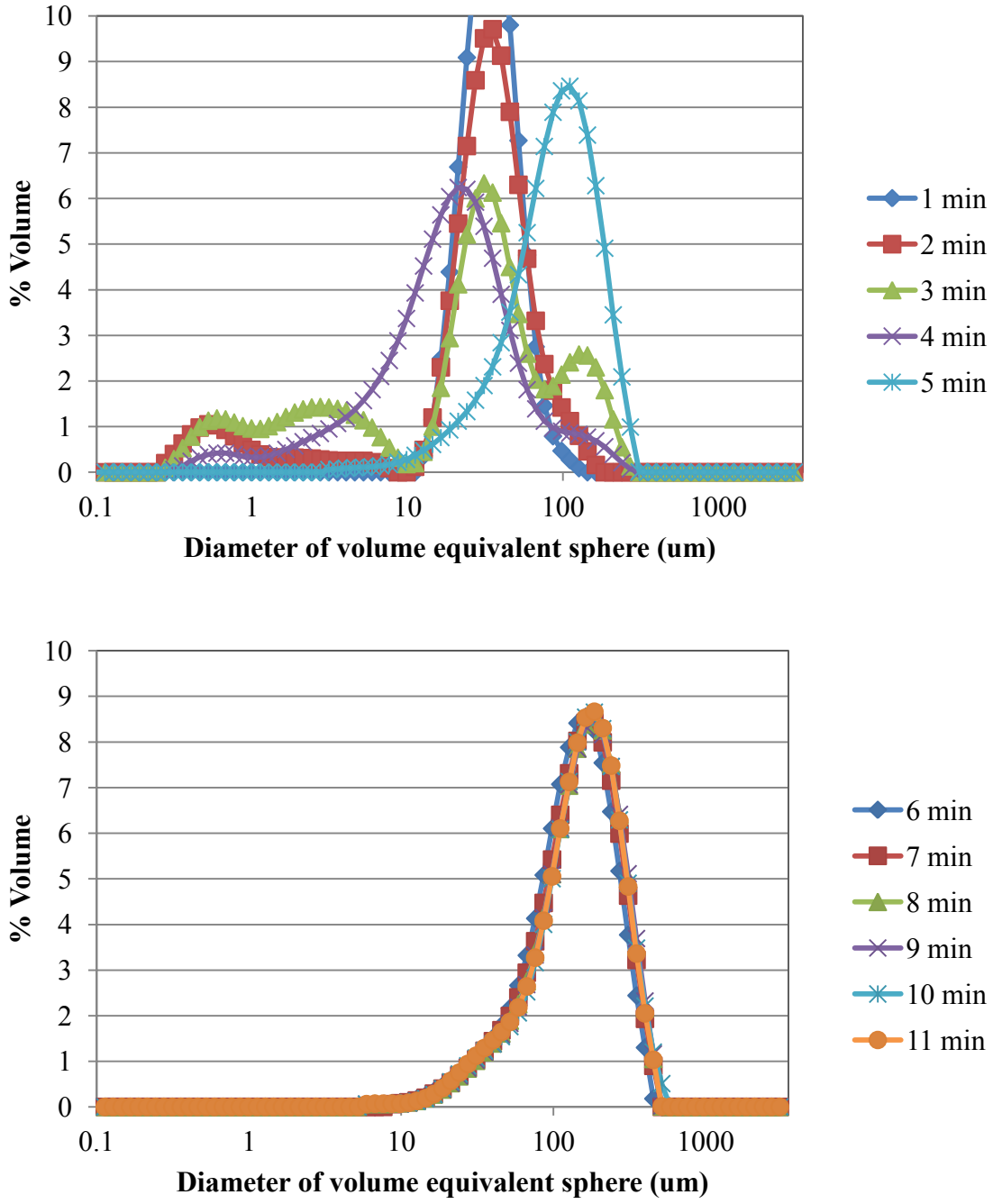

Figure B.11: Floc size distributions generated over time for Case No. 6 (Replicate No. 2). Iron was continuously generated from a sacrificial anode for the first five minutes, after which the iron dosing was stopped.

APPENDIX C: CHAPTER 6 DATA

Table C.1: Experimental Conditions

Case No.	Method of Dosing	Salt Concentration	Final pH
1	CC	Low Salt	pH 6.0
2	CC	Low Salt	pH 8.3
3	CC	High Salt	pH 6.0
4	CC	High Salt	pH 8.3
5	EC	Low Salt	pH 6.0
6	EC	Low Salt	pH 8.3
7	EC	High Salt	pH 6.0
8	EC	High Salt	pH 8.3

Table C.2: Iron and Current

Case(Rep)*	Median Current (A)	Final Iron Conc. (mg/L)
1(1)	n/a	4.77
1(2)	n/a	4.52
2(1)	n/a	5.07
2(2)	n/a	5.15
3(1)	n/a	4.50
3(2)	n/a	4.19
4(1)	n/a	4.65
4(2)	n/a	4.71
5(1)	0.106	6.19
5(2)	0.113	6.41
6(1)	0.108	6.54
6(2)	0.109	6.60
7(1)	0.113	5.90
7(2)	0.113	6.69
8(1)	0.109	6.37
8(2)	0.106	6.05

*Case No. (Replicate No.)

Table C.3: pH over Time

Case(Rep)*	0 min	0.5 min	2.5 min	5 min	11.5 min
1(1)	6.20	6.22	6.17	6.12	6.10
1(2)	6.17	6.17	6.14	6.08	6.08
2(1)	9.01	9.06	8.87	8.37	8.22
2(2)	9.07	9.09	8.94	8.46	8.30
3(1)	6.12	6.05	6.00	5.94	5.92
3(2)	6.04	6.01	5.97	5.91	5.91
4(1)	8.76	8.83	8.71	8.44	8.37
4(2)	8.85	8.87	8.75	8.53	8.43
5(1)	6.06	6.08	6.08	5.94	5.96
5(2)	6.09	6.09	6.08	5.96	6.01
6(1)	8.30	8.28	8.36	8.29	8.31
6(2)	8.14	8.32	8.21	8.23	8.30
7(1)	5.84	5.86	5.92	5.99	5.97
7(2)	5.95	5.98	6.03	6.07	6.07
8(1)	8.23	8.23	8.23	8.23	8.23
8(2)	8.26	8.26	8.26	8.26	8.26

*Case No. (Replicate No.)

Table C.4: Conductivity (mS/cm) over Time

Case(Rep)*	0 min	0.5 min	2.5 min	5 min	11.5 min
1(1)	1.188	1.188	1.191	1.192	1.191
1(2)	1.181	1.179	1.182	1.183	1.182
2(1)	1.107	1.106	1.104	1.101	1.100
2(2)	1.101	1.100	1.096	1.092	1.093
3(1)	40.64	40.59	40.36	40.20	40.31
3(2)	41.65	41.60	41.41	41.42	41.19
4(1)	41.62	41.59	41.45	41.30	41.28
4(2)	41.11	41.15	41.00	40.86	40.70
5(1)	1.131	1.139	1.132	1.148	1.142
5(2)	1.125	1.114	1.120	1.121	1.114
6(1)	1.072	1.067	1.066	1.066	1.058
6(2)	1.067	1.062	1.060	1.060	1.060
7(1)	44.55	43.77	43.70	43.72	43.58
7(2)	41.87	41.16	41.36	40.46	40.32
8(1)	43.81	43.43	43.40	43.13	43.59
8(2)	44.00	43.78	43.14	43.25	43.48

*Case No. (Replicate No.)

Table C.5: Zeta Potential (mV) over Time

Case(Rep)*	Time (min)	ZP Read1	ZP Read2	ZP Read3
1(1)	0	-40.7	-43.5	-46.8
1(1)	0.5	-26.9	-21.3	-28.2
1(1)	2.5	-12.1	-12.6	-12.1
1(1)	5	-9.6	-11.6	-13.4
1(1)	11.5	-7.5	-9.2	-8.3
1(2)	0	-8.1	-8.8	-12.0
1(2)	0.5	-24.3	-26.2	-26.5
1(2)	2.5	-12.5	-13.7	-12.1
1(2)	5	-6.5	-5.4	-7.3
1(2)	11.5	-8.0	-8.3	-9.4
2(1)	0	-22.3	-21.5	-25.9
2(1)	0.5	-25.9	-27.0	-29.4
2(1)	2.5	-28.2	-28.9	-28.8
2(1)	5	-31.5	-30.6	-31.5
2(1)	11.5	-33.2	-32.0	-33.1
2(2)	0	-41.1	-35.2	-34.4
2(2)	0.5	-28.5	-30.1	-35.2
2(2)	2.5	-34.6	-36.1	-35.8
2(2)	5	-22.2	-26.5	-28.1
2(2)	11.5	-29.1	-30.2	-34.5
3(1)	0	-1.3	-8.0	-16.6
3(1)	0.5	-3.3	3.8	3.5
3(1)	2.5	-1.0	-2.5	-2.1
3(1)	5	0.2	2.3	4.6
3(1)	11.5	3.6	4.7	5.7
3(2)	0	-5.1	-13.6	10.4
3(2)	0.5	-2.2	-17.0	-5.8
3(2)	2.5	-2.5	-2.3	-0.4
3(2)	5	-3.3	-5.8	-3.4
3(2)	11.5	-6.1	6.0	5.0
4(1)	2.5	-10.4	-8.2	0.4
4(1)	5	-11.4	-10.0	-12.3
4(1)	11.5	-7.8	1.8	-2.4
4(2)	0	-11.7	-11.4	-13.2
4(2)	0.5	-9.8	-4.9	-5.0
4(2)	2.5	-10.1	-5.5	-7.6
4(2)	5	-12.4	-11.7	-12.3

Case(Rep)*	Time (min)	ZP Read1	ZP Read2	ZP Read3
4(2)	11.5	-12.4	-4.9	-1.4
5(1)	0	-19.3	-27.0	-25.5
5(1)	0.5	-26.8	-26.5	-25.1
5(1)	2.5	-20.4	-21.2	-21.4
5(1)	5	-12.0	-10.6	-9.3
5(1)	11.5	-12.8	-11.9	-12.3
5(2)	0	-34.7	-35.8	-32.9
5(2)	0.5	-18.9	-18.1	-22.2
5(2)	2.5	-12.3	-12.0	-11.2
5(2)	5	-16.0	-13.6	-13.1
5(2)	11.5	-16.5	-17.0	-17.8
6(1)	0	-7.6	-12.4	-9.5
6(1)	0.5	-33.6	-35.4	-36.5
6(1)	2.5	-22.5	-21.6	-23.3
6(1)	5	-24.7	-25.4	-24.2
6(1)	11.5	-22.8	-25.2	-27.2
6(2)	0	-44.4	-44.4	-38.1
6(2)	0.5	-31.8	-32.9	-30.5
6(2)	2.5	-26.3	-23.6	-23.1
6(2)	5	-25.0	-24.1	-23.6
6(2)	11.5	-28.8	-24.2	-29.0
7(1)	0	-10.4	-2.6	-8.2
7(1)	0.5	-13.8	-13.4	-16.1
7(1)	2.5	-4.9	-3.1	-2.9
7(1)	5	3.3	-1.4	4.6
7(1)	11.5	-5.2	-4.2	-5.7
7(2)	0	-5.4	-12.4	-12.5
7(2)	0.5	1.3	8.9	6.7
7(2)	2.5	-1.9	-2.5	-4.1
7(2)	5	-6.1	-6.8	-6.8
7(2)	11.5	-2.4	-1.7	-2.2
8(1)	0	-12.1	-8.0	-9.2
8(1)	0.5	-12.2	-10.0	-12.7
8(1)	2.5	-9.8	-11.0	-11.0
8(1)	5	-13.4	-13.4	-12.1
8(1)	11.5	-7.9	-11.8	-11.2
8(2)	0	-5.9	-22.3	-14.9
8(2)	0.5	-3.2	-17.2	-1.4
8(2)	2.5	-10.4	-10.8	-11.1

Case(Rep)*	Time (min)	ZP Read1	ZP Read2	ZP Read3
8(2)	5	-11.6	-11.0	-9.1
8(2)	11.5	-16.3	-0.3	-0.3

*Case No. (Replicate No.)

Table C.6: Scattering exponent and percentile particle size (μm) data over time

Case(Rep)[a]	Time (min)	D_x (10)	D_x (50)	D_x (90)	Scattering Exponent	R^2 [b]
1(1)	1	5.7	232.6	487.3	1.50	0.97
1(1)	2	1.4	80.1	164.1	1.59	0.98
1(1)	3	4.3	12.1	222.2	2.24	1.00
1(1)	4	16.6	45.0	92.8	2.43	1.00
1(1)	5	43.2	118.4	235.3	2.49	1.00
1(1)	6	72.6	205.2	445.2	2.57	1.00
1(1)	7	90.5	269.0	727.4	2.60	1.00
1(1)	8	93.9	287.2	580.4	2.64	1.00
1(1)	9	97.2	297.9	617.7	2.65	1.00
1(1)	10	89.9	274.2	572.5	2.67	1.00
1(1)	11	85.3	254.5	521.0	2.69	1.00
1(2)	1	78.9	121.9	187.0	n/a	n/a
1(2)	2	79.9	186.8	1969.2	1.82	0.99
1(2)	3	6.5	807.6	2030.7	2.20	1.00
1(2)	4	12.7	33.3	65.1	2.41	1.00
1(2)	5	39.4	102.2	209.5	2.51	1.00
1(2)	6	76.0	200.1	416.0	2.59	1.00
1(2)	7	98.2	287.2	609.3	2.65	1.00
1(2)	8	98.9	295.9	593.5	2.69	1.00
1(2)	9	99.8	295.1	583.1	2.73	1.00
1(2)	10	98.4	288.3	562.1	2.74	1.00
1(2)	11	94.9	289.7	575.1	2.74	1.00
2(1)	1	26.1	51.1	85.1	2.52	0.97
2(1)	2	20.4	59.1	104.3	1.82	0.98
2(1)	3	10.9	69.1	106.5	1.63	0.99
2(1)	4	2.6	41.3	83.5	1.53	0.99
2(1)	5	3.4	10.7	40.8	2.14	1.00
2(1)	6	13.5	35.6	72.9	2.43	1.00
2(1)	7	41.8	113.4	222.6	2.56	1.00
2(1)	8	70.1	191.6	394.4	2.64	1.00
2(1)	9	87.0	253.0	578.4	2.65	1.00
2(1)	10	91.9	291.4	613.7	2.68	1.00
2(1)	11	91.5	283.5	585.0	2.70	1.00
2(2)	1	0.2	0.7	1.3	1.42	0.93
2(2)	2	40.8	978.9	2140.1	1.41	0.96
2(2)	3	50.9	909.5	2017.5	1.53	0.99

Case(Rep)[a]	Time (min)	D_x (10)	D_x (50)	D_x (90)	Scattering Exponent	R^2 [b]
2(2)	4	0.9	25.9	49.1	1.72	0.99
2(2)	5	2.9	11.3	118.3	2.00	1.00
2(2)	6	11.6	30.8	63.8	2.32	1.00
2(2)	7	38.3	102.8	201.2	2.49	1.00
2(2)	8	66.4	183.0	371.1	2.58	1.00
2(2)	9	85.5	249.3	539.2	2.59	1.00
2(2)	10	96.3	293.3	717.8	2.61	1.00
2(2)	11	91.3	265.4	601.4	2.64	1.00
3(1)	1	0.1	0.4	1.6	1.06	0.95
3(1)	2	0.5	5.7	23.8	1.12	0.99
3(1)	3	1.3	5.1	15.9	1.74	0.99
3(1)	4	6.6	15.0	29.8	2.05	0.98
3(1)	5	19.0	45.2	97.3	2.30	0.99
3(1)	6	43.7	107.6	205.0	2.43	0.99
3(1)	7	69.9	175.0	336.0	2.47	0.99
3(1)	8	80.7	201.1	398.2	2.51	0.99
3(1)	9	82.1	207.6	406.4	2.53	0.99
3(1)	10	84.5	208.8	428.8	2.55	0.99
3(1)	11	81.2	198.3	386.5	2.57	0.99
3(2)	1	47.6	105.7	311.3	n/a	n/a
3(2)	2	42.8	70.0	435.6	1.05	0.91
3(2)	3	61.4	110.9	292.9	1.67	0.99
3(2)	4	7.6	90.3	265.9	1.86	0.98
3(2)	5	13.9	45.5	157.0	2.16	0.99
3(2)	6	32.0	85.8	170.2	2.34	0.99
3(2)	7	60.0	156.2	305.1	2.44	0.99
3(2)	8	78.3	206.9	437.3	2.47	0.99
3(2)	9	86.9	229.2	455.0	2.49	0.99
3(2)	10	89.5	239.6	497.7	2.50	0.99
3(2)	11	89.7	233.5	478.6	2.49	0.99
4(1)	1	0.2	1.3	5.6	1.20	0.97
4(1)	2	4.9	77.9	193.1	1.40	1.00
4(1)	3	5.0	51.0	114.8	1.60	1.00
4(1)	4	6.2	30.1	94.7	1.86	1.00
4(1)	5	12.4	34.3	80.8	2.13	0.99
4(1)	6	27.6	73.4	151.5	2.27	0.99
4(1)	7	51.4	138.9	291.1	2.40	0.99
4(1)	8	70.0	197.5	394.5	2.43	0.99

Case(Rep)[a]	Time (min)	D_x (10)	D_x (50)	D_x (90)	Scattering Exponent	R^2 [b]
4(1)	9	86.7	252.3	1410.2	2.46	0.99
4(1)	10	83.2	234.6	506.5	2.47	0.99
4(1)	11	85.7	233.8	456.4	2.49	0.99
4(2)	1	3.9	66.7	108.6	1.13	0.98
4(2)	2	29.3	87.2	2040.7	1.36	1.00
4(2)	3	3.8	36.1	70.5	1.61	1.00
4(2)	4	5.3	19.4	69.8	1.94	0.99
4(2)	5	12.4	33.4	83.1	2.18	0.99
4(2)	6	27.2	71.0	138.2	2.32	0.99
4(2)	7	50.9	135.9	263.6	2.41	0.99
4(2)	8	69.6	193.4	405.3	2.46	0.99
4(2)	9	85.5	234.2	517.0	2.48	0.99
4(2)	10	89.6	246.8	511.4	2.50	0.99
4(2)	11	96.5	274.4	573.5	2.50	0.99
5(1)	1	28.5	1051.7	2372.8	2.16	0.99
5(1)	2	52.5	400.9	2338.8	1.98	0.99
5(1)	3	22.7	134.8	1041.0	1.79	1.00
5(1)	4	17.3	86.7	605.2	1.65	1.00
5(1)	5	11.3	75.5	545.7	1.53	0.99
5(1)	6	5.8	81.2	468.3	1.42	0.99
5(1)	7	3.3	68.3	476.0	1.51	0.99
5(1)	8	4.5	29.0	288.9	1.87	1.00
5(1)	9	10.3	34.1	119.6	2.00	1.00
5(1)	10	25.3	73.9	157.1	2.13	1.00
5(1)	11	45.8	124.5	245.0	2.21	1.00
5(2)	1	33.0	61.9	153.7	1.86	0.98
5(2)	2	29.2	56.3	160.2	1.71	0.96
5(2)	3	30.8	78.1	163.6	1.70	0.98
5(2)	4	22.2	93.1	604.6	1.57	0.99
5(2)	5	20.4	96.0	1471.4	1.41	0.99
5(2)	6	4.6	65.6	156.4	1.55	1.00
5(2)	7	5.7	51.8	155.2	1.82	1.00
5(2)	8	13.1	45.2	130.2	2.00	1.00
5(2)	9	34.5	97.3	201.5	2.15	1.00
5(2)	10	58.6	155.2	314.2	2.22	1.00
5(2)	11	72.3	191.8	376.8	2.24	0.99
6(1)	1	58.7	251.0	403.1	1.87	1.00
6(1)	2	49.8	1168.7	2388.8	1.50	0.99

Case(Rep)[a]	Time (min)	D_x (10)	D_x (50)	D_x (90)	Scattering Exponent	$R^{2\,b}$
6(1)	3	34.5	221.8	2263.3	1.59	0.99
6(1)	4	8.9	111.3	2103.5	1.63	0.99
6(1)	5	10.6	37.7	127.2	2.00	1.00
6(1)	6	37.6	103.4	208.7	2.21	0.99
6(1)	7	63.1	170.7	340.4	2.33	0.99
6(1)	8	71.5	184.3	366.2	2.38	0.99
6(1)	9	70.3	188.2	359.8	2.42	0.99
6(1)	10	72.5	193.3	389.4	2.44	1.00
6(1)	11	71.2	194.3	406.1	2.45	0.99
6(2)	1	5.1	136.6	563.4	2.16	0.99
6(2)	2	11.8	75.8	182.2	1.45	1.00
6(2)	3	11.8	93.1	199.6	1.54	0.99
6(2)	4	4.7	70.5	157.8	1.56	1.00
6(2)	5	8.7	46.2	151.6	1.92	1.00
6(2)	6	29.5	87.8	182.8	2.15	1.00
6(2)	7	55.2	149.7	306.9	2.28	1.00
6(2)	8	63.9	167.7	343.3	2.34	1.00
6(2)	9	67.7	181.3	364.4	2.38	1.00
6(2)	10	67.1	176.7	375.6	2.40	1.00
6(2)	11	64.2	171.8	342.4	2.42	1.00
7(1)	1	9.7	85.5	706.5	2.24	0.99
7(1)	2	14.7	69.5	120.5	1.91	0.99
7(1)	3	81.3	253.7	639.6	1.67	1.00
7(1)	4	10.5	87.7	143.0	1.53	1.00
7(1)	5	17.3	91.0	154.1	1.38	0.99
7(1)	6	6.9	103.3	163.3	1.35	0.99
7(1)	7	4.7	112.3	176.6	1.36	0.98
7(1)	8	4.2	116.7	197.8	1.48	0.99
7(1)	9	4.9	120.6	225.0	1.73	1.00
7(1)	10	6.0	99.4	228.9	1.87	1.00
7(1)	11	8.1	31.9	198.9	1.96	1.00
7(2)	1	162.2	260.9	412.9	2.15	0.97
7(2)	2	27.0	164.2	279.3	1.51	0.99
7(2)	3	25.3	227.6	444.1	1.41	0.98
7(2)	4	1.7	50.5	595.5	1.07	0.99
7(2)	5	0.8	136.6	490.0	1.29	0.97
7(2)	6	1.7	138.6	570.9	1.35	0.99
7(2)	7	1.0	30.6	399.5	1.37	0.98

Case(Rep)[a]	Time (min)	D_x (10)	D_x (50)	D_x (90)	Scattering Exponent	R^2 [b]
7(2)	8	2.7	43.1	418.5	1.64	1.00
7(2)	9	5.3	21.0	186.8	1.82	1.00
7(2)	10	12.8	35.3	77.4	1.99	0.99
7(2)	11	28.6	77.1	156.1	2.13	0.99
8(1)	1	1.5	34.9	54.2	1.17	0.99
8(1)	2	1.4	57.0	594.3	0.99	1.00
8(1)	3	0.7	5.1	39.9	1.69	0.99
8(1)	4	2.3	9.9	40.2	1.87	1.00
8(1)	5	9.9	27.2	56.5	2.10	1.00
8(1)	6	26.7	68.0	130.5	2.26	0.99
8(1)	7	42.6	106.1	208.4	2.39	1.00
8(1)	8	47.6	121.0	237.7	2.44	1.00
8(1)	9	50.7	128.0	263.3	2.48	1.00
8(1)	10	50.7	128.4	247.3	2.50	1.00
8(1)	11	50.2	129.0	255.7	2.52	1.00
8(2)	1	0.4	9.5	33.6	n/a	n/a
8(2)	2	0.6	21.9	57.3	1.38	0.98
8(2)	3	0.6	3.0	13.3	1.66	0.99
8(2)	4	3.7	198.6	371.9	1.84	1.00
8(2)	5	8.9	24.8	53.9	2.10	1.00
8(2)	6	25.2	64.3	126.8	2.27	0.99
8(2)	7	38.9	100.2	190.9	2.40	1.00
8(2)	8	45.7	114.8	219.7	2.46	1.00
8(2)	9	47.9	120.9	245.0	2.50	1.00
8(2)	10	48.7	124.1	245.9	2.52	1.00
8(2)	11	47.8	121.0	243.7	2.54	1.00

[a]Case No. (Replicate No.)

[b]R^2 is the coefficient of determination calculated for the linear relationship between *log(I)* and *log(Q)*. The calculation of scattering exponent is described in Section 3.2.4.

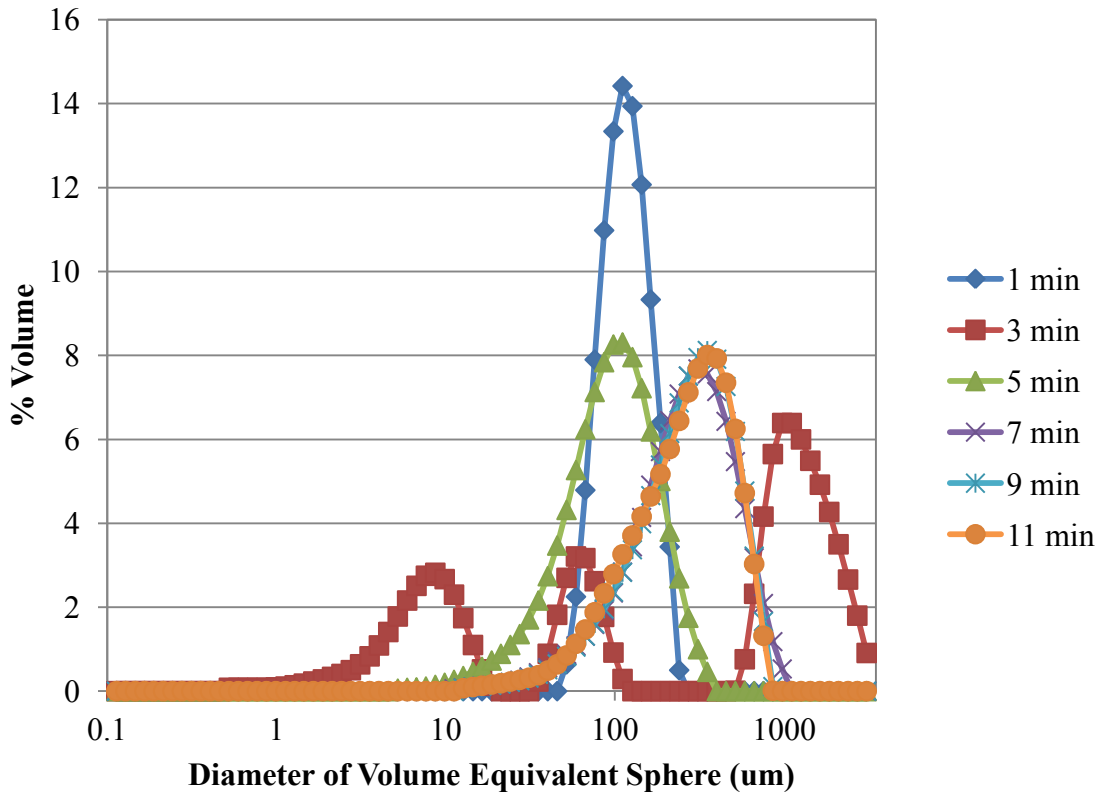

Figure C.1: Floc size distributions generated over time for Case No. 1 (Replicate No. 2). Coagulant dosing occurred continuously during the first 5 minutes.

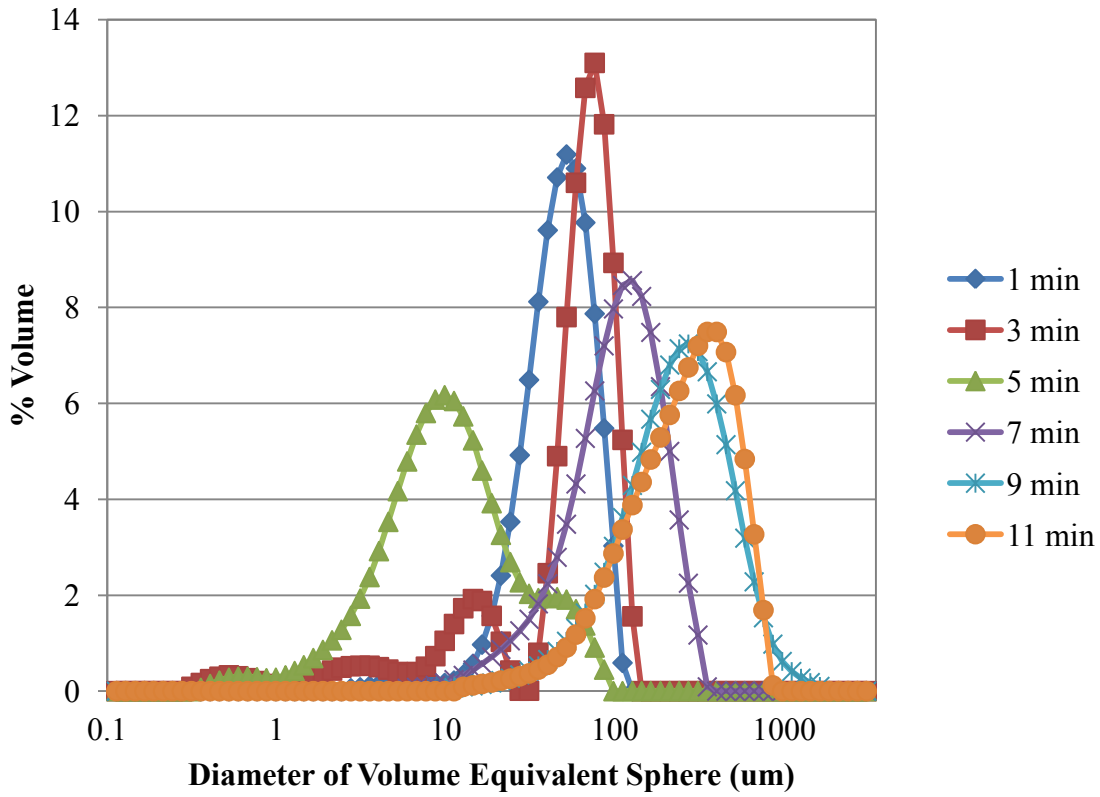

Figure C.2: Floc size distributions generated over time for Case No. 2 (Replicate No. 1). Coagulant dosing occurred continuously during the first 5 minutes.

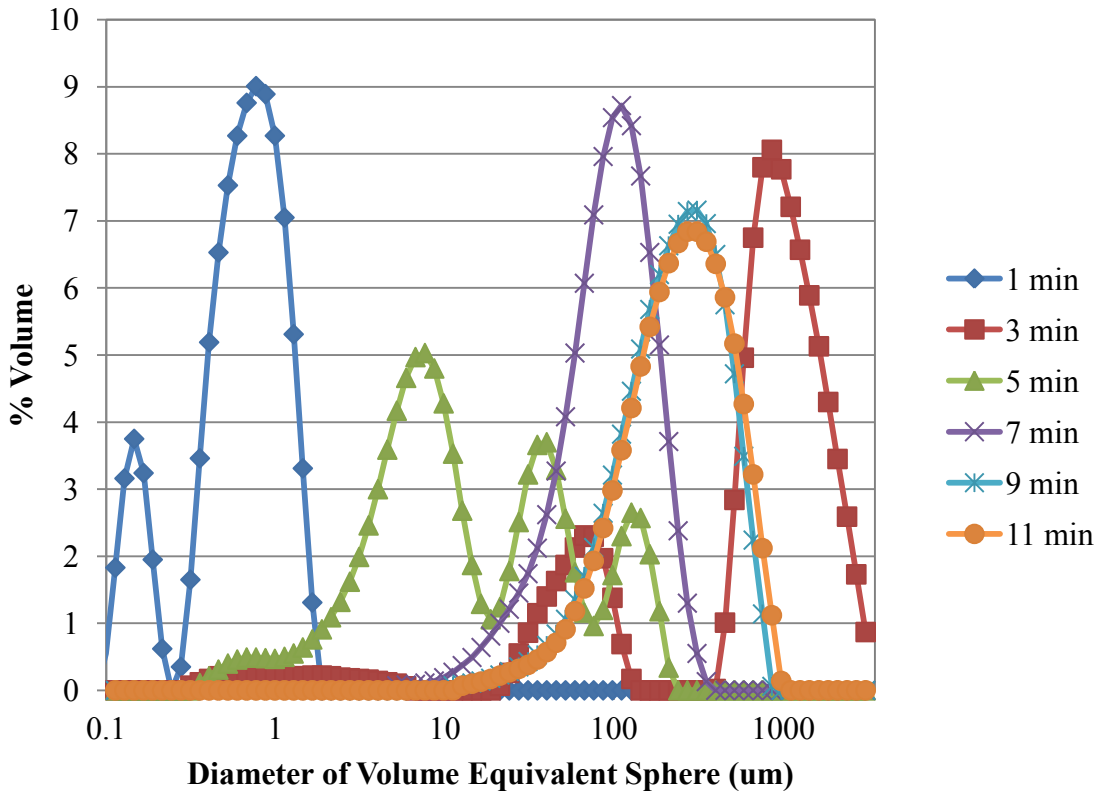

Figure C.3: Floc size distributions generated over time for Case No. 2 (Replicate No. 2). Coagulant dosing occurred continuously during the first 5 minutes.

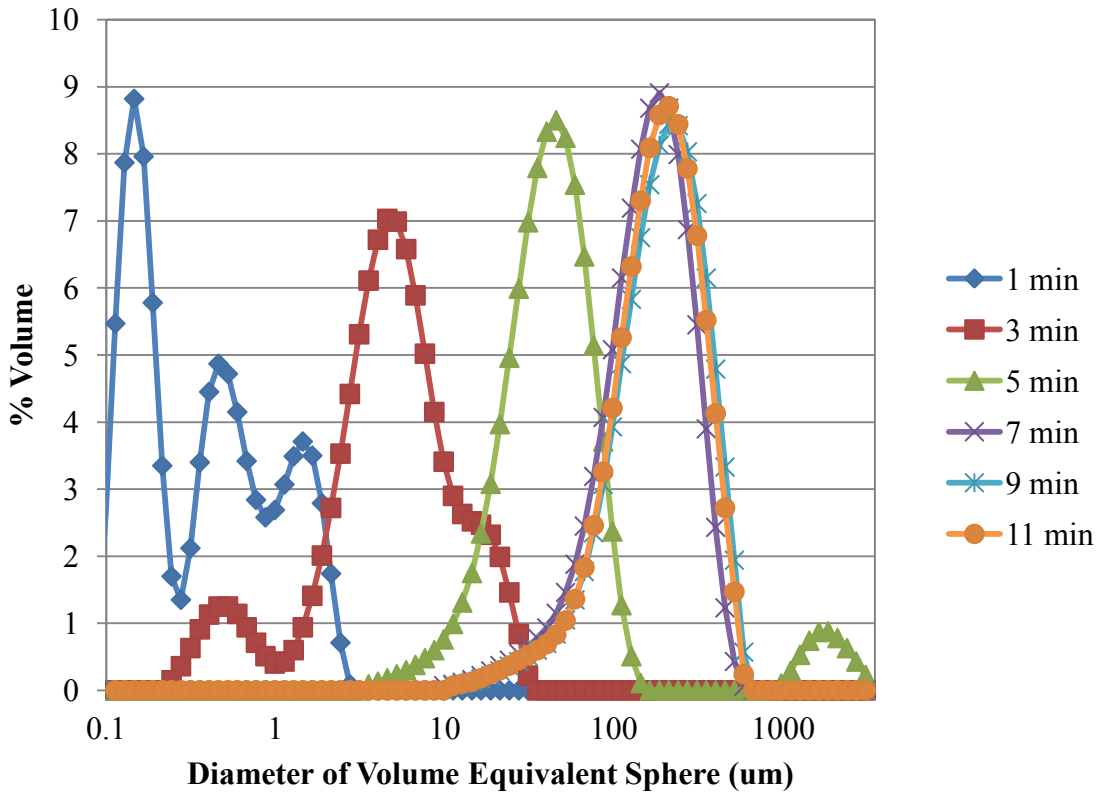

Figure C.4: Floc size distributions generated over time for Case No. 3 (Replicate No. 1). Coagulant dosing occurred continuously during the first 5 minutes.

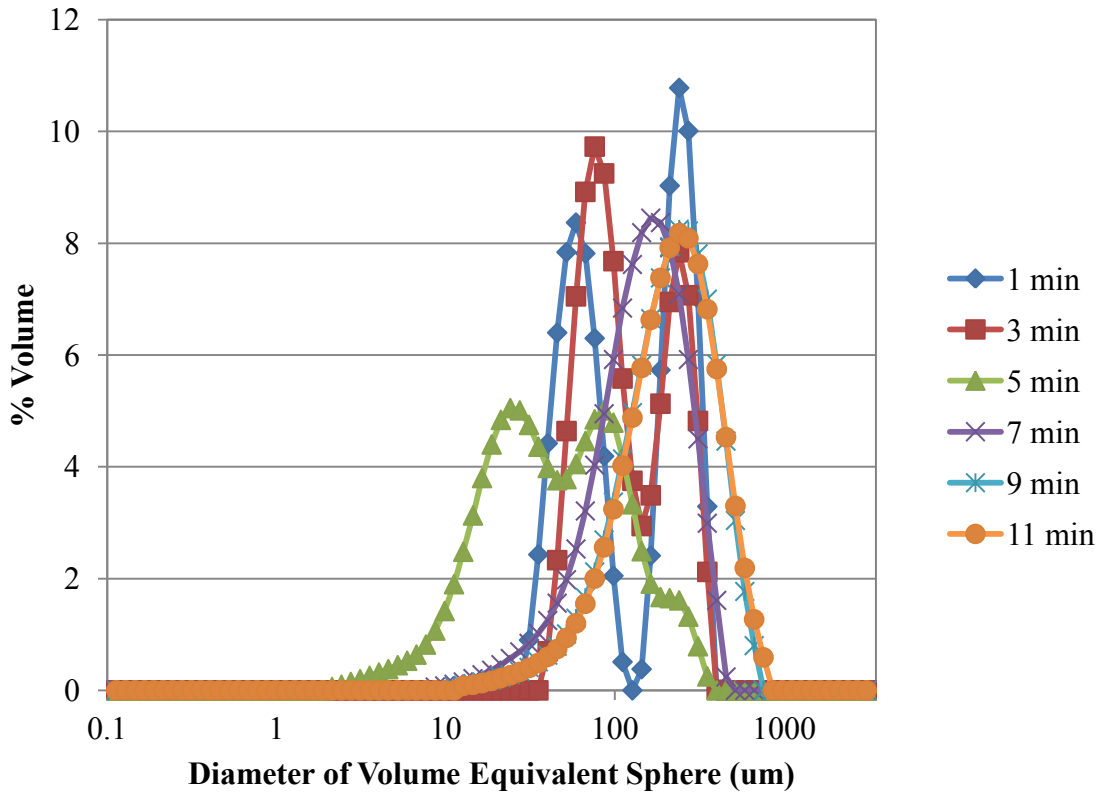

Figure C.5: Floc size distributions generated over time for Case No. 3 (Replicate No. 2). Coagulant dosing occurred continuously during the first 5 minutes.

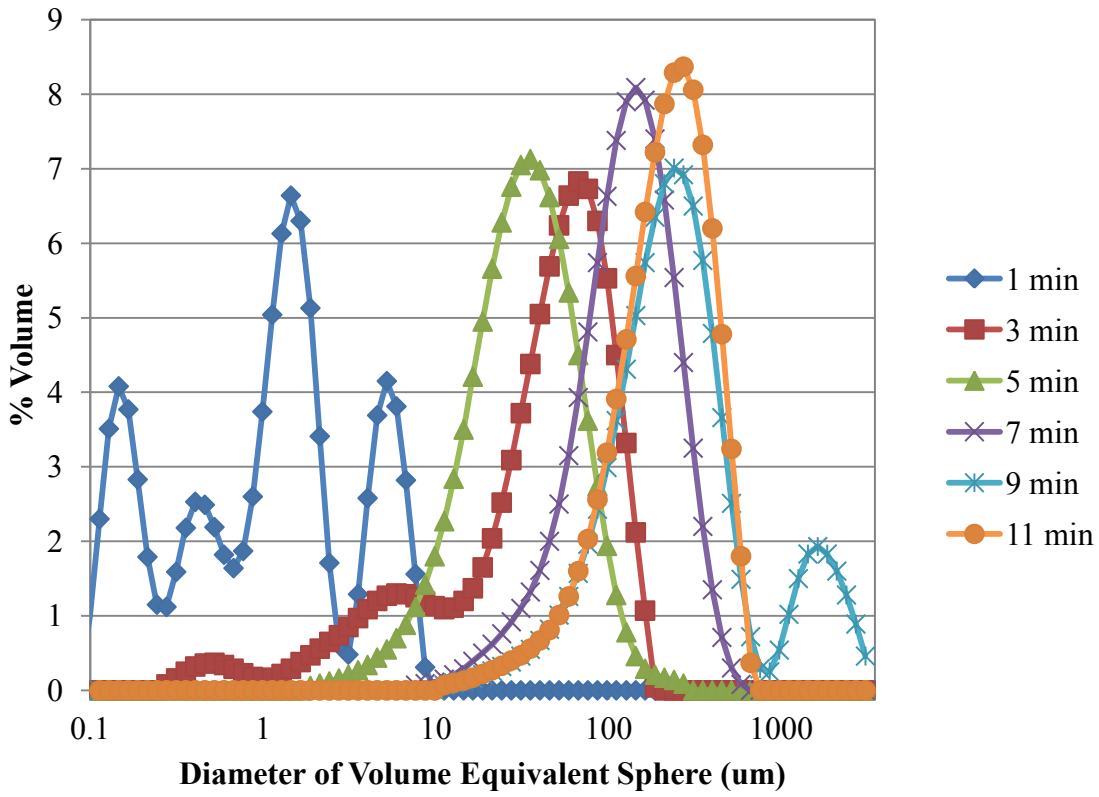

Figure C.6: Floc size distributions generated over time for Case No. 4 (Replicate No. 1). Coagulant dosing occurred continuously during the first 5 minutes.

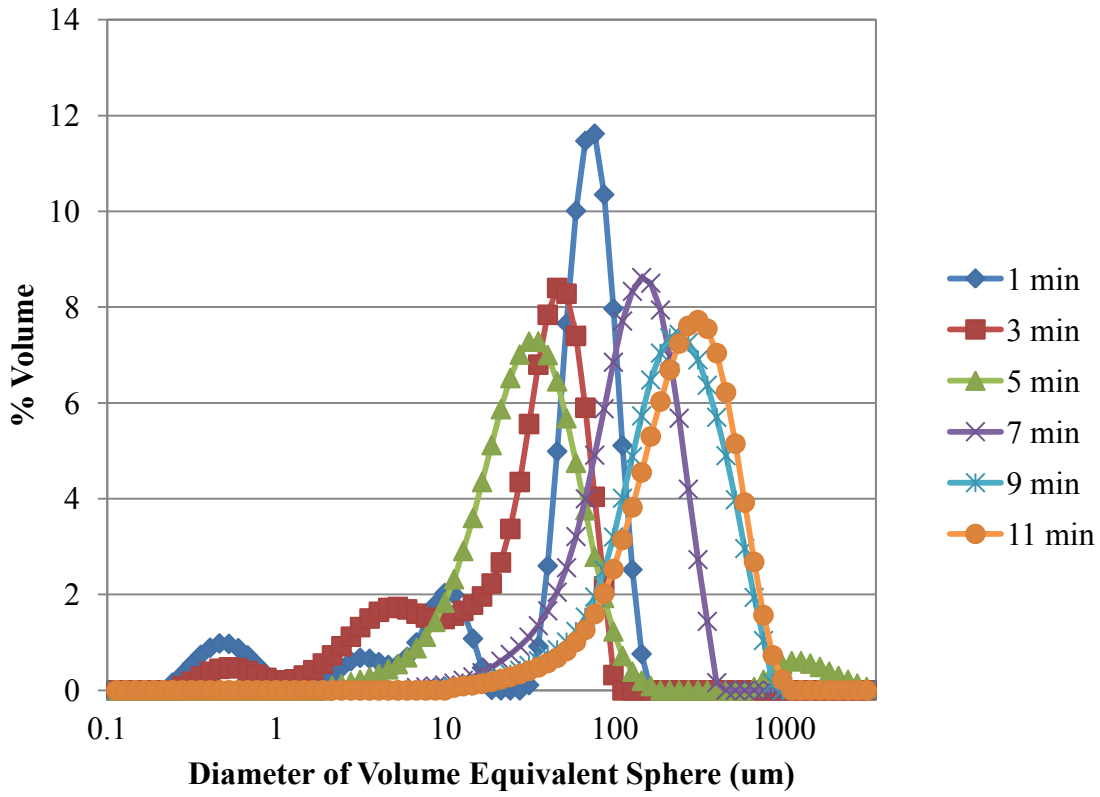

Figure C.7: Floc size distributions generated over time for Case No. 4 (Replicate No. 2). Coagulant dosing occurred continuously during the first 5 minutes.

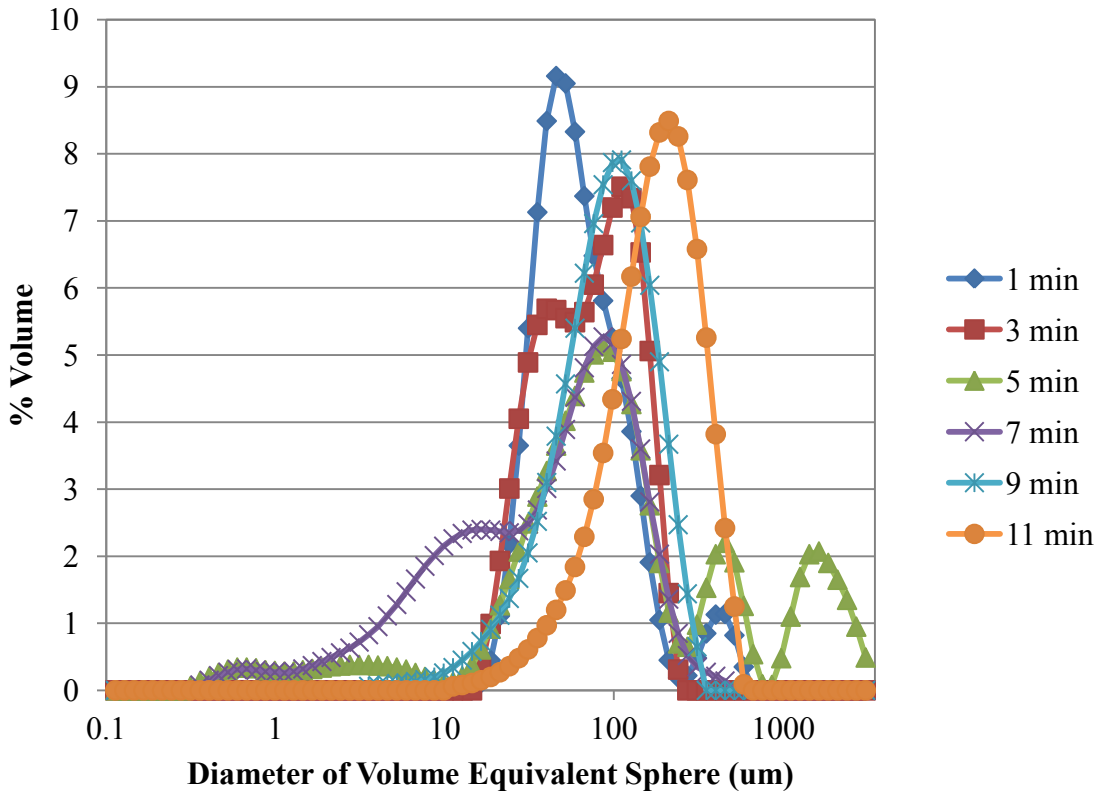

Figure C.8: Floc size distributions generated over time for Case No. 5 (Replicate No. 2). Coagulant dosing occurred continuously during the first 5 minutes.

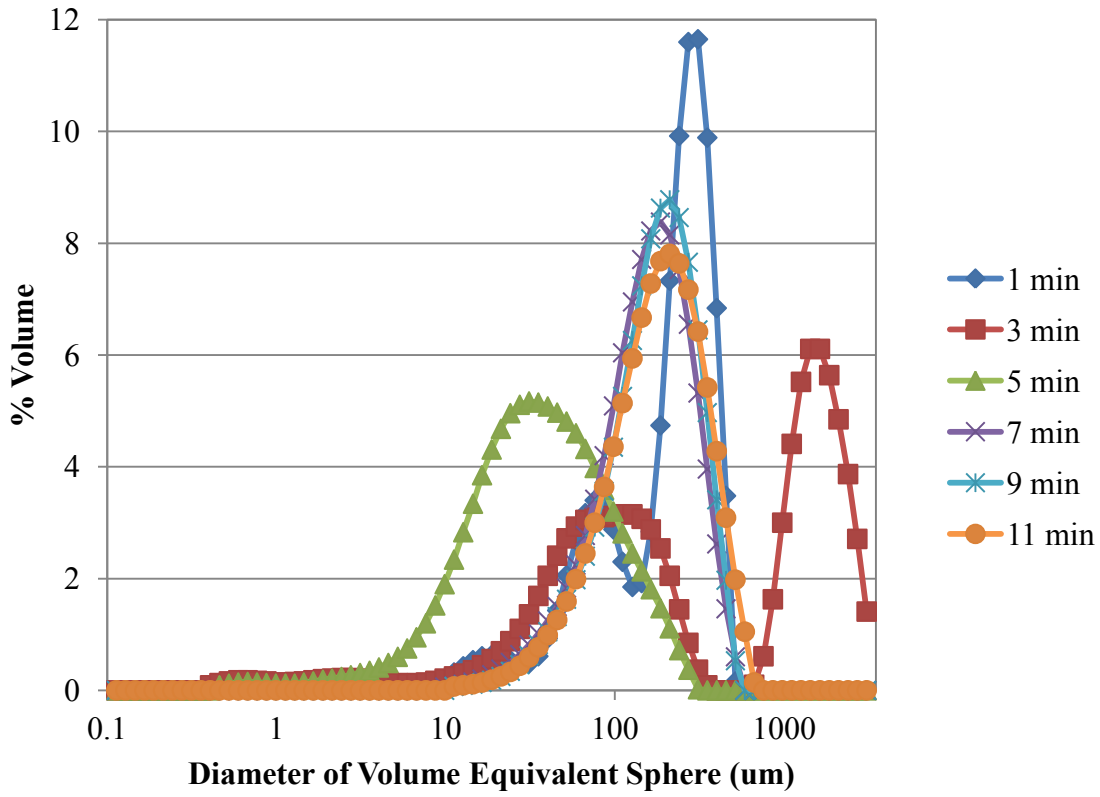

Figure C.9: Floc size distributions generated over time for Case No. 6 (Replicate No. 1). Coagulant dosing occurred continuously during the first 5 minutes.

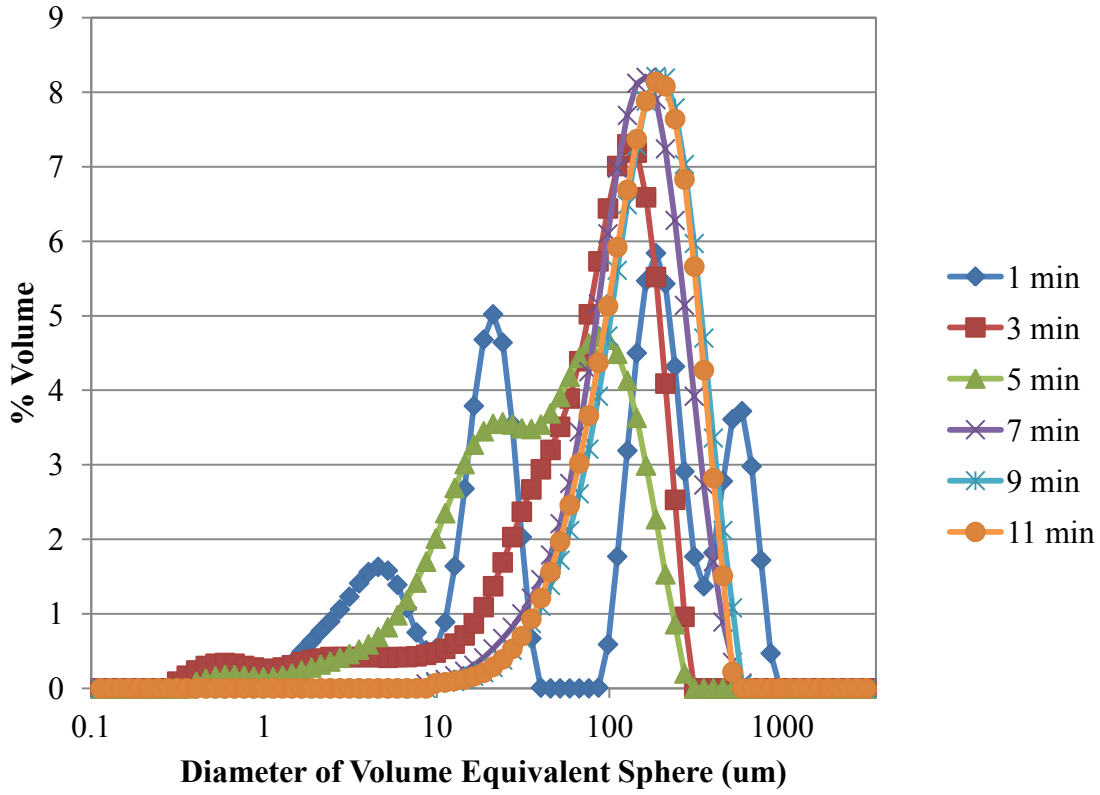

Figure C.10: Floc size distributions generated over time for Case No. 6 (Replicate No. 2). Coagulant dosing occurred continuously during the first 5 minutes.

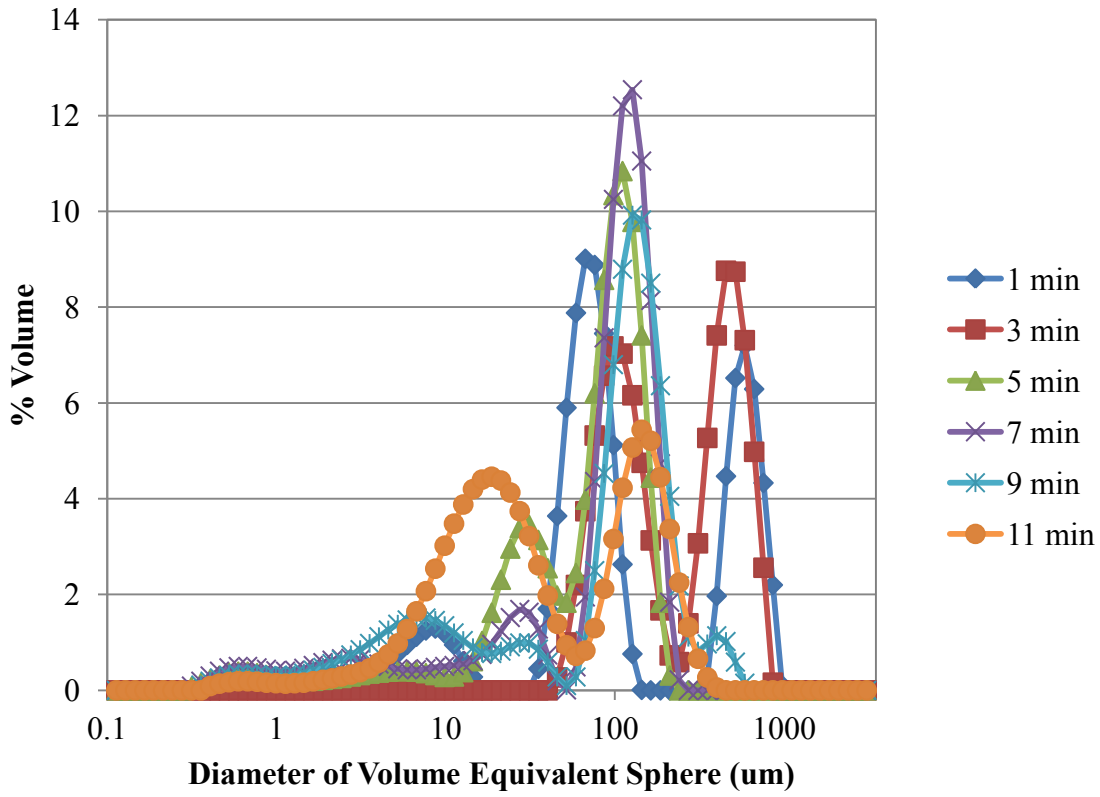

Figure C.11: Floc size distributions generated over time for Case No. 7 (Replicate No. 1). Coagulant dosing occurred continuously during the first 5 minutes.

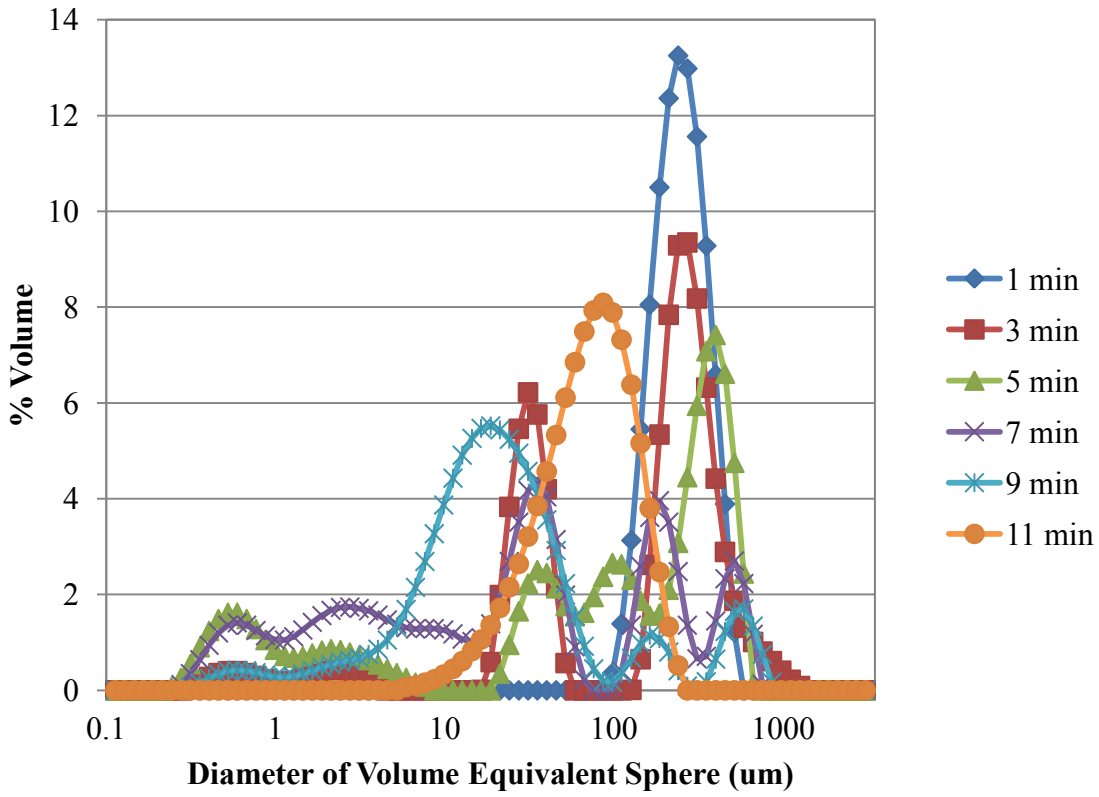

Figure C.12: Floc size distributions generated over time for Case No. 7 (Replicate No. 2). Coagulant dosing occurred continuously during the first 5 minutes.

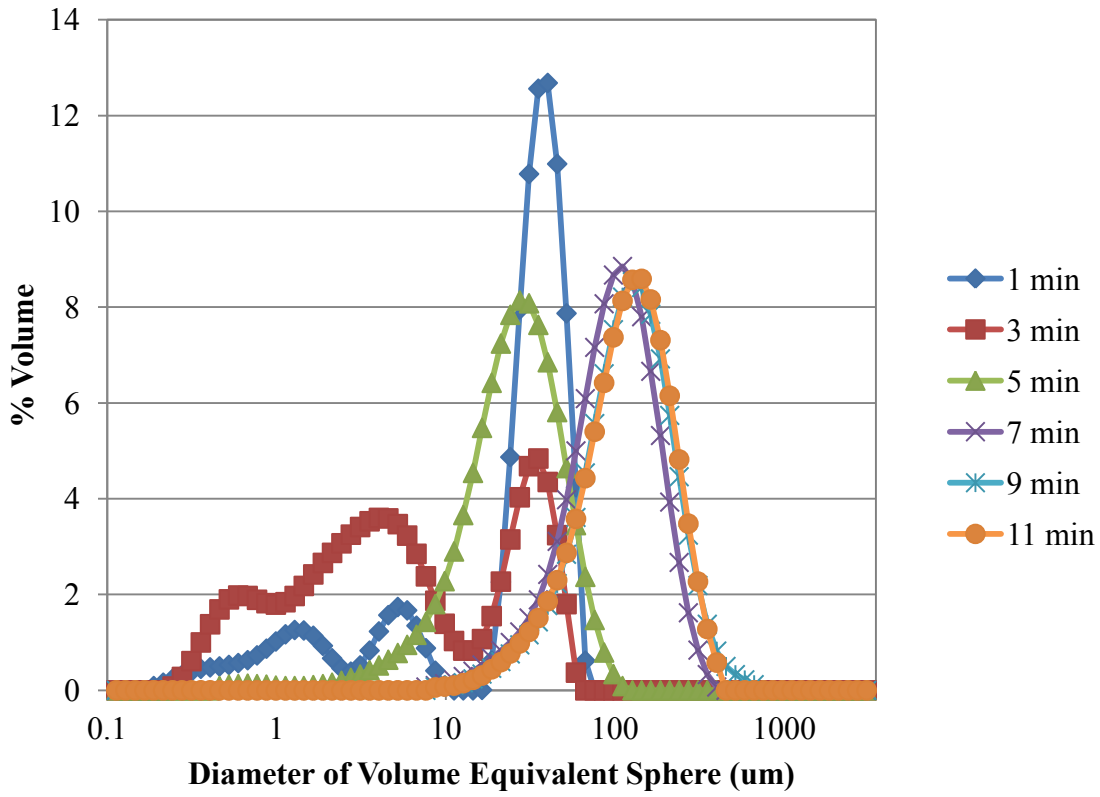

Figure C.13: Floc size distributions generated over time for Case No. 8 (Replicate No. 1). Coagulant dosing occurred continuously during the first 5 minutes.

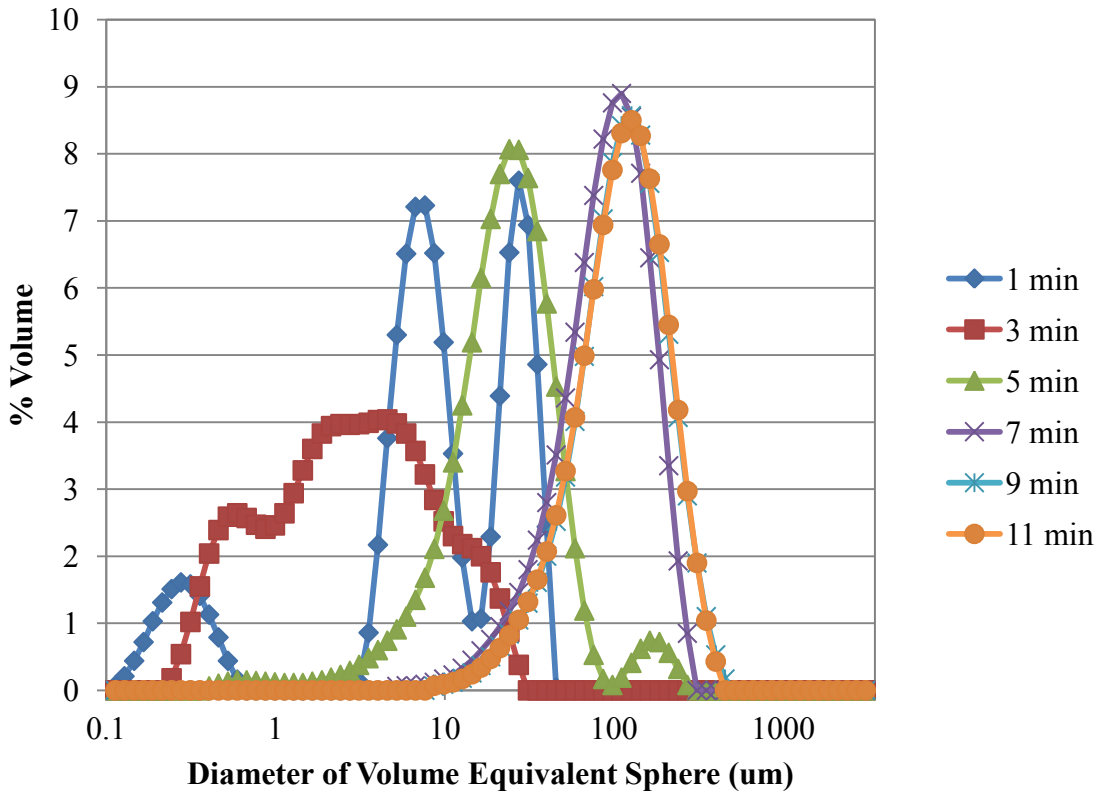

Figure C.14: Floc size distributions generated over time for Case No. 8 (Replicate No. 2). Coagulant dosing occurred continuously during the first 5 minutes.

APPENDIX D: COPYRIGHT PERMISSION LETTER FROM JOURNAL ENVIRONMENTAL REVIEWS

RE: Reproducing paper in PhD thesis

pubs@nrcresearchpress.com

Wed 2/11/2015 3:12 PM

To: Sin Yin Lee;

Dear Sin Yin Lee,

Please review: http://www.nrcresearchpress.com/page/authors/information/rights

As one of the authors of this paper, you may reuse your published material.

Permission is granted.

Thank you for checking.

Best regards,

Eileen Evans-Nantais

Client Service Representative

Canadian Science Publishing

65 Auriga Drive, Suite 203, Ottawa, ON K2E 7W6

T: 613-656-9846 ext.232 F: 613-656-9838

Please Note: My email has changed, please add me to your contacts and use eileen.evans-nantais@cdnsciencepub.com for future correspondence.

From: Sin Yin Lee [mailto:leesinyin@Dal.Ca]

Sent: February-05-15 3:37 PM

To: pubs@nrcresearchpress.com

Subject: Reproducing paper in PhD thesis

Dear Sir or Madam,

In 2014 I co-authored a paper that was published in *Environmental Reviews:*

S.Y. Lee and G.A. Gagnon. (2014). Review of the factors relevant to the design and operation of an electrocoagulation system for wastewater treatment. *Environmental Reviews, 22(4):*421-429.

I am currently preparing my PhD thesis for submission at Dalhousie University (Halifax, NS, Canada). As it is required by my university, could I please get a return email or letter

stating that I have your permission to reproduce a manuscript version of this paper in my thesis?

Please also note that Canadian graduate theses are reproduced by the Library and Archives of Canada (formerly National Library of Canada) through a non-exclusive, world-wide license to reproduce, loan, distribute, or sell theses. I am thus also seeking your permission for said paper to be reproduced and distributed by the LAC (NLC).

Yours sincerely,

Sin Yin Lee

APPENDIX E: COPYRIGHT PERMISSION LETTER FROM JOURNAL ENVIRONMENTAL TECHNOLOGY

East, Deborah <Deborah.East@tandf.co.uk>

Wed 5/13/2015 10:47 AM

To: Sin Yin Lee;

Our Ref: DE/TENT/P3836

Date 13th May 2015

Dear Sin Yin Lee,

Thank you for your correspondence requesting permission to reproduce the following material from our Journal in your thesis:

The rate and efficiency of iron generation in an electrocoagulation system – Environmental Technology – Authors – Sin Yin Lee and Graham A. Gagnon.

We will be pleased to grant entirely free permission on the condition that you acknowledge the original source of publication and insert a reference to the Journal's web site: http://www.tandfonline.com

We are happy for you to post the preprint version on the website of www.nlc-bnc.ca.

Please include the following:

This is a preprint of an article whose final and definitive form has been published in Environmental Technology © 16th April 2015 Copyright Taylor & Francis; Environmental Technology is available online at:

http://www.tandfonline.com/doi/full/10.1080/09593330.2015.1032367

Please note we are unable to grant you permission to include the final published version within the 18 month embargo period.

Thank you for your interest in our Journal.

Yours sincerely

Debbie East– Permissions & Licence Administrator - Journals.

Routledge, Taylor & Francis Group.

3 Park Square, Milton Park, Abingdon, Oxon, OX14 4RN, UK.

Tel :+44(0)20 7017 6960

Fax:+44 (0)20 7017 6336

Web: www.tandfonline.com

E-mail: deborah.east@tandf.co.uk

From: Sin Yin Lee [mailto:leesinyin@dal.ca]

Sent: 02 April 2015 17:24

To: Academic UK Non Rightslink

Subject: tent20:The rate and efficiency of iron generation in an electrocoagulation system

Permissions Request

Contact name: Sin Yin Lee

Street address: 502-1271 Church Street

Town: Halifax

Postcode/ZIP code: B3J3L3

Country: Canada

Contact telephone number: 902-412-7900

Contact email address: leesinyin@dal.ca

Article title: The rate and efficiency of iron generation in an electrocoagulation system

Article DOI: 10.1080/09593330.2015.1032367

Author name: Sin Yin Lee, Graham A. Gagnon

Journal title: Environmental Technology

Volume number: *

Issue number: *

Year of publication: *

Page number(s): All

Are you the sole author/editor of the new publication?: No

Are you requesting the full article?: Yes

If no, please supply extract and include number of word:

If no, please supply details of figure/table:

Name of publisher of new publication: Dalhousie University (and by extension, the Library and Archives of Canada)

Title of new publication: Electrocoagulation for wastewater treatment (working title)

Course pack: No

Number of Students:

Is print: Yes

Electronic: Yes

E-reserve: No

Period of use:

Short loan library?: No

Thesis: Yes

To be reprinted in a new publication?: No

In print format:

In ebook format?:

ISBN:

Languages:

Distribution quantity:

Retail price:

Additional comments: I am currently preparing my PhD thesis for submission to the Faculty of Graduate Studies at Dalhousie University, Halifax, Nova Scotia, Canada. I am seeking your permission to include a manuscript version of the above paper as a chapter in the thesis. Please note that Canadian graduate theses are reproduced by the Library and Archives of Canada (formerly National Library of Canada) through a non-exclusive, world-wide license to reproduce, loan, distribute, or sell theses. I am thus also seeking your permission for said paper to be reproduced and distributed by the LAC(NLC). Further details about the LAC(NLC) thesis program are available on the LAC(NLC) website (www.nlc-bnc.ca). Full publication details and a copy of your permission will be included in the thesis.